Modelling of photocatalytic degradation of pharmaceuticals in water by multi-faceted approach

Tomić, Antonija

Permanent link / Trajna poveznica: https://urn.nsk.hr/urn:nbn:hr:149:221286

Download date / Datum preuzimanja: **2025-02-12**

FACULTY OF CHEMICAL ENGINEERING AND
TECHNOLOGY

Antonija Tomić

MODELLING OF PHOTOCATALYTIC DEGRADATION OF PHARMACEUTICALS IN WATER BY MULTI-FACETED APPROACH

DOCTORAL THESIS

Zagreb, 2022

Sveučilište u Zagrebu

FAKULTET KEMIJSKOG INŽENJERSTVA I TEHNOLOGIJE

Antonija Tomić

MODELIRANJE FOTOKATALITIČKE RAZGRADNJE FARMACEUTIKA U VODI VIŠESTRANIM PRISTUPOM

DOKTORSKI RAD

Zagreb, 2022.

University of Zagreb

FACULTY OF CHEMICAL ENGINEERING AND TECHNOLOGY

Antonija Tomić

MODELLING OF PHOTOCATALYTIC DEGRADATION OF PHARMACEUTICALS IN WATER BY MULTI-FACETED APPROACH

DOCTORAL THESIS

Supervisor: Prof. Ana Lončarić Božić, Ph.D.

Zagreb, 2022

Sveučilište u Zagrebu

FAKULTET KEMIJSKOG INŽENJERSTVA I TEHNOLOGIJE

Antonija Tomić

MODELIRANJE FOTOKATALITIČKE RAZGRADNJE FARMACEUTIKA U VODI VIŠESTRANIM PRISTUPOM

DOKTORSKI RAD

Mentor: prof. dr. sc. Ana Lončarić Božić

Zagreb, 2022.

Bibliographic page

Bibliographic data:

The topic of the dissertation was approved at the session of the Faculty Council of the Faculty of Chemical Engineering and Technology, University of Zagreb on December 16, 2019, and approved at the 10th session of the Senate of the University of Zagreb on June 9, 2020.

ACKNOWLEDGMENTS

SUMMARY

Pharmaceuticals, as one of the largest groups of contaminants of emerging concern (CECs), pose a threat to the environment and human health. Advanced Oxidation Processes (AOPs) have proven to be effective in the degradation of persistent, toxic, and non-biodegradable pollutants in water. Heterogeneous photocatalytic processes are multiparameter systems pertaining to AOPs based on *in-situ* generated radical, with overall effectiveness influenced by the different process parameters. Predicting the behaviour of photocatalytic AOPs by means of mathematical simulations is crucial not only for scale-up and process optimization, but also for controlling undesirable environmental effects such as the formation of by products with a higher toxicity than the parent compound.

In this work, a multi-faceted approach was applied to develop a simulation model for the photocatalytic process for the degradation and mineralisation of pharmaceutical ibuprofen by UV-A/TiO_2 P25. The mathematical – mechanistic model of heterogeneous photocatalysis includes a set of differential equations and takes into account the configuration of the photocatalytic reactor, the irradiation emission, the scattering of irradiation, the process parameters, the reaction kinetics and the degradation mechanism. The developed model was verified by experimental results obtained at different photocatalyst loadings. Coumarin and 1,4-benzoquinone were used as chemical probes to confirm the generation of hydroxyl and superoxide radicals and to fine-tune the chemical reactions in the model. To increase the robustness of the developed model, a variety of organic compounds whose structural features influence important mechanisms in photocatalytic treatment, such as adsorption on the TiO_2 P25 surface and the prevalence of degradation by hydroxyl and superoxide radicals, were investigated using quantitative-structure activity/property relationship (QSA/PR) modelling. Adsorption was first investigated by a combined experimental/statistical approach using response surface method (RSM), which yielded a quadratic polynomial equation (QPE) describing adsorption for each organic compound studied. The coefficients of the QPE were related to structural features employing QSA/PR. The degradation of organic compounds by the UV-A/TiO_2 P25 process in the presence of coumarin and 1,4-benzoquinone was studied, common radical scavengers for hydroxyl and superoxide radicals were investigated and coefficients were determined based on the kinetics obtained, that diversified the prevalence of oxidation or reduction mechanisms in the degradation of organic compounds. The

determined coefficients were correlated with structural features of the investigated organic compounds by QSA/PR modelling.

The simulation model developed by the proposed multi-faceted approach achieved good agreement between the predicted and experimental data. The QSA/PR modelling combined with RSM methodology accurately predicted the adsorption of organic compounds with complex molecular structure. The QSA/PR technique also successfully captured relevant structural features that determine degradation kinetics, so it can be used to increase the robustness of mathematical – mechanistic models which ensures their simulation capability for a wide range of organic structures.

SAŽETAK

Farmaceutici, kao jedna od najvećih skupina onečišćivala koji izazivaju zabrinutost (eng. *contaminants of emerging concern*, CECs), predstavljaju prijetnju za okoliš i ljudsko zdravlje. Napredni oksidacijski procesi (eng. *advanced oxidation processes*, AOPs) su se pokazali učinkovitim u razgradnji postojanih, toksičnih i biološki nerazgradivih onečišćenja u vodi. Heterogeni fotokatalitički procesi kao dio AOP-a su višeparametarski sustavi, koji se temelje na *in-situ* generiranju radikala, pri čemu na ukupnu učinkovitost utječu različiti parametri procesa. Predviđanje ponašanja fotokatalitičkih AOP-a primjenom matematičkih simulacija važno je ne samo za uvećanje i optimizaciju procesa, nego i za kontrolu nepoželjnih učinaka na okoliš kao što su stvaranje toksičnijih nusprodukata u odnosu na primarni spoj.

U ovom radu primijenjen je višestrani pristup za razvoj simulacijskog modela fotokatalitičke razgradnje i mineralizacije farmaceutika ibuprofena UV-A/TiO$_2$ P25 procesom. Razvijeni matematičko – mehanistički model za heterogenu fotokatalizu sastoji se od seta diferencijalnih jednadžbi koje uključuju konfiguraciju fotokatalitičkog reaktora, emisiju zračenja, raspršenje zračenja, parametre procesa, kinetiku reakcije te mehanizam razgradnje. Razvijeni model verificiran je eksperimentalnim rezultatima dobivenih pri različitim koncentracijama fotokatalizatora. Kumarin i 1,4-benzokinon primijenjeni su u svrhu potvrde generiranja hidroksilnih i superoksidnih radikala te za fino podešavanja kemijskih reakcija na koje utječu u razvijenom modelu. Kako bi se povećala robusnost razvijenog modela istraženi su utjecaji strukturnih značajki različitih organskih spojeva na važne mehanizme fotokatalitičkog procesa, ponajprije na adsorpciju onečišćivala na površini TiO$_2$ P25 te relativni doprinos razgradnji hidroksilnim i superoksidnim radikalima, primjenom kvantitativnog odnosa aktivnosti/svojstava strukture (eng. *quantitative structure activity/property*, QSA/PR) modeliranja. Adsorpcija je ispitana objedinjenim eksperimentalno/statističkim pristupom korištenjem metode odzivnih površina (eng. *response surface methodology*, RSM), a rezultat su kvadratne polinomne jednadžbe (eng. *quadratic polynomial equation*, QPE) koje opisuju adsorpciju za svaki pojedini ispitivani organski spoj. Koeficijenti iz QPE jednadžbi korelirani su sa strukturnim značajkama organskih spojeva primjenom QSA/PR modeliranja. Razgradnjom odabranih organskih spojeva UV-A/TiO$_2$ P25 procesom u prisutnosti kumarina i 1,4-benzokinona, hvatača hidroksilnih i superoksidnih radikala, dobiveni su kinetički modeli te su određeni koeficijenti iz kojih je razvidan doprinos

oksidacijskih i redukcijskih mehanizama prilikom razgradnje organskih spojeva. Dobiveni koeficijenti su zatim uspješno korelirani sa strukturnim značajkama ispitivanih organskih spojeva primjenom QSA/PR modeliranja.

Simulacijski model, razvijen predloženim višestranim pristupom, ukazuje na dobro slaganje predviđenih i eksperimentalnih podataka. QSA/PR modeliranje kombinirano s RSM metodologijom točno predviđa adsorpciju organskih spojeva složenih molekulskih struktura. QSA/PR metodologija je uspješno ukazala na relevantne strukturne značajke koje određuju kinetiku razgradnje te se može primijeniti za uvećanje robusnosti matematičko – mehanističkog modela, što osigurava sposobnost simulacije modela za širok raspon organskih spojeva.

Ključne riječi: adsorpcija, farmaceutici, heterogena fotokataliza, matematičko – mehanističko modeliranje, napredni oksidacijski procesi, RSM, TiO_2 P25, QSA/PR

CONTENT

1. INTRODUCTION

The presence of contaminants of emerging concern (CECs) in the aquatic environment has been identified as a global issue. This common denominator is given for chemical, physical or biological compounds for which there are no regulatory standards, but which may have harmful effects. CECs include cyanotoxins, flame retardants, organohalogens and perfluorinated compounds, personal care products, pesticides, plasticizers, and pharmaceuticals. Besides CECs, single-benzene ring compounds with various substituents are also widely distributed chemical structures in the aquatic environment, many of these are also intermediate chemicals in production of various CECs, as well as by-products of their degradation. The chemicals in both groups are generally characterized with moderate to high solubility, low biodegradability and toxicity towards aquatic organisms and humans [1, 2, 3]. CECs pose a particular challenge to wastewater treatment plants (WWTP) that rely on primary and secondary treatment because they occur in very low concentrations and are therefore continuously discharged into the aquatic environment through large volumes of effluents [4, 5]. Uncontrolled discharge of vast array of hazardous and toxic compounds presents a serious threat to environment and have to be minimized employing either biological, physical, chemical, or their combined treatment. The application of WWTP depends on various parameters, such as: nature and concentration of pollutants, specific parameters of the applied processes that influence the overall effectiveness of the treatment, and economic aspects [6]. Today, one of the most effective methods of removing very low concentrations of pollutants are advanced oxidation processes (AOPs), classified as destructive and low– or non–waste generation technologies, which are performed at mild conditions of temperature and pressure. Accordingly, upgrading WWTP with advanced processing methods promotes greater pollutant removal efficiency but also energy efficiency [2]. Among various AOPs, photocatalysis is a promising tool to ensure complete removal of pollutant or at least partial degradation with the formation of less toxic and more biodegradable structures, seems as a promising option for CECs removal [7].

However, photocatalytic processes are systems with numerous parameters that affect their efficiency. The experimental determination of the different aspects for each pollutant is a rather time-consuming and expensive process. Therefore, it is necessary to use computational techniques to minimize experimental efforts, optimize processes, save time and money. Hence, modelling is used to determine the mechanism and efficiency of pollutant degradation and to predict the

influence of processing characteristics within or outside the studied system. Mathematical – mechanistic modelling, for example, attempts to mathematically describe the chemistry of the processes and phenomena that occur in the degradation of pollutants, and it is possible to predict the behaviour of the system beyond the range of the investigated process parameters [8]. To increase the robustness of the models, the quantitative structure activity/property relationship (QSA/PR) can be used to predict different properties or activities of pollutants based on their chemical structures, as well as the response surface methodology (RSM), which can be used to optimise and robustly predict system responses that depend on input parameters within a certain range [9]. If the above modelling approaches are not applied synergistically, it is not possible to gain a complete insight into the whole process or to predict the behaviour of the water treatment system. Therefore, to gain a complete insight into the aspects of water treatment systems, a multifaceted approach that combines and integrates experimental data with different modelling approaches is required. Given the complexity of photocatalytic processes and their integration models, advanced computer tools such as artificial intelligence and genetic algorithms are used in their creation. By applying the previous methodologies, it is possible to create relatively reliable predictive models that allow us to propose sustainable technologies for water treatment.

2. GENERAL PART

2.1. Pharmaceuticals as emerging contaminants of water

Pharmaceuticals are biologically active substances that produce a certain therapeutic effect. The very structure of pharmaceuticals has a major impact on their fate in the environment, with pharmaceuticals differing in structure and behaviour in the environment from most conventional industrial pollutants. In the last two decades, pharmaceutical compounds have been identified as emerging contaminants for aquatic ecosystems. There are 4000 different pharmaceuticals in use in Europe today. Their use is constantly increasing, and with it, the emergence of new unexplored compounds in the environment, which are a cause for concern of water quality, human health, and the entire ecosystem [10]. Pharmaceuticals detected in the environment are grouped as follows: (i) anti-inflammatory analgesics, (ii) antibiotics, (iii) antiepileptics, (iv) antidepressants, (v) antihistamines, (vii) β-blockers, and (viii) other substances (barbiturates, narcotics) [2]. Unlike conventional industrial chemical pollutants, pharmaceuticals with a molecular weight of less than 500 Da (a) can form chemically more complex molecules with a wide range of molecular weights, different structures and functional groups; (b) are polar molecules with multiple ionising groups, lyophilic and moderately or poorly soluble in an aqueous medium; (c) are persistent in the environment; (d) undergo metabolic reactions that alter their structure [11]. The use of antibiotics is the most common and their spread in the environment is high, leading to the development of multi-resistant bacteria that pose a threat to humans and animals [12]. Relatively high concentrations of antibiotics in the environment are the result of their persistence and continuous inflow into the environment. In general, WWTPs comprise a primary system of physical-chemical treatments and a secondary system that consists of a biological reactor formed by active sludge [11]. Conventional plants have limited ability to remove pharmaceutical products from wastewater because most compounds cannot be metabolised by microorganisms that use the pollutants as a carbon source and may even inhibit the activity of microorganisms or cause their bioaccumulation in effluent or sludge and thus in the food chain. For example, subsequent biological treatments remove 30 – 75% of anti-inflammatories and antibiotics [11]. On the other hand, penicillin is readily hydrolysed in water, whereas fluoroquinolones, macrolides and tetracyclines are much more stable, which leads to their accumulation in higher concentrations [5, 6]. In general, most pharmaceuticals are not completely eliminated in WWTPs, so they remain in effluents and

contaminate surface and groundwater. Figure 1 shows the status of European countries in terms of the number of pharmaceuticals detected in the aquatic environment. As of 2019, a total of 381 different parent pharmaceutical compounds and 66 metabolites and transformation products have been found in European surface waters [15]. The highest number of pharmaceuticals are found in countries where monitoring is most frequently conducted, e.g., United Kingdom, Germany, or Spain. At the same time, this suggests to insufficient monitoring in the countries of Eastern and South-Eastern Europe, where there is almost no data on the detection of pharmaceuticals.
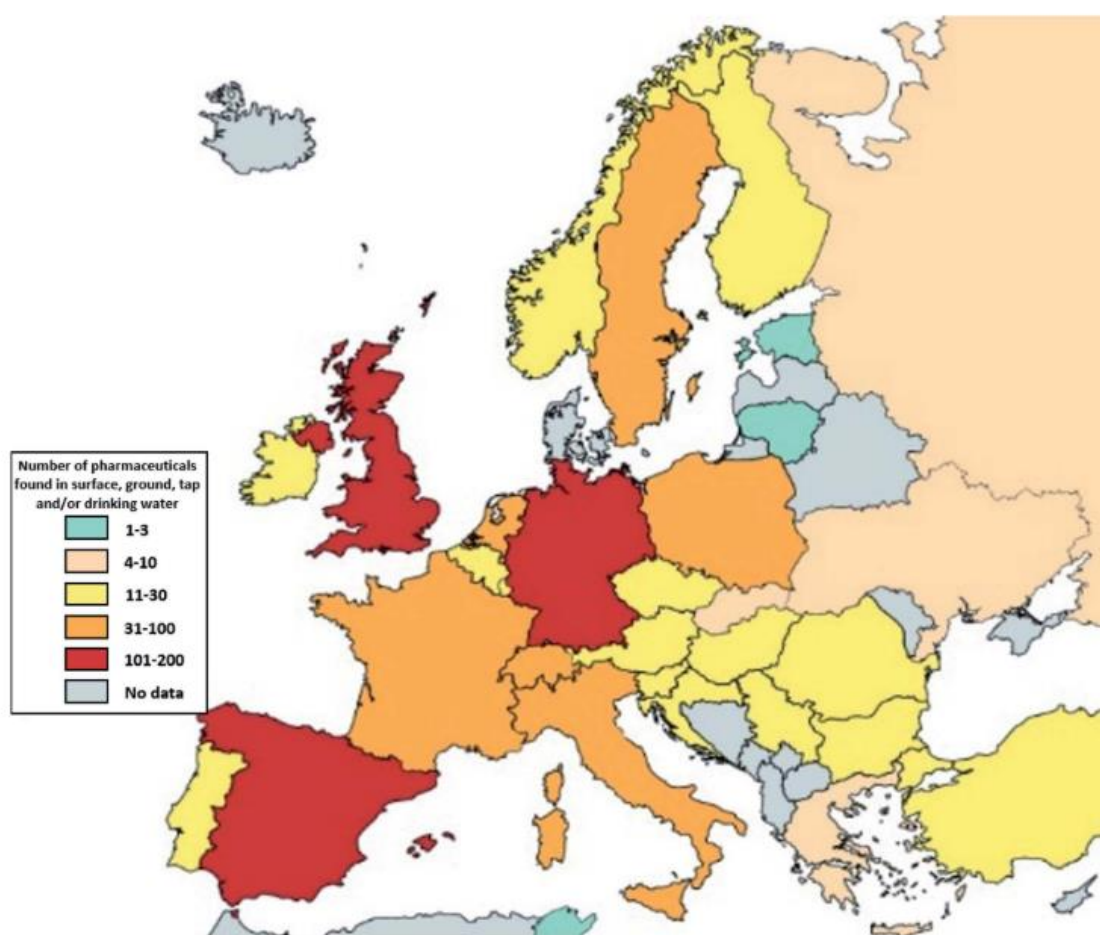
Figure 1 Overview of European countries by number of pharmaceuticals detected in surface waters, groundwater and drinking waters [16].

The presence of pharmaceuticals has been detected in the pristine polar areas of the Earth. Respectively, several antimicrobials and synthetic estrogens have been detected in northern

Antarctica, while recently a German team of scientists collected data on the presence of pharmaceuticals in the environment in 71 countries around the world [8, 9]. After their use, pharmaceuticals are excreted into the environment unchanged or as metabolites from human and animal faeces or urine. The main sources are wastewater treatment plants [19]. They are often detected in large numbers together with their metabolites, which can lead to their synergistic effect [20]. This can lead to the formation of more complex and hazardous compounds that enter surface waters in concentrations of $\mu g \cdot L^{-1}$ – $mg \cdot L^{-1}$ [21]. The pollution of drinking water is also a consequence of the excretion of faeces of human or animal organisms because the wastewater from the sewage system is used for the irrigation of agricultural land after treatment. Another major source of pollution is the pharmaceutical industry. This is due to the direct discharge of wastewater from the production plant into the treatment plant [22]. Farms are also one of the main sources of pharmaceuticals and their metabolites in the environment and can be said to be one of the most dangerous sources, as excreta are often discharged directly into surface waters without pre-treatment, making them much more difficult to control and monitor [2]. In this way, they enter the soil and water and then the food chain [19]. Interesting data from studies in the Northeast of England, where 66% of the population improperly dispose of unused pharmaceuticals in household waste. 12% of disposed pharmaceutical enter the sewerage system via household drains and only 22% of unused pharmaceuticals are properly disposed of properly by being returned to pharmaceutical facilities [23]. Over the last two decades, numerous studies have been conducted on the detection of pharmaceuticals in the environment, especially antibiotics and endocrine disruptors due to their increasing use [8, 9, 15, 16, 17].

2.1.1. Transformation of pharmaceuticals in environment

Pharmaceuticals are designed to be chemically stable compounds, but they are subject to physicochemical and biotic transformations in the environment [27]. Pharmaceuticals that enter the environment via the human and animal body are usually metabolised in the environment under certain conditions [28]. With the continuous input of pharmaceuticals into the environment, they become pseudo persistent, although they are susceptible to biodegradation processes, photodegradation and sorption [19]. Monitoring of metabolites in the environment is limited by the small number of reference standards for pharmaceutical metabolites in the environment, resulting

in limited information on the occurrence, behaviour, and half-lives of metabolites in the environment. Awfa et al. and Wales et al. [19, 20] reported the detection of carbamazepine epoxide that is a metabolite of carbamazepine, in wastewater at concentrations ranging from 880 to 4026 ng·L^{-1}, while the concentration of the parent compound carbamazepine was 1.5 to 113 ng·L^{-1}. For these reasons, it is necessary to identify transformation processes in the environment, transformation metabolites and perform various analyses of pharmaceutical metabolites in order to reduce the concentration of pharmaceuticals and their metabolites in the environment. Understanding pharmaceutical biodegradation, conjugation and deconjugation, metabolic pathways, persistence and sorption is important for pharmaceutical transformation processes to predict their fate in the environment [2]. The high stability of pharmaceuticals indicates persistence in the environment when exposed to environmental factors. However, the metabolites of pharmaceuticals, which are formed by oxidation, reduction, or hydrolysis, are very often susceptible to transformation processes, making them less stable in the environment than the primary substance.

Biodegradation, photodegradation and abiotic transformation processes, such as hydrolysis, can reduce the concentration of pharmaceutical products in the environment through partial degradation or mineralisation [22, 23]. Chiron et al. [33] shows that in simulated estuarine waters an acridine intermediate is formed by photodegradation of carbamazepine. The metabolite discovered is more toxic, mutagenic, and carcinogenic than the primary carbamazepine. Another study conducted in the Elbe river showed that the antibiotic tetracycline adsorbs on the sediment and is not subject to photodegradation [34]. However, the analgesic diclofenac, which is one of the most frequently detected pharmaceuticals in the environment, can be degraded very effectively by direct photolysis in a very short period of 1h, according to studies [19].

Different pharmaceuticals have large differences in their physicochemical properties, thus great differences in behaviour can be assumed. For example, water solubility, hydrophobicity, and volatility can significantly affect the fate of pharmaceuticals in the environment [22, 26]. The dissociation constant (pK_a), solid-water partition coefficient (logK_d), organic carbon sorption coefficient (logK_{oc}), and octanol-water partition coefficient (logK_{ow}) also affect the transformation of pharmaceuticals as well as their fate in the environment, hydrolysis by sorption, and biodegradation processes [31].

Many pharmaceuticals have an acidic or basic functional group, so they can exist in cationic, anionic, neutral, and zwitterionic forms under environmental conditions. They depend on the pK_a and $logK_{ow}$ values, which are very different for each individual compound. This adds to the complexity of understanding the behaviour of pharmaceuticals in the environment [2]. The Henry coefficient (K_H) is also one of the important parameters for pharmaceuticals in the environment. Some researches suggests that pharmaceutical fractions obtained by evaporation should be neglected due to the low value of the Henry coefficient [27, 28]. The role of chirality of molecules is of great importance for the fate of pharmaceuticals in the environment, since almost half of pharmaceuticals are sold as single enantiomers and are more dangerous than achiral molecules [38]. Enantiomeric reactions produce different enantiomers in different biotransformation reactions, which are mirror images of the original enantiomer. However, metabolism can alter the enantiomeric ratio of racemic pharmaceuticals in the environment. Microbiological transformation of racemic pharmaceuticals can produce different compounds from each enantiomer, selectively altering one enantiomer in which both are present [39]. Therefore, microbial metabolism can accumulate a particular enantiomer, as shown by research on the biodegradation of naproxen in wastewater treatment plants [40]. The (S) enantiomer was transformed into O-desmethylnapraxene due to microbiological activity, enriching the enantiomeric excess of the (R) enantiomer, which leads to an increase in toxicity [39].

Pharmaceutical transformation depends on many environmental parameters such as pH, temperature, sunlight, etc., which accelerate various degradation processes [41]. Transformations are also influenced by dilution, adsorption in soils, sediments, natural organic materials and suspended particles [42]. Turbidity, hydraulic regime, boundary layer conditions together with light intensity, presence of photosensitive substances and presence and type of microbial communities, and seasons are necessary factors for determining the concentration of pharmaceuticals in the environment and their transformation [43]. For many pharmaceuticals, the presence of photosensitive functional groups leads to their more successful removal from surface waters by photodegradation [44]. In addition, the efficiency of photodegradation depends on the intensity of solar radiation, water depth, organic matter composition, eutrophic conditions, latitude, and time zones [19]. Photodegradation can be induced directly by adsorption of UV radiation or indirectly by the generation of hydroxyl radicals. Propranolol, ketoprofen, naproxen, ibuprofen and many other antibiotics are known to undergo photodegradation after their release into the environment

[45]. Photodegradation also depends on various environmental parameters, such as vegetation, vegetation shading, radiation intensity, particle suspension, dissolved organic matter, seasonal changes in sunlight, temperature, and depth in aquatic systems [36, 37]. However, the presence of various suspended organic particles and dissolved organic matter can slow photodegradation because they absorb some sunlight and reduce the light intensity for photoexcitation of pharmaceuticals and their metabolites. An example is the presence of humic acids, which can reduce or enhance photodegradation of pharmaceuticals in the environment [48]. The effect of humic acids depends on the absorption spectrum of the compound. The process of direct photolysis is possible when the compounds absorb light with a wavelength of more than 290 nm, which leads to the degradation of the chemical compounds. Such compounds are photosensitizers and examples are humic acid and nitrates. Humic acid has been found to enhance the photochemical degradation of the pharmaceuticals diclofenac and naproxen by indirect photolytic processes [49]. Andreozzi [50], found that humic acid or nitrates enhanced the photodegradation kinetics of chlorofibric acid, which he attributed to an indirect photolytic effect.

2.1.2. Environmental risk of pharmaceuticals

Human exposure to pharmaceuticals results from the direct effects of the therapeutic use of pharmaceuticals but may also be a consequence of the indirect effects of pharmaceuticals released into the environment. The increasingly frequent detection of pharmaceuticals in the aquatic environment and their incomplete removal from wastewater have led to the presence of a wide range of pharmaceuticals in drinking water worldwide that can cause a threat to human health and wildlife. Furthermore, very little is known today about the potentially harmful effects of pharmaceuticals on the environment and human health, and further research is necessary. An indirect consequence of pharmaceutical exposure for human health is associated with exposure to antimicrobial resistant organisms (AMR), as AMR poses a severe threat to both animal and human health. For example, the presence of antibiotics in the environment such as ciprofloxacin and sulfamethoxazole can influence the development and spread of AMR, bacteria, fungi, and biofilms [16]. Furthermore, AMR bacteria found in fish have been shown to transfer this resistance to human microbiota [25]. This research, as well as general research on the potentially harmful effects of pharmaceuticals in the aquatic environment on human health, has not been fully explored and

further research is needed and is still being conducted today. In the case of testing the toxicity and potential harmfulness of pharmaceuticals to fauna and flora, worrying results were found regarding their effects. When determining endpoints in ecotoxicology, four main categories from aquatic systems are examined: fish, invertebrates, algae, and plants. Studies on the potential toxicity of azithromycin to the alga *Chlorella pyrenoidosa* and the freshwater shrimp *Daphnia magna* conducted by Li et al. [26], concluded that azithromycin inhibits digestive enzymes and causes oxidative stress in *Daphnia magna*. Fu et al. [51] studied the toxicity of 13 antibiotics on freshwater green algae and showed that of the 13 antibiotics, azithromycin had the highest toxicity. Sulfamethoxazole can be classified as highly toxic to photosynthetic organisms, especially aquatic plants, algae and cyanobacteria [52]. The mechanism of action of sulfamethoxazole is the inhibition of folate synthesis in bacteria. This mechanism of action is similar to that of many photosynthetic organisms that cause inhibition of *Lemna gibba* growth [53]. Furthermore, Jijies et.al. studies [54] have shown that exposure of healthy zebrafish larvae to sulfamethoxazole leads to inflammation of the immune system, which in turn results in the hatching of embryos with shortened body length. Antibiotic ciprofloxacin is highly toxic to organisms such as gram-negative bacteria *Pseudomonas putida*, freshwater and marine cyanobacteria *Microcystis aeruginosa*, *Synechococcus leopolensis*, and *Cyclotella meneghiniana* platons [55]. According to research Martins et. al. [56] exposure to *D. magna* to low concentrations of ciprofloxacin reduced fertility, larval size in the first brood, and number of broods per female. This confirms that ciprofloxacin is toxic to the most sensitive organisms in the aquatic ecosystem. In general, the concentrations of antibiotics in Asian developing countries tend to be higher than countries in European and North American countries [57]. For example, in India, enormously high levels of ciprofloxacin were detected in WWTP effluents (up to 14000 $\mu g \cdot L^{-1}$) and in lakes (2500 – 6500 $\mu g \cdot L^{-1}$), and elevated levels were found also in groundwater (0.044 – 14 $\mu g \cdot L^{-1}$) [9, 13] compared to ng$\cdot L^{-1}$ levels in surface and groundwaters of the USA and the European Union [25, 26, 27].

Diclofenac is a pharmaceutical widely used in the form of sodium salt for the treatment of painful inflammatory rheumatoid and non-rheumatoid diseases. It is one of the most used pharmaceuticals of today, primarily because of its wide range of activities, and its harmful effects are also well known, therefore it is still the subject of research. In aquatic environment diclofenac has recently been found in low concentrations of approximately 2 ng$\cdot L^{-1}$. However, chronic exposure to lower concentrations affects the degradation potential of naturally occurring microbial populations and

lead to significant impacts on fish health [61]. Diclofenac has a very high biological activity that can potentially be toxic to non-target organisms [62]. Biotransformation of diclofenac into reactive intermediate acyl glucuronides, which may bind to intracellular and extracellular proteins, results in adverse effects. Diclofenac has been shown to cause oxidative stress and affect the metabolism of carbohydrates and fatty acids in *C. pyrenoidosa* in low concentrations [63]. It is also associated with reduced egg growth in Japanese medaka which causes a reduced ability to hatch eggs [64]. Diclofenac has also been observed to affect the biochemical functions of California trout resulting in tissue damage [65].

By the 2015 revision of the Watch list, based on collected data, antibiotics amoxicillin and ciprofloxacin have been identified as suitable candidates for inclusion [66]. Amoxicillin has been detected at concentrations around 200 ng·L^{-1} in surface water in Spain, while ciprofloxacin was detected to 19 ng·L^{-1}. The consequence of their use is antibacterial resistance.

The relatively small dataset for amoxicillin is not surprising, because amoxicillin belongs to β-lactam class of antibiotics that are structurally characterized by the β-lactam ring. Although β-lactams are the most commonly prescribed antibiotic class around the world, but amoxicillin is usually not detected in surface waters as it degrades easily and is mostly removed during the wastewater treatment process. Amoxicillin is susceptible to degradation when exposed to light, heat, extreme pH, and solvents like water and methanol. Furthermore, β-lactam antibiotics hydrolyse easily under environmental conditions and only low levels are usually detected in the water despite their high consumption [67]. Nonetheless, it has been detected in some European and Australian surface waters, but the highest concentration of amoxicillin identified was 1.67 mg·L^{-1} which was detected in effluent water entering Victoria Harbor in Hong Kong, China [68].

Ibuprofen is a nonsteroidal anti-inflammatory drug that is used for treating pain, fever, and inflammation. As a consequence of the inadequate removal using conventional wastewater treatment, especially biological process-based methods, the presence of ibuprofen in surface waters has been detected at different concentrations from 10 ng·L^{-1} to 169 000 ng·L^{-1} that could be potentially harmful to the environment [69]. Ibuprofen has been reported to have toxic impact on microbial communities [70]. Wastewater from WWTPs containing ibuprofen is mainly treated with AOP, which results in formation of various metabolites with higher or indefinite toxicity compared to the parent compounds [38, 39]. Furthermore, Han et al. [73] investigated chronic toxicity of ibuprofen for three freshwater species, *Oryzias latipes, Daphnia magna*, and *Moina macrocopa*

and its influence on hormone balance in in vitro conditions using H295R cell line. The results of the research showed that ibuprofen at concentration of 0.1 µg·L^{-1}, increased production of 17 β-estradiol and aromatase activity and decreased testosterone production. Additionally, ibuprofen at the same concentration was responsible for a delay in hatching of eggs in *Oryzias latipes.*

Venlafaxine is a prodrug which means it is biologically inactive in its parent form. Its metabolite, the biologically active drug desvenlafaxine, has been classified as persistent and toxic in the environment [74]. However, research conducted by Jijie et al. [54] has shown that exposure to venlafaxine significantly increases the hyperactivity of *Danio rerio* larvae by approximately 25%. Furthermore, Painter et al. [75] showed that low doses of venlafaxine reduced the reactions of the predator *Pimephales promelas*. However, no such behaviour was observed at higher doses. This result is significant because lower doses of antidepressants have shown higher toxicity than higher doses.

In the environment, pharmaceuticals are usually found as a multi-component mixture of pharmaceuticals and other pollutants. It is necessary to study the effect of a mixture that poses a higher risk in relation to the individual effect of pharmaceuticals. A combination of several different pharmaceuticals can cause a synergistic effect (the effect of a mixture is greater than the sum of the effect of individual pharmaceuticals), an additive effect (the effect of a mixture is the sum of the effect of individual pharmaceuticals), or an antagonistic effect (a mixture of pharmaceuticals has less effect than individual pharmaceuticals) [76]. Drzyma and Kalka's investigated the toxicity of sulfamethoxazole and diclofenac on *Vibrio fischeri*, *Dapnia magna* and *Lemna minor* [77]. Their research confirmed the synergistic effect of two pharmaceuticals and the partially additive effect on the test organisms. Furthermore, investigation of the chronic toxicity of sulfamethoxazole and ciprofloxacin on marine peripheral algae and bacteria has shown inhibition of the organisms ability to metabolize carbon sources as a function of concentration. This change in metabolism leads to a change in biodiversity and community function [78].

2.2. Water treatment methods

Wastewater treatment methods depend on the amount and composition of wastewater, the possibility of reuse or release into watercourses and economic viability. Conventional wastewater treatment is a combination of physical, chemical, and biological processes to remove suspended solids, dissolved solids, biological decomposition of organic pollutants, and nutrients from wastewater [23]. Today, it is estimated that almost 80% of currently used pharmaceuticals enter the environment in their original form or as metabolites [79]. Entering in wastewater, they are taken to treatment plants where they try to be removed by various processes. However, many conventional wastewater treatment plants are not able to completely remove pharmaceuticals and their metabolites. As a result of the incomplete removal of the pollutants, they appear as residues in sediments, sludge, effluents, and surface waters [80]. The removal efficiency of pharmaceuticals in conventional wastewater treatment plants range from 50% to 90% [49, 50] and depends on the physical and chemical properties of the compounds as well as on the configuration of the biological reactors and operating parameters such as hydraulic retention time and sludge retention time [83]. In addition, biological processes are carried out by degradation with activated sludge, which is widely used under suitable conditions, especially in the treatment of municipal water. However, despite numerous advantages of biological processes, such as simplicity, economic justification and maintenance, the disadvantage is that the degradation of toxic organic compounds is impossible or very slow and the process conditions required for microbial growth are difficult to adjust. Physical methods of wastewater treatment, such as coagulation, flocculation and sedimentation as well as activated sludge are also mainly used in conventional wastewater treatment plants [52, 53] and generally involve the transfer of contaminants from one medium to another. Therefore, solving problems such as the disposal of secondary waste and the regeneration of adsorbents further reduces the economic viability of these processes. Adsorption on activated carbon or other adsorbent is one of the methods of physical wastewater treatment used to remove poorly degradable organic and inorganic pollutants (such as aromatic compounds, i.e., nitrates, sulphates and/or heavy metals). Coagulation/flocculation can also be very effective, but large amounts of secondary waste (sludge) must be processed, which significantly increases the cost of the treatment process itself [69, 70, 71]. The insufficient efficiency of physical methods is also due to the physicochemical

properties, hydrophobicity and poor biodegradability of pharmaceuticals, as well as the operating parameters of processes in wastewater treatment plants [80].

For example, Berset et al. [89] reported that cocaine and benzoylecgonine were not removed when using conventional methods without biological processes, which include dioxychlorination and sand filtration, while they were completely removed when using ozonation. The dioxychlorination process is usually used to disinfect water with chlorine dioxide, which is also the most effective process for disinfecting drinking water because chlorine dioxide is a stronger oxidant than chlorine. Removal of non-steroidal anti-inflammatory drugs in wastewater treatment plants is achieved to varying degrees. After treatment with a dioxychlorination mixture and sand filtration, diclofenac was almost completely removed (over 99%); naproxen was partially removed (48%), while ibuprofen was almost marginally removed (14%) [89]. However, when ozonation was used as the treatment process, more than 40% of ibuprofen, naproxen and diclofenac were removed, and dioxychlorination and the sand filtration process effectively removed sulfonamides and macrolides [90]. Thermal destruction of contaminants, i.e., incineration at high temperatures, is also one of the removal techniques. However, this technique can lead to unwanted emissions and destruction of beneficial microbes but is technically and economically very challenging. Since conventional methods of removing pharmaceuticals from the environment are not sufficiently effective, more attention is being paid to advanced methods of water treatment.

2.3. Advanced oxidation processes

The ubiquity of pharmaceuticals in the aquatic environment, as well as their persistence, necessitates advanced water treatment methods. Since conventional wastewater treatment has a number of disadvantages in the form of limited efficacy for the removal of pharmaceuticals, hence advanced oxidation processes (AOPs) represent a great potential [91]. They are defined as a water treatment process whose efficiency is based on the activity of *in-situ* generated highly reactive radicals, such as hydroxyl radicals, which can decompose and mineralize persistent organic pollutants [92]. AOPs can be used on their own, but usually as a pre-treatment process in wastewater treatment plants to increase the biodegradability of organic pollutants, or as post-treatment process to remove certain pollutants, such as pharmaceuticals. Primary, AOPs were first introduced for drinking water treatment and later, in the 1980s, for the treatment of various wastewaters [93].

The hydroxyl radical (•OH) is the backbone of most advanced oxidation processes due to its extremely high oxidation potential ($E°_{•OH/H_2O} = 2.8$ V), reactivity and extreme non-selectivity [94]. The radical •OH is an unstable, charge-neutral radical with a short half-life of only 10^{-9} s. The reaction with low molecular weight organic molecules is extremely fast with constant rates in the order of $10^8 – 10^{10}$ $M^{-1} \cdot s^{-1}$. The advantage of advanced oxidation processes, besides the extremely rapid degradation of persistent pollutants, is the low or almost negligible amount of secondary waste produced during treatment due to the complete oxidation (mineralisation) of the organic compound to carbon dioxide and water [95]. Advanced oxidation processes have been shown to be effective in removing persistent pollutants such as dyes, cyanotoxins, pharmaceuticals, volatile organic compounds, and pesticides [65, 66, 67]. Therefore, AOPs are attractive as pretreatment processes immediately prior to secondary treatment or as a tertiary treatment step in wastewater treatment plants [68, 69]. Sources of energy in AOPs for generation •OH are chemical, electrical, mechanical energy and electromagnetic radiation. The oldest advanced oxidation process, the Fenton process, generate an •OH by catalytic redox reaction of hydrogen peroxide reduction with simultaneous oxidation of Fe^{2+} to Fe^{3+}. Another chemical source of generation •OH is the reaction of ozone with hydrogen peroxide under alkaline conditions (pH > 8) [101]. Electrical sources are used in "corona" processes where •OH is generated by a high-voltage electrical discharge in water [102]. In processes based on the energy of electromagnetic radiation, the photons can have a wide

range of energies, from visible radiation to X-rays and γ-rays. If the visible or UV radiation is applied, it is referred to as photo processes; while at higher energies, it is referred to as radiolysis [72, 73]. Among the advanced oxidation processes, the photo processes are particularly interesting, such as photooxidation and photocatalysis, which stand out as very efficient processes.

2.3.1. Heterogeneous photocatalytic processes

After the discovery of photocatalytic water splitting by Fujishima and Honda in 1972, the researchers turned their point of convergence toward semiconductor photocatalysis which proved very effective in the degradation of even those pollutants which are highly difficult to remove by the other means [105]. In comparison with the conventional wastewater treatments, the heterogeneous photocatalysis has significant advantages, for example, they can be used to degrade and mineralize the pollutants completely to CO_2 and H_2O, but also can degrade very stable compounds which cannot be easily degraded by the other processes. Furthermore, they can work efficiently at ambient temperature and pressure conditions, and they do not need any special supply of oxygen. The other advantage of the photocatalysis is that it is a low-cost process as compared to the other oxidation process having no waste disposal problems [106]. To date, heterogeneous photocatalysis has been known as the most distinctive, popular, effective, interesting, and promising wastewater treatment technique for the removal of recalcitrant and persistent contaminants [95, 96, 97]. A large number of semiconductor photocatalysts have been investigated for degradation of various pollutants, such as ZnO, WO_3, Fe_2O_3, CdSe, SnO_2 [110, 111]. In general, an ideal photocatalyst should have some basic properties, such as activity under UV, visible light, or solar light, they should have property of chemical and biological robustness, as well as they should be stable toward photocorrosion [112].

The most commonly used photocatalyst is titanium dioxide, TiO_2, due to its biological and chemical inertness, non-toxicity, low cost, high catalytic efficiency, photochemical stability, low energy band gap, and high UV absorptivity [109]. Heterogeneous photocatalysis is essentially a process of surface chemical reactions driven by photons. Figure 2 illustrates the simplified mechanism for the photoactivation of photocatalyst TiO_2. As shown in Figure 2, the valence and conduction bands of a TiO_2 are separated by a band gap.
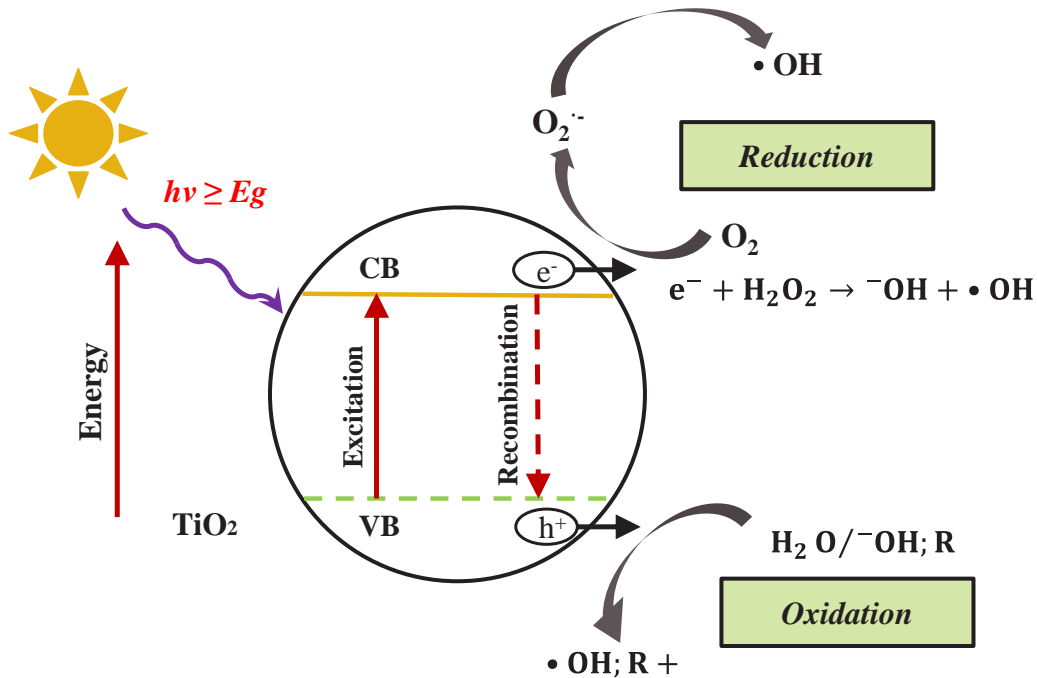
Figure 2 Simplified mechanism of the photocatalytic process [109].

In order to initiate the degradation process, TiO_2 requires photoexcitation with light at a wavelength of < 387 nm, to exceed the band gap of the active anatase phase of 3.2 eV and the rutile phase of 3.0 eV with onset wavelength of 413 nm [113]. Hence, photocatalysis over a TiO_2 is initiated by the absorption of photons with energy equal to or greater than its band gap that promotes the movement of electron from the valence band to the conduction band of TiO_2. Using a simplified correlation, the wavelength of the photon needed to excite the photocatalyst can be calculated from the energy of the forbidden zone:

$$\lambda = \frac{hc}{E_g} \approx \frac{1240}{E_g} \tag{1}$$

where h is the Planck constant (6.626×10^{-34} J·s), and c is the speed of the light in vacuum (3.0×10^8 m·s^{-1}). We can approximate the expression in numerator (1) with a constant of 1240 after considering that 1 eV = 1.6×10^{-19} J·s, and express λ in nm (10^{-9} m) [114]. Therefore, this process generates positive valence band hole (h_{vb}^+) and negative conduction band electron (e_{cb}^-):

$$TiO_2 + hv \rightarrow e_{cb}^-(TiO_2) + h_{vb}^+(TiO_2) \tag{2}$$

These photogenerated electron-hole pairs may also be involved in the following three possible processes: (i) the electron-hole pairs are separated and successfully migrate to the surface of semiconductor and then transfer to adsorbed organic or inorganic species or to the solvent (ii) the separated charge carriers are trapped by the defect sites in the bulk and/or surface region of semiconductor; (iii) the separated charge carriers recombine and release the energy in the form of heat or photons in the bulk and/or surface region of semiconductors [115]. The last two processes are usually referred to as deexcitation processes because the photogenerated charges do not have the ability to drive the photocatalytic reaction, so only the photogenerated charges that are transferred to the reactants via the surface of semiconductor could contribute to photocatalytic reactions. The electron and hole can recombine when there is a lack of oxygen to react with the electron for the formation of superoxide radicals, $O_2^{-\bullet}$. During the recombination, the absorbed light energy released as heat with no chemical reaction takes place [113]. Therefore, TiO_2 can act as a molecule's acceptor or electron donor. The powerful oxidant, h_{vb}^+, oxidizes the water and hydroxide ion (OH⁻) to produce the •OH, whereby the reductant, e_{cb}^-, reduces the oxygen to form superoxide radical anion ($O_2^{-\bullet}$) [109]. Superoxide radical can than react with hydrogen ion (H⁺) to form hydrogen peroxide radical ($HO_2^{\bullet}$) and hydrogen peroxide (H_2O_2) that is protonated by H⁺ ion. These reduction and oxidation processes take place on the surface of the photoexcited semiconductor to prevent the recombination of e_{cb}^- and h_{vb}^+ but also to produce reactive oxygen species (ROSs) such as •OH, $O_2^{-\bullet}$, $HO_2^{\bullet}$ and H_2O_2 which takes part in the contaminant degradation process. The following reactions have been widely postulated [109]:

$$TiO_2(h_{vb}^+) + H_2O \rightarrow TiO_2 + \bullet OH + H^+ \tag{3}$$

$$TiO_2(h_{vb}^+) + OH^- \rightarrow TiO_2 + \bullet OH \tag{4}$$

$$TiO_2(e_{cb}^-) + O_2 \rightarrow TiO_2 + O_2^{-\bullet} \tag{5}$$

$$O_2^{-\bullet} + H^+ \rightarrow HO_2^{\bullet} \tag{6}$$

$$HO_2^{\bullet} + H^+ + TiO_2(e_{cb}^-) \rightarrow H_2O_2 \tag{7}$$

$$O_2^{-\bullet} + O_2^{-\bullet} + 2H^+ \rightarrow H_2O_2 + O_2 \tag{8}$$
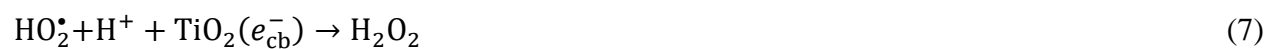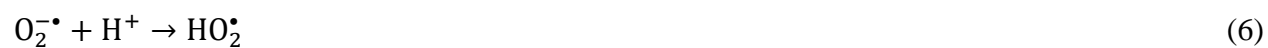
However, when H_2O_2 is split off by the reactions mentioned below, HO• can also be formed:

$$H_2O_2 + h\nu \rightarrow 2HO \bullet \tag{9}$$

$$H_2O_2 + O_2^{-\bullet} \rightarrow HO\bullet + O_2 + OH^- \tag{10}$$

$$H_2O_2 + TiO_2(e_{cb}^-) \rightarrow HO\bullet + OH^- + TiO_2 \tag{11}$$

Organic compounds adsorbed on the surface of the photocatalyst and present in the bulk can be degraded by ROSs (HO•, $O_2^{-\bullet}$, $HO_2^{\bullet}$, H_2O_2) including h_{vb}^+ and e_{cb}^-. Although the degradation commences with a partial degradation, the term photocatalytic degradation usually refers to the complete photo mineralisation or oxidation, essentially to the harmless end products of water and carbon dioxide [116].

2.3.2. Titanium dioxide

The most common photocatalysts are metal oxides of transition metals, phosphates, carbides, nitrides. The advantage of metal oxides is their amphotericity, their surface can be positively or negatively charged, i.e., protonated, or deprotonated, at different pH values, allowing them to adsorb a wide range of pollutants. The width of the forbidden zone of most metal oxides in photocatalysis (CeO_2, SnO_2, TiO_2, ZnO) is generally greater than 3 eV, they are active under UV radiation [106, 107]. However, if the width of the forbidden zone is less than 2.7 V, the oxidation of water to HO• is thermodynamically impossible, considering the reduction potential of HO•. Complex oxides, such as $BiVO_4$ have a larger band gap, often greater than 3.5 eV, which limits their application in photocatalytic wastewater treatment [110]. Photocatalyst TiO_2 remains the benchmark among other semiconductors with its ideal properties such as high UV absorption and resistance to photocorrosion in aqueous environments, environmental friendliness, low energy gap, and ability to be deposited individually without additional chemicals [105, 110]. Compared to other semiconductor photocatalysts, TiO_2 has so far proven to be the most promising material for both fundamental research and practical applications because it is highly photoreactive, cheap, nontoxic, chemically, and biologically inert, and photostable [108, 109]. The structure of the photocatalyst also plays a critical role in the efficiency of photocatalysis [122]. TiO_2 polymorphs anatase, rutile and brookite are naturally occurring, with band gaps between 3.0 and 3.3 eV. Rutile and brookite are rarely used because of their wider band gap and lower photocatalytic activity [123]. It is known that the photocatalytic activity of TiO_2 increases with an increase in the crystallinity fraction upon short-term heat treatment up to 700 °C, after which the phase transformation from anatase to rutile

occurs. Despite the smaller band gap width compared to anatase, the recombination of photogenerated charges is higher in rutile [124]. The photocatalytic efficiency of TiO_2 photocatalysts is usually limited due to the fast recombination of the electron–hole pairs and recombination is an undesirable process and must be prevented. The commercial TiO_2 powder, such as anatase crystalline, and the combinations of anatase and rutile (Degussa P25, 25:75 or 80:20 anatase/rutile) have been the most extensively used heterogeneous catalysts in the photocatalysis treatment process due to their numerous positive characteristic [109].

In photocatalytic processes, TiO_2 is usually used as a powder or in immobilized form. Suspended TiO_2 has been the most used system because of its simplicity in terms of preparation and application. The suspended TiO_2 system can provide a higher efficiency than the immobilized system, mainly due to a higher ratio of catalyst active site to reaction volume [109]. However, at the end of the treatment process, it is necessary to use a separation process to recover the TiO_2 powder, e.g., filtration or centrifugation. This separation process not only increases the complexity and cost of the overall process, but it is also time-consuming [125]. Furthermore, the suspended TiO_2 powder tends to agglomerate into larger particles at high concentration, which could reduce the catalytic activity [122, 123]. On the other hand, the immobilized TiO_2 system allows the direct discharges of decontaminated water effluent without the recovery of TiO_2 since the catalyst remains confined to the packed-bed [111]. This avoids the need for post-processing, which saves time and money. However, as compared to the suspended catalyst, it is reported that 60 – 70% of reduction in performance has been observed in the aqueous system for immobilized TiO_2 since the latter system offers a lower reaction surface area for the photocatalysis reaction to take place [109]. In addition, the immobilised catalyst is more difficult to synthesise and requires inert support materials such as glass or ceramic fibres, alumina pellets or molecular sieves [125].

2.3.3. Operating and affecting parameters of photocatalysis

The design and configuration of the reactor are critical to the performance of the photocatalytic reaction. The photodegradation of organic pollutants in the reactor involves mass transfer of the corresponding pollutants to the catalyst surface, i.e., adsorption, followed by photodegradation of the substrates and their desorption at a certain point. An ideal photocatalytic reactor should demonstrate a high mass transfer speed, kinetic rate and reaction surface area [128]. Over the years,

most photocatalytic reactors have been tested on a laboratory scale. This is due to the numerous limitations and criteria encountered during the design phase. One of the obstacles is that the extremely low pollutant concentration may result in a slow photodegradation rate, as the pollutants usually present in the water with a trace amount [128]. The reaction time may be prolonged to fully degrade the pollutants and produce harmless products. The main features used to categorise reactor configuration are suspended or immobilized catalysts [129]. Furthermore, the efficiency of photodegradation processes depends on the following parameters: photocatalyst dosage, catalyst morphology, pollutant concentration, irradiation intensity, and pH value as well as the temperature of the system.

Photocatalyst dosage

The amount of photocatalyst during the photocatalytic process is essential for promoting the photodegradation. Increasing the photocatalyst dosage leads to an increase in the total catalyst surface area. A larger surface area indicates that there are more active sites on the semiconductor surface [130]. As a result, more reactive radicals ($HO\bullet$ and $O_2^{-\bullet}$) will be produced to carry out the mineralisation. In short, there is a positive correlation between photocatalyst dosage and degradation rate. However, this relationship is invalid if the photocatalyst dosage is above the optimal amount. The reaction can be slowed down if there is an excess of photocatalyst. This scenario can be explained by the fact that the irradiation can no longer penetrate deep into the solution due to the agglomeration of the photocatalyst [126, 127, 131]. Consequently, the clusters of the photocatalyst hindered and constrained the light from irradiating on a large catalytic area and more irradiations will be scattered off. The complexity of the chemical structures may affect the interaction between the photocatalysts and the degradation efficiency. If the catalyst dosage is insufficient, the degradation rate is reduced. However, too high a catalyst dosage may not be able to further increase the removal efficiency. For example, Elhalil et al. [131] found that the photodegradation efficiency was boosted with the increase of photocatalyst dosage from 0.1 to 0.3 $g \cdot L^{-1}$.

Effect of initial pollutant concentration

The amount of organic pollutant in solution is an important parameter, especially in real wastewater where the concentration always varies. Different initial substrate concentrations require different irradiation times to reach a certain mineralisation stage with constant operating parameters. At a low pollutant concentration, the amount of reactive radicals (HO• and $O_2^{-•}$) is greater than the amount of organic pollutants. Therefore, the low collision rate between the pollutant molecules and radicals results in fewer pollutant molecules being degraded in bulk. Thus, the concentration of the initial substrate should be optimized with the number of active reactive sites, increasing the chance of collision between the organic pollutant and the respective sites [134]. Photodegradation efficiency is always highest when the pollutant concentration is kept low. Babu et al. [135] investigated the effect of initial substrate concentration on sonophotocatalytic degradation in a range between 0.01 mM and 0.04 mM. They reported that the initial pollutant concentration of 0.01 mM showed the highest degradation rate in 90 minutes. The adsorption of the pollutant molecules on the photocatalyst surface suppressed the generation of reactive radicals.

Effect of intensity and wavelength of irradiation

The wavelength and intensity of the UV irradiation source affects the degradation of pollutant in photocatalytic processes [136]. The artificial UV irradiation is more reproducible than sunlight and can bring higher efficiency in the degradation of pollutant. Ollis et al. [137] stated that: (1) at low irradiation intensities $(0 – 20 \; mW·cm^{-2})$, the rate would increase linearly with increasing irradiation intensity; (2) at intermediate irradiation intensities beyond a certain value (approximately 25 $mW·cm^{-2}$), the rate would depend on the square root of the irradiation intensity; (3) at high irradiation intensities, the rate is independent of the irradiation intensity. There are more photons per unit of time and area; therefore, the chances of photon activation on the catalyst surface increase and the photocatalytic force is stronger. However, as the irradiation intensity increases, the number of activation sites remains the same, so the reaction rate only reaches a certain level even if the irradiation intensity continues to increase.

Neppolian et al. [138] investigate the photocatalytic degradation of Reactive Yellow 17 and Reactive Blue 4 dyes using TiO_2 as photocatalyst and solar/UV irradiation and found that UV

irradiation to be more effective than solar radiation. The difference in the input energy cause difference in the rate of degradation. The energy of UV irradiation is large compared to band gap energy of TiO_2, so problem of electron – hole recombination is avoided with UV irradiation. But in the sunlight spectrum only 5% of the total radiation possesses the optimum energy for the band gap excitation of electrons [139]. Therefore, the percentage of degradation is lower with solar radiation, and in case of both dyes percentage of degradation increase with increasing solar irradiation intensity. At a higher intensity of irradiation, the amplification of degradation was significantly higher, because the formation of electron holes predominates and therefore recombination is negligible. However, at lower irradiation intensity, electron – hole pair separation competes with recombination which in turn decreases the formation of free radicals, thereby causing less effect on the percentage degradation of the dyes [140].

Effect of initial pH

One of the very important and determining factors for the photocatalytic degradation of pollutants is the pH of the reaction solution. The reaction rate in surface photocatalytic degradation has a strong dependence on pH, whereby the surface charge of the photocatalyst and ionization state of the parent pollutant are affected by pH [112]. Different photocatalysts have different point of zero charge (pH_{pzc}) and the state of surface charges depend on this value. The point zero charge is defined as the limiting pH when the net catalyst surface charge is zero [141]. Hydroxyl radicals can be formed by the reaction between hydroxide ions and positive holes in a photocatalytic process with TiO_2 as photocatalyst. Therefore, positive holes are considered the main oxidation species at low pH, while hydroxyl radicals are considered the predominant species at neutral or high pH. It was stated that in alkaline solution, HO• are easier to be generated by oxidizing more hydroxide ions available on TiO_2 surface, thus the efficiency of the process is logically enhanced [142]. It should be noted, that in alkaline solution there is a Coulombic repulsion between the negatively charged surface of the photocatalyst and the hydroxide anions. This fact could prevent the formation of HO• leading to a decline of photocatalytic reaction.

The surface of TiO_2 can be protonated or deprotonated under acidic or alkaline condition, respectively, according to the following reactions:

$$pH < pH_{pzc}: TiOH + H^+ \rightarrow TiOH_2^+ \tag{12}$$

$$pH > pH_{pzc}: TiOH + OH^- \rightarrow TiO^- + H_2O \tag{13}$$
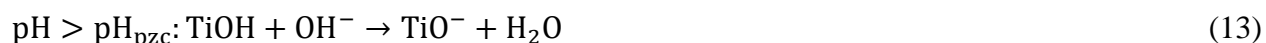
The pH_{pzc} of TiO_2 is reported in the range of 6.5 – 6.7 by various researchers [143]. The TiO_2 surface will be charged negatively when $pH > pH_{pzc}$, positively when $pH < pH_{pzc}$ and neutrally when $pH \approx pH_{pzc}$. Also, the structural properties of the pollutant will change with pH. The effect of pH on the photocatalytic degradation can be explained as electrostatic interaction between the catalyst surface and the target pollutant.

Effect of the temperature

Another factor that plays an important role in the photocatalytic degradation of organic compounds is temperature. The influence of temperature is not profound if the observed reaction rate shows only small variations; however, if the temperature is too high or too low, this can change the course of the degradation reaction. Dissolved oxygen is one of the key elements of photocatalysis, as it helps to scavenge CB electrons and leads to the formation of hydroxyl radicals. The percentage of dissolved oxygen depends on the temperature and can cause changes in the rate of degradation of the reaction in the samples, as the oxygen concentration decreases with increasing temperature. The decrease in temperature favours adsorption of the pollutant which is a spontaneous exothermic phenomenon [144]. In addition, the lowering in temperature also favours the adsorption of the final reaction product, whose desorption tends to inhibit the reaction. On the contrary, when temperature tends to the boiling point of water, the exothermic adsorption of reactant becomes disfavoured and tends to limit the reaction [145]. The influence of temperature on the photocatalytic reaction was also investigated by Soares et al. [146]. They found an optimal range of operating temperatures in the range of 40 °C – 50 °C for the photocatalytic degradation of rhodamine B. At low temperatures, desorption of the products formed limits the reaction, as it is slower than surface degradation and adsorption of the reactants. On the other hand, at a higher temperature, the limiting stage becomes the adsorption of the dye on TiO_2. Zhou and Ray [147] postulated that the reduction of the adsorptive capacity associated with the organics and dissolved oxygen at higher temperatures decreases the rate constant.

2.4. Modelling approaches

Among various AOPs, photocatalytic process shown to be promising option for tertiary treatment, aiming at removal of CECs which may often remain in water effluents after secondary (i.e., biological) treatment due to inadequate effectiveness owing to CECs recalcitrant properties. Applicability of wastewater treatment depends on numerous factors, including those: related to the nature and concentration of pollutants present in wastestreams, strongly determining treatment adequacy, then specific parameters of processes applied, influencing the overall treatment effectiveness; and of course, the economic aspects, often considered as major decision-making stepping stone although chosen solution does not satisfy set limits [8]. AOPs are multi-parameter systems as well as water treatment processes in general. Hence, the optimization and prediction of system behaviour to maximize its effectiveness, but also to control unwanted implications, which may rise during the application, are of great importance for large-scale applications. The optimization using empirical approach based on a single-factor-at-a-time experimental prediction in laboratory environment and subsequent scale-up is not appropriate because such an approach does not consider the impact of interaction factors, can be complicated and costly, and may often yield misleading information. To reduce laboratory studies and save time and money, the application of modelling tools in combination with experimental results approach, such as artificial neural networking (ANN), response surface modelling (RSM) and mathematical – mechanistic modelling (MM), is highly desired. The first two "black-box" modelling approaches, ANN and RSM, are excellent choices for "closed" systems, enabling simple and fast detection of influential process parameters providing straightforward correlation with process effectiveness in the term of chosen responses [121, 122, 123]. Besides, it may provide system optimization within the tested range of process parameters [151]. However, such modelling schemes do not enable the extrapolation outside of studied range of process parameters, and do not provide any information on chemistry or physical-hydraulic processes occurring within the system [121, 126]. Various licensed software packages are available with "ready-to-use" instructions for users among chemical and environmental engineering community, requiring moderate knowledge in statistics and planning. On the other hand, the MM approach, usually presented as a set of differential equations, along with the specific predetermined process parameters input, that are numerically solved, provides insight in the chemical and/or physical processes occurring within the studied system, and may ensure

extrapolation outside of tested boundaries for multi-responses [153]. However, such an approach requires more advanced knowledge of mathematics and programming through the use of commercially available software platforms for computing. Besides, the knowledge on detail system chemistry and physical process may yield with rather complicated and excessive models, particularly in the case when mixtures of CECs are present in wastestreams to be processed. The combination of both approaches can be helpful; however, it still requires adaption of models for each CECs or any other chemical compounds. The viable solution for solving such an issue, which would lead to the significantly increase of the robustness of models in both cases is the inclusion of quantitative-structure activity/property relationship (QSA/PR) modelling approach in modelling and simulation process for specific pollutant-structure dependent process variables/parameters. Namely, QSA/PR brings into relationship various properties (including process and kinetic parameters) or activities of organic pollutants (e.g. toxicity, biodegradability, physical and chemical properties including reaction rates, adsorption rate) and their structural features [128, 129, 130, 131].

2.4.1. Statistical design of experiments

One of the major challenges in utilization of different physicochemical processes for wastewater treatments is the proper selection of experimental conditions which can be achieved under a broader concept called design of experiments (DoE). In experimental planning, the independent variable is changed to assess the effects of the change on the dependent variable. Usually, without DoE, the experiments are carried out in such a way that one factor is being analysed, while the others are kept constant. This procedure is called single-factor-at-a-time. Furthermore, the objective of present methodology is to plan and conduct experiments to extract the maximum amount of information from the collected data in the smallest number of experiments. DoE is a systematic procedure to determine the relationships between factors affecting a process and the outputs [158]. The main advantage of DoE in environmental processes is the reduction in the number of experiments that need to be performed, resulting in less material consumption and a significant reduction in laboratory work. Furthermore, DoE provides the development of mathematical models that permit assessment of the relevance and statistical significance of the factor-effects being studied as well as an evaluation of the interaction-effects between the factors [159]. A well-designed experiment has a clearly defined goal, the possibility to estimate errors, sufficient

precision, and the possibility of adjusting for various influences by mathematical approaches such as Randomized Blocks, Latin Squares, Full Factorial Plan, Fractional Factorial Plan, and others [160]. The simplest experimental design is a Full factorial design (FFD), whose experimental matrix is carried out by exponentiating the number of factors with levels, testing each factor at each given level. Thus, with two factors and three levels (k), there are a total of 8 trials ($N = 2^k$). The most common levels are expressed in coded form, i.e., as -1, 0, 1, which corresponds to the minimum, mean and maximum value of the respective factor [161]. In the case of a larger number of factors and FFD levels, the experimental design becomes too extensive. Graphically, we can denote the 2^3 design by a cube shown in Figure 3:
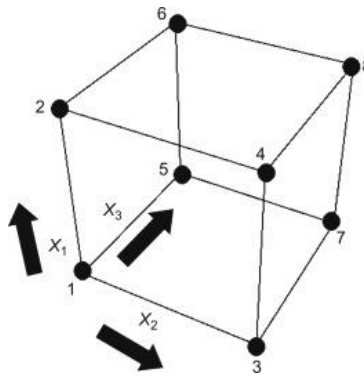
Figure 3 Representation of a 2^3 FFD as a cube.

The arrows show the direction of increase of the factors, and the numbers 1 through 8 at the corners of the design box represent the standard order of runs. Among many multivariate DoE-based methods, response surface methodology (RSM) has drawn extensive attention specially in design, modelling, and optimization of environmental and chemical experiments. The interdependence of the individual parameters is usually described by a quadratic equation. Therefore, the variance analysis method (ANOVA) is used to analyse the total variance of the dependent variable with the aim of examining the differences in arithmetic mean values between the individual groups within the data set. The total variance of the dependent variable is the sum of the variances of the changes in the individual factors and the rest of the variance is considered as random error. The analysis of variance avoids the usual measurement in triplicates. Therefore, the significance of individual parameters in the mathematical model of the investigated process is determined using the F-ratio

and the p-values. If the F-ratio is greater than 1 and the p-value is less than 0.05, a single parameter in the equation of the process model is considered influential [134, 132].

2.4.2. Response surface methodology

Response surface methodology (RSM) is a collection of statistical and mathematical techniques useful for developing, improving, and optimizing processes [148]. It has very important applications in the improvement of existing product designs as well as in the design, development, and formulation of new products. The RSM methodology is typically used in industry, usually in situations where several input variables potentially affect a performance measurement or quality characteristic of the product or process. Therefore, performance measure or quality characteristic is called the response. In most real-world applications of RSM, will involve more than one response. The response variables are usually referred to as dependent variables and the input variables as independent variables, so they are subject to the control of the engineer or scientist, at least for the purposes of a test or experiment. RSM is based on fitting the mathematical models (linear, square polynomial functions and others) to the experimental results from the designed set of experiments and verification of the model obtained by the statistical techniques [163]. The main objective of RSM is to obtain the optimum operational conditions for the system or to acquire a region that satisfies the operating specification [164]. The RSM methodology for optimising physicochemical processes can be divided into six successive steps: (i) selection of independent variables and dependent variables (responses), (ii) selection of strategy for experimental design, (iii) conducting experiments and obtaining the results, (iv) fitting the obtained mathematical model to experimental data, (v) obtaining response graphs and analysis of variance, and (vi) determination of optimal conditions. Generally, the relationship between the dependent variable or response (y) and the set of independent variables (x_1, x_2,..., x_n) in RSM is presented by eq. 14:

$$y = f(x_1, x_2, \dots, x_n) + \varepsilon \tag{14}$$

where ε is a statistical error in a response y. In the case of a 3D system with two independent variables x_1 and x_2, the surface obtained from f(x_1, x_2) is called the response surface and can be represented graphically as a three-dimensional diagram or as a contour plot. Several types of models are usually used in the response surface method such as linear, i.e., the first-order model or

quadratic, i.e., the second-order model and cubic model. The advantage of the second-order model compared to the first-order model is that it can significantly improve the optimization process due to the mutual interaction of the variables and the curvature of the surface it describes. To fit the second-order model, a full factorial design can be used that includes all main effects and interactions by eq. 15 [148]:

$$y = \beta_0 + \sum_{i=1}^{k} \beta_i x_i + \sum_{i=1}^{k} \sum_{j=1}^{k} \beta_{ij} x_i x_j + \sum_{i=1}^{k} \beta_{ii} x_i^2 + \varepsilon' \tag{15}$$

where the parameters of the eq. are:

- y – the chosen response (dependent variable),
- k – the number of patterns,
- x_i – coded independent variables
- i and j – index numbers for patterns,
- β_0 – the offset term,
- β_i – the first-order effect,
- β_{ii} – the second-order effect,
- β_{ij} – the interaction effect,
- ε' – the random error

allowing for the discrepancy or uncertainty between predicted and observed values.

The second – order model is widely used in response surface methodology for several reasons:

1) The second-order model is very flexible. It will often work well as an approximation to the true response surface because it can take on a wide variety of functional forms.
2) With the second-order model is very easy to estimate the parameters (β's).
3) There is considerable practical experience indicating that second-order models work well in solving real response surface problems.

The response surface method is widely used. It is mostly used for process optimization, i.e., to determine the values of the factors for which the best or required response value is achieved. It is also applied to determine the values of the process factors that satisfy certain process operating conditions with respect to the target range of values [165].

2.4.3. Mathematical – mechanistic modelling

The mathematical – mechanistic model can be defined as a mathematical description of the elements that make up the system, their mutual interactions, and their interactions with the environment. Such models are used in engineering systems to enable the extrapolation of systems behaviour based on the mathematically described features of the elements and the mechanisms of their interaction [166].

As previously explained, photocatalytic processes are a multi-parameter system. Therefore, the approach of formulating a mathematical – mechanistically based predictive model of photocatalysis is important for two reasons: it verifies what we know and shows what we do not yet understand. The development of the model is intended to demonstrate that it may be possible to kinetically model the complex series of reactions that occur during photocatalytic degradation and to gain valuable insight into the complicated interactions of the photocatalytic process and to examine processes outside the examined boundaries of the system. The modelling of photocatalysis takes into account next aspects: configuration of reactor, radiation emission, radiation scattering, mixing, and the most important, reaction kinetics. Numerous studies have been conducted in the literature on the modelling of photocatalytic reactors and the influence of the photoreactor configuration and irradiation intensity on the efficiency of the process [158, 159, 160].

The mathematical – mechanistic models are usually built from ordinary differential equations (OED) describing the balance of the compounds in the system and are solved by numerical methods. According to the literature, chemism of degradation of organic compounds by advanced oxidation processes, mathematical models have been developed for the kinetics of degradation of pollutants by UV-C/H_2O_2 and UV-C/$S_2O_8^{2-}$ processes [138, 158, 159]. When defining the mathematical model, idealized states were assumed. During the process, the density of the reaction mixture does not change, which means that the volume of the mixture is constant and independent of time. In the ideal batch reactor model, a constant temperature is assumed, while the composition of the reaction mixture depends on time. The composition of the reaction mixture is the same at every point, so the mass balance equations can be written for the reactor as a whole [170].

It is well known that the reaction rate of a chemical reaction depends on the number of collisions, but also on the success of the particle collisions. Thus, there are many factors that influence the reaction rate of a chemical reaction, for example, the type of reactant, the initial concentration of

the reactant, the temperature, the contact area, the influence of the catalyst, the influence of radiation and, of course, the reaction mechanism of the process.

First-order chemical reactions are those in which a reactant decomposes or is transformed to form products. The rate of such a reaction is generally defined as the change in initial concentration of the substance over time. The reactions of the transition given by eq. 16 belong to the first order reactions:

$$X \xrightarrow{k} Y \tag{16}$$
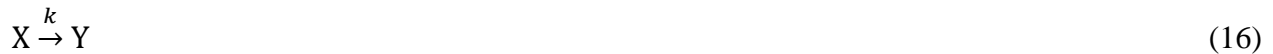
in which substance X transforms into substance Y over time. During the reaction, the concentration of substance X decreases, while at the same time the concentration of substance Y increases, which can be described by the following mathematical equations:

$$\frac{\mathrm{d}c(X)}{\mathrm{d}t} = -k \cdot c(X) \tag{17}$$

$$\frac{\mathrm{d}c(Y)}{\mathrm{d}t} = k \cdot c(Y) \tag{18}$$

In eq. 17, the reaction rate constant has a negative sign (-k) because the concentration of substance X decreases with time. Conversely, the formation of substance Y and its concentration increases. It is important to note that in these reactions the amount of substances in the closed system is constant.

Dissociation is a reaction in which a molecule decomposes into smaller components, either smaller molecules or ions. Such a reaction can be represented by a hypothetical chemical reaction:

$$X \xrightarrow{k} nY + Z \tag{19}$$

In this case, rate of formation of substances Y and Z is proportional to the rate of disappearance of substance X, which can be shown by the following equation:

$$-n\frac{\mathrm{d}c(X)}{\mathrm{d}t} = \frac{\mathrm{d}c(Y)}{\mathrm{d}t} = n\frac{\mathrm{d}c(Z)}{\mathrm{d}t} \tag{20}$$

In contrast to the previous example, the balance of the amounts of substances in the system should be taken into account.

Second-order chemical reactions are bimolecular reactions whose rate is proportional to the product of the concentration of the reactants, or the concentration of the reactant squared. They can be expresses as follows [172]:

$$X + Y \xrightarrow{k} Z \tag{21}$$

The reaction rate (k) provides information on how much reactant is spent in a unit of time, i.e., how much product is formed in a unit of time, and can be described for a second-order reaction by the following expressions:

$$\frac{dc(X)}{dt} = -k \cdot c(X) \cdot c(Y) \tag{22}$$

$$\frac{dc(Y)}{dt} = -k \cdot c(X) \cdot c(Y) \tag{23}$$

$$\frac{dc(Z)}{dt} = k \cdot c(X) \cdot c(Y) \tag{24}$$

Chemical reaction described by eq. 21, shows that the concentration of reactants X and Y decreases, and the concentration of product Z increases (eq. 24). The sums of the concentrations of substances A and C, or B and C, are constant at each point in the reaction, as in the previous examples.

The combination of the reaction and its reversible reactions represented by the expressions (25) are more complex compared to the examples shown before.

$$X + Y \mathrel{\mathop{\rightleftarrows}^{k_1}_{k_2}} Z \tag{25}$$

Based on eq. 25 differential equations are derived, which are represented in the following expressions:

$$\frac{dc(Z)}{dt} = k_1 \cdot c(X) \cdot c(Y) - k_2 \cdot c(Z) \tag{26}$$

$$\frac{dc(X)}{dt} = -k_1 \cdot c(X) \cdot c(Y) + k_2 \cdot c(Z) \tag{27}$$

$$\frac{dc(Y)}{dt} = -k_1 \cdot c(X) \cdot c(Y) + k_2 \cdot c(Z) \tag{28}$$

Thus, an increase or decrease in the concentration of each component indicates the direction of the reaction. Also in this case, the sums of the concentrations of components X and Z or Y and Z are constant at any time of the reaction.

The complex nature of AOPs, especially photocatalytic processes in which the generated radical species are responsible for the degradation of organic substances, requires often numerous and complex differential equations. All possible chemical reactions occurring in the system during the process must be taken into account, as well as the influence of the reactor system configuration and the radiation source, so any reaction that affects the concentration of the reactants also affects the overall kinetics. Therefore, the chemical reactions of the photocatalytic process can be described by a set of differential equations, which are set up considering the possible kinetic reactions described earlier, including the specifics of the reactor and the radiation source.

2.4.4. Quantitative structure-activity/property relationship modelling

The physical, chemical, and biological properties of pollutants can be related to their molecular structure. However, in order to predict the properties of a substance, the relationship between the molecular structure and the observed property must be determined. Ideally, the relationship is expressed quantitatively, and to obtain a statistically significant relationship, a relatively large number of parameters describing the desired property is required due to the complexity of the relationship [131, 140]. Therefore, the modelling strategy that shows relationships between various properties (physical, chemical, and biological) or activities of organic pollutants and their structural features is called the quantitative structure activity/property relationship approach, QSA/PR. This methodology was established by Corwin Hansch more than 50 years ago and was initially considered to be a branch of physical organic chemistry [174]. Since then, QSA/PR models have been developed and have evolved from simple regression series to methods of analysing very large data sets consisting of numerous molecules with different structures, using various machine learning techniques. Therefore, the models can interpolate the unknown properties of compounds of a given group using either measured or calculated molecular parameters of the whole group and appropriate mathematical and statistical methods. The presented methodology is used in many areas of science [175]. For example, in order to minimize experimental testing work in the development of pharmaceuticals, the pharmaceutical industry applies QSAR models that can

predict pharmaceutical metabolic activity and toxicity a priori using molecular descriptors [176]. However, there are also numerous application studies focused on using the QSA/PR modelling approach to describe the influence of structural features of wastewater treatments such as adsorption, photooxidative or photocatalytic processes [130, 144, 145, 146]. Descriptors are the predictor variables, also called quantum chemical parameters, features, attributes, independent variables, or structural/compositional components, that describe the properties of molecules.

The use of QSA/PR models are based on two main principles:

(1) under similar environmental conditions, compounds with similar structures show comparable behaviour,

(2) variations in structure and composition among compounds are responsible for their behavioural differences [180].

In general, the development of QSA/PR models begins with the selection of the molecular descriptors and the response variable. Molecular descriptors can be collected from experiments, literature or usually they are computed. Therefore, response variables are the most determined experimentally or collected from the other studies. Collected data must be divided in two sets for running and validating the model. Then, a statistical tool is used to determine the appropriate model for the collected data, and it is fitted to the curve using regression analysis, generalized linear model, machine learning, etc. After validation is complete, the model can be used to predict the behaviour of new molecules that belong to the group used in the model. Next step is a validation of data, and the model can be used to predict the behaviour of new molecules that belong to the group used in the model. The typical simplified flow diagram for a QSA/PR model is present in Figure 4:
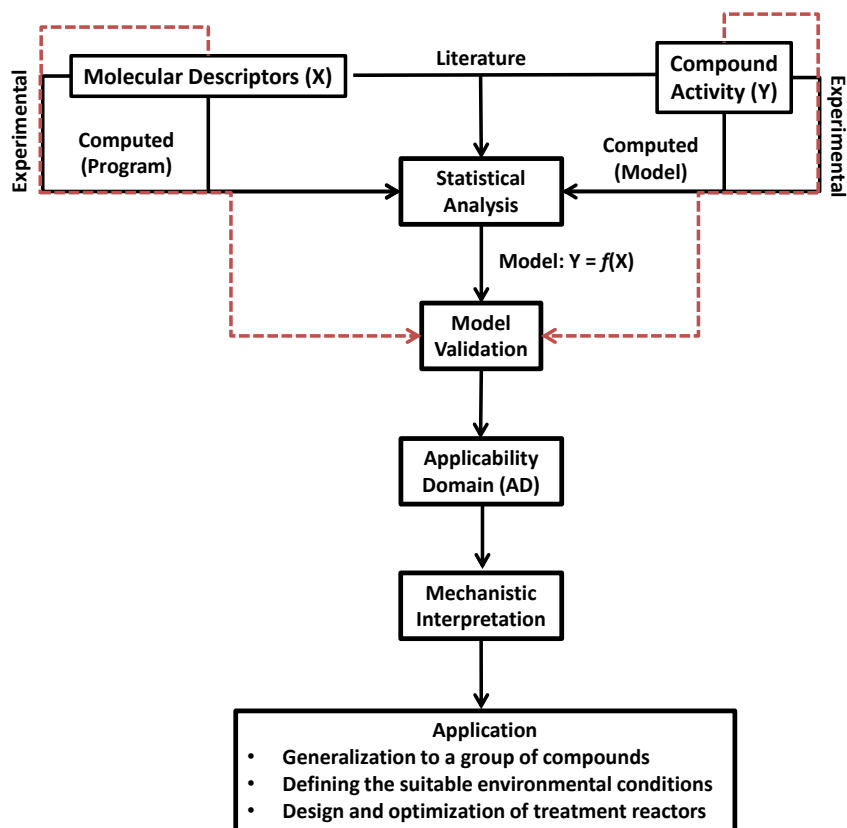
Figure 4 Simplified flow diagram for the development of a QSA/PR model [181].

The Organization for Economic Cooperation and Development (OECD) has proposed principles for the validation of QSA/PRs, and they might be of more importance for evaluating and characterizing a QSA/PR and hence to determine whether an individual prediction is valid [175]. Hence, developed QSA/PR model must include the next information:

    (i)   a defined endpoint,

    (ii)   an unambiguous algorithm,

    (iii)   a defined domain of applicability,

    (iv)   appropriate measures of goodness-of-fit, robustness and predictive ability,

    (v)   a mechanistic interpretation, if possible.

A final step in the development of QSA/PR models is statistical validation to assess the significance of the model and its ability to predict the studied activities of other (novel) compounds. In the most QSA/PR studies in the literature, the leave-one-out (LOO) cross-validation procedure has been used for this purpose. The output of this procedure is the cross-validated (Q_2) parameter which is

commonly regarded as an ultimate criterion of both robustness and predictive ability of a model [175]. The simplest cross-validation method is LOO, where one compound at a time is removed from the dataset, and the N-1 remaining compounds are used to predict its value and it is done systematically N times. The resulting N predictions are then compared with measured values for their respective compounds to enable computation of Q_2 [182]. A more robust and reliable method is the leave-many-out cross-validation, LMO. In the leave-20%-out cross-validation, for example 80% of the compounds are randomly selected to create a model that is used to predict the remaining compounds, and this process must be repeated several times to obtain reliable statistical results. Results obtained in this way are much better indicators for the robustness and the predictive ability of a QSA/PR model than the usually used LOO procedure [183]. Internal validation can also be performed using the method of changing the data of the input variable, the Y-scramble. The Y-mixture is performed to ensure the robustness of the developed QSA/PR model. In this test, validation is performed by replacing the Y values while leaving the X values unchanged. By finding that a model for a system with mixed values does not account for the correlation of the data (the model is not applicable) confirms that the existing correlation in the unmixed data set is not random. Gramatica [184], suggested that for the most stringent evaluation of model applicability for prediction of new chemicals, external validation verified by Q^2_{EXT} or R^2_{EXT} (R^2 is the linear regression coefficient when calculated removals are correlated with experimental data) is recommended as the last step after model development. The satisfactory model is the one with the highest values for the prediction parameters and the most balanced results between the cross-validation parameters for the training chemicals and the strength predictions (Q^2_{EXT} or R^2_{EXT}), which are verified later the external prediction chemicals.

2.4.4.1. Molecular descriptors

Molecular modelling involves the application of various theoretical approaches and computational techniques with the aim of describing and understanding the behaviour of molecules. The process of molecular modelling starts with a design of the structures of the analysed molecules in one of the molecular modelling software packages. Since such a virtual representation does not provide a

realistic insight into the actual structure of the molecule, it is optimised by energy minimisation, i.e. by solving the N-electron Schrödinger equation [175].

Two data sets are required to develop a QSA/PR model: the first contains the observed activity values, the second the descriptor values. Descriptors can be theoretical or empirical. They are derived from the representation of the molecular structure, and to calculate this molecular structure, the molecule must be correctly represented. The information obtained depends on the way the structure is represented, so specially designed software packages are used for molecular modelling: ChemOffice, Hyperchem, Avogadro, Gaussian, or others [185]. It is desirable to make the virtual representation of the structure as close as possible to the real one, and therefore one of the methods of molecular modelling is to search for the conformer with the lowest energy, i.e., to optimise the structure of the molecule. Therefore, semiempirical quantum mechanical descriptors are calculated from the optimised structures, i.e., theoretical structural parameters of the substance such as ionisation potential, energy of the highest occupied molecular orbital (HOMO) and energy of the lowest unoccupied molecular orbital (LUMO), dipole moment and enthalpy. More detailed information on structural features is derived from optimised structures by calculating molecular descriptors, including constitutional, topological, empirical, and geometric descriptors, charge-related descriptors and many others related to 2D and 3D representations of molecular structures, as well as functional groups and physical properties [186]. Each descriptor takes into account a small part of the chemical information contained in the actual molecule. As recent research provides new insights into chemical and biological systems, the number of descriptors is constantly increasing, so that there are software packages that can be used to calculate more than 6000 descriptors (Dragon 6, Talete) [187].

Molecular descriptors obtained from the chemical formula of a substance, i.e., the simplest representation of a molecule, are called 0D descriptors. If the complexity of the representation of the molecule is increased further, 1D, 2D, 3D and 4D descriptors are obtained. 1D molecular descriptors are obtained from the list of structural fragments of the molecule and their calculation does not require complete knowledge of the molecular structure. Therefore, 0D and 1D descriptors are easy to interpret and their calculation does not require optimising the geometry of the molecular structure.

2D descriptors take into account the chemical bonds between the atoms of a molecule and are obtained from a topological representation called a molecular graph. A molecular graph describes the bonds between atoms without taking metric parameters into account.

3D molecular descriptors are calculated based on a three-dimensional representation of the molecule, taking into account the nature of the atoms and the bonds between them, as well as their spatial arrangement. A molecule is defined by the type of atoms it is made of and their (x, y, z) coordinates, and such a representation of a molecule is called a geometric representation.

4D descriptors are obtained from the stereo electronic representation of the molecule resulting from the distribution of electrons and the interactions of the molecule that characterise the space around the molecule (field of molecular interactions) [188].

2.4.5. Density functional theory

Density functional theory (DFT) is a computational method that derives properties of the molecule based on a determination of the electron density of the molecule [175]. Unlike the wavefunction, which is not a physical reality but a mathematical construct, electron density is a physical characteristic of all molecules.

Thomas and Fermi provided the first concept of DFT, which can be described by the following integral:

$$n(r) = N \int dr_2 \ldots \int dr_n \Psi(r, r_{2,} \ldots r_n) \times \Psi(r, r_{2,} \ldots r_n) \tag{29}$$

where $n(r)$ describe electron density. The theorem for DFT was established by Hohenberg and Kohn and later adapted by Levy [175]. It is based on two conclusions that are now theorems of quantum mechanics:

1) The ground state function is a unique function of the particle density, i.e., a functional which means that the wave function can be calculated from the particle density and all other physical quantities from the wave function.
2) The ground state energy is a function of the particle density and has a minimum value for the true particle density [189].

In DFT, electron density is represented as a functional, i.e., as a function of space and time. Unlike the wavefunction, which becomes significantly more complicated as the number of electrons increases, the determination of the electron density is independent of the number of electrons. Thus, unlike the many-body electron wavefunction which is a function of $3N$ variables, the electron density is only a function of the variables x, y, and z. According to the Kohn-Sham theorem, the total ground state energy of the many-electron system is a functional of the electron density. Thus, if the electron density functional is known, the total energy of the system is known as well.

Hybrid functionals are a class of approximations to the exchange-correlation energy functional in DFT that incorporate a portion of exact exchange from Hartree-Fock theory with the rest of the exchange-correlation energy from other sources (ab initio or empirical). Among the ever-increasing number of DFT methods, the hybrid functional B3LYP (Becke 3-term correlation functional; Lee, Yang, and Parr exchange functional) method, initially developed to study vibrational absorption and circular dichroism, has proven to be a good compromise between computational cost, coverage, and accuracy of results [157]. It has become the most used method in computational chemistry practise and is often the method of choice for reaction calculations or molecular optimisation.

2.4.6. Multiple linear regression

Linear regression is a mathematical method for quantifying the relationship between a dependent variable and one or more independent variables. Linear regression between a dependent variable and more than one independent variable is multiple linear regression (MLR). Multiple linear regression as one of the semi-empirical methods is a commonly used method in QSA/PR modelling due to its simplicity, reproducibility and easy of interpretation. The MLR model assumes that the dependent variable is related to the independent variables according to the following expression:

$$y_i = \beta_0 + \beta_1 x_{i,1} + \beta_2 x_{i,2} + \ldots + \beta_k x_{i,k} + \varepsilon_i \qquad (30)$$

where y_i is the response or dependent variable, $x_{i,1} - x_{i,k}$ are descriptors or independent variables with appropriate β regression coefficients (parameters of the model) and ε_i is residuals. Every regression coefficient should be significant at the 5% level ($p < 0.05$), which is verified by a t-test

[190]. The validity of the MLR model can be determined by two statistical variables: the coefficient of determination, R^2 and the adjusted coefficient of determination, R_{adj}^2.

The coefficient of determination can be defined with the following expression:

$$R^2 = 1 - \frac{\Sigma\,(Y_{obs} - Y_{calc})^2}{\Sigma\,(Y_{obs} - \overline{Y_{obs}})^2} \tag{31}$$

In the eq. 31 Y_{obs} represents the observed values and Y_{calc} is the expected values (calculated by the model), Y_{obs} is the average of the observed values. Ideally, the sum of the squared residuals should be 0 and the value of R^2 should be 1. If the value of R^2 differs from 1, the validity of the model decreases. The root of the R^2 value represents the multiple correlation coefficient (R).

Furthermore, in the case of adjusted coefficient of determination, if we increase the number of descriptors in the model for a fixed number of observations, the value of the coefficient of determination increases, but the degrees of freedom and statistical reliability decrease. It follows that a high coefficient of determination is not necessarily an indication of a good statistical model. The corrected coefficient of determination is calculated as follows:

$$R_{adj}^2 = \frac{(N-1)R^2 - p}{N - 1 - p} \tag{32}$$

where p is the number of predictor variables in the model [190].

2.4.7. Genetic algorithm

Genetic algorithms imitate biological evolution in the process of optimizing complex problems, and their most important feature is that they use a population of potential solutions. The following can be established for the genetic algorithm:

(i) there is a population of individuals,

(ii) some individuals are better (better adapted to the environment),

(iii) better individuals have a higher probability of survival and reproduction,

(iv) the characteristics of individuals are written in chromosomes using the genetic code,

(v) children inherit the properties of parents and

(vi) mutation of the individual may occur.

In the genetic algorithm, the chromosome is an abstract representation of the solution and consists of a set of characters (genes). The initial population is usually formed by random sampling from space. The objective function, i.e., the function whose maximum or minimum is sought, is used to evaluate the validity of the individuals (i.e. the chromosomes) in the population. Based on the value of the objective function, the better individuals (chromosomes) are selected to participate in the creation of a new generation. The exchange of genes during reproduction is called crossbreeding. Crossbreeding creates offspring that are a combination of their parents, and a small part of the chromosome may be changed by mutation. The process of selecting the most capable individuals within each generation is called selection. This determines the individuals to which the genetic operators crossover and mutation will be applied, resulting in their offspring. The resulting offspring form a new population, completing a genetic cycle. The process of evaluating individuals, selection, crossing, and mutation is repeated on the newly created population, i.e., a new genetic cycle is performed. The cycles of the genetic algorithm are repeated until a predefined stop criterion is reached. The execution of the genetic algorithm can be improved by applying elitism, where the parents (the best individuals of the previous genetic cycle) are included in the new population in addition to the offspring, thus preventing the loss of quality solutions already found [191].

3. EXPERIMENTAL PART

3.1. Chemicals

The list of chemicals used for research are given in Table 1 and Table 2.

Table 1 List of organic compounds used for the research:

#	Compound	Abbreviation	CAS	Molecular formula	Manufacturer	Purity
1	Amoxicillin	AMX	26787-78-0	$C_{16}H_{19}N_3O_5S$	Acros Chemicals	96%
2	Ciprofloxacin	CIP	85721-33-1	$C_{17}H_{18}FN_3O_3$	Acros Chemicals	$\geq 98\%$
3	Diclofenac	DCF	15307-79-6	$C_{14}H_{10}Cl_2NNaO_2$	Sigma Aldrich	p.a.
4	Donepezil HCl	DPH	120011-70-3	$C_{24}H_{30}ClNO_3$	Pliva	98%
5	Desloratadine	DSL	100643-71-8	$C_{19}H_{19}ClN_2$	Pliva	98%
6	Desvenlafaxine	DVF	93413-62-8	$C_{16}H_{25}NO_2$	Pliva	98%
7	17α-Ethynylestradiol	EE2	57-63-6	$C_{20}H_{24}O_2$	Sigma Aldrich	$\geq 98\%$
8	Etodolac	ETD	41340-25-4	$C_{17}H_{21}NO_3$	Pliva	98%
9	Hydrochlorothiazide	HCTZ	58-93-5	$C_7H_8ClN_3O_4S_2$	Pliva	98%
10	Ibuprofen	IBP	15687-27-1	$C_{13}H_{18}O_2$	Sigma Aldrich	$> 99\%$
11	Omeprazole HCl	OMP	73590-58-6	$C_{17}H_{20}ClN_3O_3S$	Sigma Aldrich	$\geq 99\%$
12	Oxytetracycline	OXY	79-57-2	$C_{22}H_{24}N_2O_9$	Sigma Aldrich	$> 95\%$
13	Tobramycin	TB	32986-56-4	$C_{18}H_{37}N_5O_9$	Pliva	98%
14	Vilazidone HCl	VZD	163521-08-2	$C_{26}H_{27}N_5O_2$	Pliva	98%
15	Alachlor	ALC	15972-60-8	$C_{14}H_{20}ClNO_2$	Sigma Aldrich	99.8%
16	Atrazine	AZN	1912-24-9	$C_8H_{14}ClN_5$	Sigma Aldrich	99.1%
17	Diuron	DIU	330-54-1	$C_9H_{10}Cl_2N_2O$	Sigma Aldrich	99.6%
18	Simazine	SZM	122-34-9	$C_7H_{12}ClN_5$	Sigma Aldrich	98.0%
19	Bisphenol A	BPA	80-05-7	$C_{15}H_{16}O_2$	Sigma Aldrich	$\geq 99\%$
20	o-Aminobenzoic acid	o-aminoBenzAc	118-92-3	$C_7H_7NO_2$	Sigma Aldrich	$\geq 97\%$
21	Benzoic acid	BenzAc	65-85-0	C_6H_5COOH	Sigma Aldrich	$\geq 99.5\%$
22	Salycilic acid	SalAc	69-72-7	$C_7H_6O_3$	Sigma Aldrich	99.5%
23	Sulfanilic acid	SA	121-57-3	$C_6H_7NO_3S$	Sigma Aldrich	$\geq 99.5\%$
24	2,4-Dichlorophenol	DCP	120-83-2	$C_6H_4Cl_2O$	Sigma Aldrich	99%
25	1,4-Dimethoxybenzene	1,4-DMB	150-78-7	$C_6H_4(OCH_3)_2$	Sigma Aldrich	99%
26	2,6-Dimethoxyphenol	2,6-DMP	91-10-1	$(CH_3O)_2C_6H_3OH$	Sigma Aldrich	$\geq 98\%$
27	p-Methoxyphenol	p-MP	150-76-5	$CH_3OC_6H_4OH$	Sigma Aldrich	99%
28	p-Nitrophenol	p-NP	100-02-7	$O_2NC_6H_4OH$	Sigma Aldrich	$\geq 99\%$
29	m-Nitrophenol	m-NP	554-84-7	$O_2NC_6H_4OH$	Sigma Aldrich	99%
30	Phenol	Ph	108-95-2	C_6H_5OH	Sigma Aldrich	$\geq 99.5\%$

The list of organic compounds used as water pollutants in the study includes 19 CECs: pharmaceuticals (#1 – #14), pesticides (#15 – #18), plasticizers (#19) and 10 single-benzene ring aromatics (#20 – #30) are listed in Table 1.

Table 2 Chemicals used for research:

Compound	Abbreviation	CAS	Molecular formula	Manufacturer	Purity
Acetonitrile	ACN	75-05-8	CH_3CN	J.T. Baker	HPLC
1,4-Benzoquinone	BQ	106-51-4	$C_6H_4O_2$	Fluke	98%
Coumarin	-	91-64-5	$C_9H_6O_2$	Alfa Aesar	98%
Dimethyl sulfoxide	DMSO	67-68-5	$(CH_3)_2SO$	Sigma Aldrich	99.9%,
Formic acid	FA	64-18-6	$HCOOH$	Sigma Aldrich	HPLC
Methanol	MeOH	67-56-1	CH_3OH	J.T. Baker	HPLC
Oxalic acid	-	144-62-7	HO_2CCO_2H	Sigma Aldrich	p.a.
Sodium hydroxide	-	1310-73-2	$NaOH$	Kemika	p.a.
Sulfuric acid	-	7664-93-9	H_2SO_4	Kemika	96%
Titanium dioxide	TiO_2 P25	13463-67-7	TiO_2	Evonik	$\geq$99.5%

3.2.   Plan and implementation of experiments and computer simulations

The aim of this thesis was to develop and evaluate a simulation model for photocatalytic degradation of ibuprofen by heterogeneous UV-A/TiO$_2$ P25 process. The simulation model is a combination of a mechanistic and structural approach, including mathematical modelling and quantitative modelling of structure-activity/property relationships.

Research plan:

1) to determine the physical properties of nanoparticles of applied photocatalyst and the characteristics of the equipment for performing photocatalysis.
2) to investigate the conversation and mineralisation of ibuprofen by the UV-A/TiO$_2$ P25 process to develop a mathematical – mechanistic model.
3) to verify the simulation model through experimental results.
4) to investigate experimentally the adsorption of organic compounds onto the TiO$_2$ P25 photocatalyst surface and to determine appropriate adsorption coefficients.
5) to correlate chemical structures of organic compounds with their adsorption coefficients using QSA/PR modelling and genetic algorithm, incorporating QSA/PR into a mathematical – mechanistic model.
6) to conduct experimentally the degradation of organic compounds by UV-A/TiO$_2$ P25 process with the purpose of optimizing the process.
7) to determine the reaction rate between HO•/O$_2^{-•}$ and organic compounds in the UV-A/TiO$_2$ P25 process as well as to identify the degradation pathway, incorporating QSA/PR into a mathematical – mechanistic model.

3.2.1. Photocatalytic degradation of ibuprofen

Ibuprofen was selected as a test compound for the development of the mechanistic model for photocatalytic processes, UV-A/TiO$_2$ P25. Experiments were conducted in a borosilicate-glass cylinder batch photoreactor (Figure 5) with initial concentration of model solutions 0.05 mM. The volume of photoreactor was 80 mL, that is equipped with water-jacket cooling. UV-A 365 nm

wavelength source (Pen-ray, UVP, UK) was placed vertically in the middle of the reactor, along with a magnetic stirrer (IKA Werke-COMBIMAG RCT, Germany) rotating at a speed of 500 rpm to provide effective mixing of reaction solution. Input power of the UV-A lamp was $P_L = 4.83$ W and radiation efficiency is $\eta = 0.037$. TiO$_2$ P25 was used as a photocatalyst at three different concentrations: 0.4 g·L^{-1}, 0.8 g·L^{-1}, and 1.2 g·L^{-1}. The duration of the experiments was 50 min, 30 min in the dark and 20 min under UV-A illumination. During the experiments, 500 μL aliquots were periodically taken at -30 (start of irradiation), 0, 2.5, 5, 10, 15, and 20 minutes, filtered with Chromafil XTRA RC (25 mm, 0.45 μm, Macherey Nagel, Germany), and analysed with a HPLC instrument to determine the extent of degradation. In addition to the HPLC analysis, the TOC was analysed according to the standard methods for drinking water and wastewater investigations. Samples were collected over a period of 150 minutes at the following intervals -30 (dark period), 0, 5, 10, 20, 40, 60, 90, 120, 150 min.
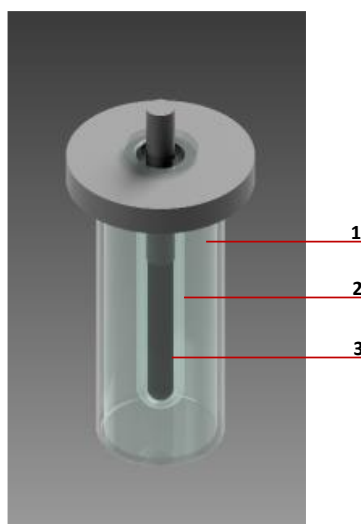
Figure 5 Photocatalytic batch reactor consisting of: (1) borosilicate-glass cylinder batch photoreactor (2) quartz tube (3) UV-A lamp.

3.2.2. Adsorption of organic compounds onto TiO₂ P25

Adsorption experiments were performed in closed 80 mL glass bottles with model solutions of the organic compounds, selected 19 CECs and (pharmaceuticals, pesticides, and plasticizers) and 11 common single-benzene ring aromatics that were listed in Table 1. The concentration of the

prepared solution was 0.05 mM for all compounds. The initial pH and mass concentration (γ) of the adsorbent TiO_2 P25 were varied from 4 to 10 and 0.4 to 1.2 g·L⁻¹, respectively, according to the Full Factorial Design (FFD) used (Table 4). A Handylab pH/LF portable pH-meter (Schott Instruments GmbH, Germany) was used to adjust the pH to the desired value. All experiments were performed at a constant temperature ($T = 25.0$ °C) in a thermostatic shaking water bath (Grant Instruments Ltd, UK) operating at 150 rpm to provide effective mixing of the reaction solution. Aliquots were taken after 24 hours, filtered through Chromafil XTRA RC 0.45 µm filters, and analysed immediately using HPLC system to determine the adsorption coefficients.

3.2.3. Photocatalytic degradation of organic compounds

Experiments of photocatalytic degradation of 30 selected compound listed in Table 1, were conducted in the same photoreactor (Figure 5) at room temperature with initial concentration of model solutions 0.05 mM. Following experimental procedure was applied: model solution of selected organics were placed into reactor and the appropriate amount of catalyst was added. The solution was stirred in a dark for 30 min to establish adsorption equilibrium. Afterwards, the warmed-up UV-A lamp was inserted in quartz cuvette and the treatment started. All experiments were performed at initial pH 7 and with TiO_2 P25 loading of 0.8 g·L⁻¹. From the point of view of practical applications, operation close to pH 7 is desirable to avoid the need for alkalization or acidification steps [169]. For each of selected organics three types of degradation experiments to investigate the mechanism of processes were performed; (i) without scavenging agents, (ii) with DMSO (10 mM) and (iii) with BQ (10 mM) to prevent bulk degradation mediated by HO• and $O_2^{-•}$, respectively. The duration of experiments was 50 min (30 min dark period and 20 min under UV-A illumination). During experiments, 500 µL aliquots were periodically taken at -20, -10 (during dark period), 0 (starting of irradiation), 2.5, 5, 10, 15, and 20 min, filtered using Chromafil XTRA RC (25 mm, 0.45 µm, Macherey Nagel, Germany), quenched with MeOH and submitted to HPLC analysis. The experiments were conducted in quintuplicates and average values were reported; the reproducibility of experiments calculated based on HPLC measurements was 97.3%.

3.2.4. Analysis of total organic carbon

The extent of mineralisation, that is, the oxidative degradation of ibuprofen to CO_2 and H_2O, was determined by measuring organic carbon in solution using an organic carbon analyser TOC-VCPN (Shimadzu, Japan). The non-purgeable organic carbon (NPOC) method was used, in which carbon is quantified by measuring the IR absorption of CO_2 produced by burning the sample in a catalytic reactor in a stream of synthetic air at 680 °C. Before injecting of sample into the reactor, the instrument acidifies the sample by adding 5% of 0.1 M HCl and blows it through with synthetic air for 3 minutes.

3.2.5. High Performance Liquid Chromatography

The concentrations of pharmaceuticals in the experiments were monitored by High Performance Liquid Chromatography (HPLC, LC20, Shimadzu, Japan). Instrument is equipped with UV-DAD detector (SPD-M20A, Shimadzu, Japan), two pumps (LC-20AD, Shimadzu, Japan) and de-gassing unit (DGU-20A3R, Shimadzu, Japan). Injection volume was 50 μL with mobile phase flow was set at 1 ml·min^{-1}, while its composition varied depending on the analysed organic pollutant; the composition of mobile phase, detection details and columns used in HPLC analysis are summarized in Table 3. All aqueous phases used for the chromatographic analyses were prepared in ultrapure water with an electrical resistance of $\varphi = 18$ MΩ·cm^{-1}, obtained by the Direct-Q 3 UV system (EMD Millipore, USA).

Table 3 Composition of mobile phases and detection details for HPLC analysis of studied organics:

Compound	w(PHASE 1)	w(PHASE 2)	λ, nm	Column
o-aminobenzoic acid	0.50 (CH_3OH)	0.50 (H_2O)	333	
17α-Ethynylestradiol	0.70 (CH_3OH)	0.30 (H_2O)	282	
Etodolac	0.60 (CH_3CN)	0.40 (H_2O)	219	
Omeprazole HCl	0.30 (CH_3CN)	0.70 (H_2O)	278	
Amoxicillin	0.10 (CH_3CN)	0.90 (H_2O)	273	
Benzoic acid	0.50 (CH_3CN)	0.50 (H_2O)	228	
Hydrochlorothiazide	0.50 (CH_3CN)	0.50 (H_2O)	270	
Diuron	0.60 (CH_3CN)	0.40 (H_2O)	219	
Diclofenac			276	
Ibuprofen	0.70 (0.1% CH_2O_2)	0.30 (H_2O)	219	
Salicylic acid			303	
Bisphenol A	0.60 (CH_3OH)	0.40 (0.2% CH_2O_2)	276	Machery Nagel C18 250 x 4.6mm, 4.6µm
Sulfanilic acid	0.10 (CH_3OH)	0.90 (0.2% CH_2O_2)	254	
Phenol			270	
p-Nitrophenol			318	
p-Methoxyphenol			318	
m-Nitrophenol	0.50 (CH_3OH)	0.50 (0.1% CH_2O_2)	318	
2,6-Dimethoxyphenol			210	
2,4-Dichlorophenol			288	
1,4-Dimethoxybenzene			288	
Alachlor			276	
Atrazine	0.40 (CH_3CN)	0.60 (0.1% CH_2O_2)	230	
Simazine			230	
1,4-Benzoquinone	0.50 (CH_3CN)	0.5 (10 mM $CH_3CO_2NH_4$)	254	
Desvenlafaxine			318	
Donepezil HCl	0.30 (CH_3OH)	0.70 (0.2% CH_2O_2)	318	
Desloratadine			276	Shodex 4.6 mm IDx150 mm
Oxytetracycline	0.35 (CH_3OH)	0.65 (10 mM $C_2H_2O_4$)	354	
Vilazodone HCl			273	
Tobramycin	0.40 (CH_3OH)	0.40 (H_2O)	273	
Ciprofloxacin	0.10 (CH_3CN)	0.90 (0.2% CH_2O_2)	273	Atlantis T3 5µm, 4.6 mm x 150 mm

3.2.6. Chemical probing of radical species in UV-A/TiO₂ P25 process

In order to confirm the generation of HO• radicals within the studied system using TiO$_2$ P25 under visible irradiation, coumarin was used as a chemical probe and monitored by an UV/Vis spectrophotometer (Lambda EZ 201, PerkinElmer, USA) at 277 nm. Namely, the degradation of coumarin yields typical fluorescent intermediate 7-hydroxycoumarin [192], so its evolution was monitored by a fluorescence spectrophotometer (Cary Eclipse, Varian) using an excitation wavelength of 332 nm and emission wavelength at 456 nm. For this purpose, 50 μM solution of coumarin containing different concentration of TiO$_2$ P25 (0.4, 0.8, 1.2 g·L^{-1}) was treated under UV-A with the purpose to monitor the evolution of 7-hydroxycoumarin. Furthermore, to investigate the generation of superoxide radicals in the study system, a 50 mM solution of BQ was used as a chemical probe containing the same concentration of TiO$_2$ P25 as mentioned earlier. All experiments were conducted in triplicates and average values were reported; the reproducibility of experiments calculated based on HPLC measurements was 97.3%.

3.2.7. Measurement of UV-A irradiation intensity

Light intensity of UV-A irradiation source was measured by UVP UVX Radiometer (Analytik Jena GmbH). The radiometer range switch provides selection from three intensity ranges: 0 to 20 mW·cm^{-2}, 0 to 200 μW·cm^{-2} and 0 to 2000 μW·cm^{-2}. Measurements were performed at 0 to 200 μW·cm^{-2} mode. The irradiation intensity $I(r, z)$ was measured at different distances between the centre of the lamp and the surface of the reactor $R_1 < r < R_2$ where r were: 0.00425, 0.0125, 0.0211 m, and at different distances along the lamp $0 < z < H$, where z were: 0.010, 0.0204, 0.037, 0.054, 0.0705, 0.088 m, and the bottom of the reactor is 0. The coordinates of the irradiation intensity measurement are shown in Figure 6.
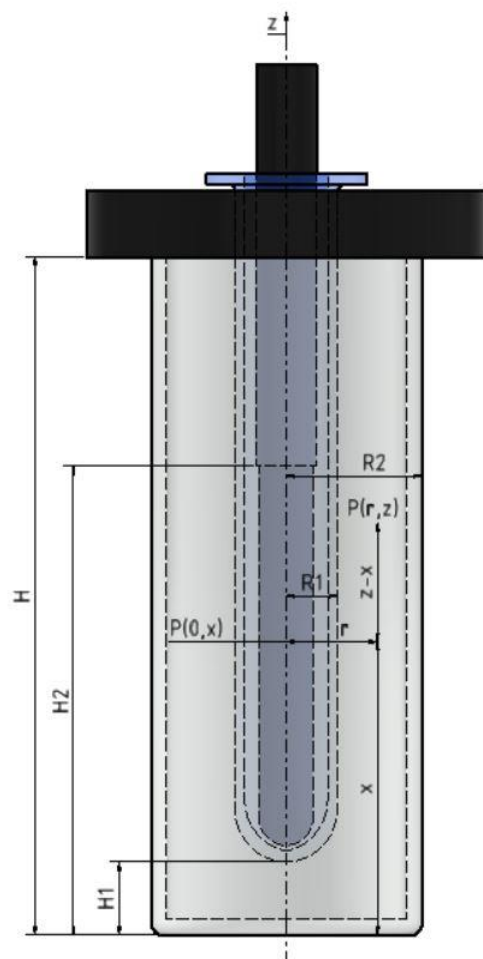
Figure 6 Diagram with the cylindrical coordinate system and geometrical parameters of the photoreactor.

3.2.8. Dynamic light scattering

Dynamic light scattering (DLS) is an established and precise measurement technique for characterizing particle sizes in suspensions and emulsions. The average radius of the TiO_2 P25 agglomerates, R_A, was determined by DLS for different catalyst concentrations, D_0. The analysis was performed using a Malvern light scattering unit, Zetasizer Ultra (Malvern Panalytical, UK). The measuring temperature was fixed at 25.0 ± 0.1 °C. Experiments were run 3 minutes after thermal equilibrium was reached, to minimize eventual drifts. The measurements were carried out

with different prepared TiO_2 P25 suspensions: 0.2, 0.4, 0.6, 0.8, 1, 1.2 $g \cdot L^{-1}$ at a natural pH. Individual peaks in the particle size distributions were derived from multi-modal correlation functions and represent the size of particles in a given suspension. The measurements were carried out in triplicate and the mean values of agglomerates, R_A, were calculated for each suspension.

3.3. Computer simulations

3.3.1. Mathematical – mechanistic modelling

For the development of a mathematical – mechanistic model for the photocatalytic degradation process of ibuprofen in water, a previously developed mathematical – mechanistic model (MM) was used. The models of MM were originally developed, verified and validated in previous studies focused on the degradation of textile dyes, p-chlorophenols, single benzene ring compounds and diclofenac by photooxidation processes: UV-C/H_2O_2 and UV-C/$S_2O_8^{2-}$ [138, 184, 185, 186, 187]. Developed MM model was modified for the simulation of photocatalytic processes as well as for the simulation of pollutant removal and mineralisation by adapting the model to the equations associated with photocatalytic reactions and the simulation of a photocatalytic reactor based on the literature and own experimental data.

The development of the mathematical – mechanistic model was based on the assumed ideal conditions [170]:

(i)   the reaction volume is constant and independent of the treatment time leading to the constant amounts of substance in the reaction mixture,

(ii) the temperature in the reactor is constant providing isothermal conditions,

(iii) the composition of the reaction mixture is time dependent,

(iv) the homogeneity of the reaction mixture is assured.

The influence of reactions, their rates and reactor parameters as well as characteristic of UV-A lamp on model performance was evaluated with the purpose to simplify mathematical – mechanistic modelling by the reduction of number of species and reactions according to their significance. The mathematical – mechanistic model for photocatalytic processes represents the system of ordinary differential equations and the calculations were performed with Mathematica 10.4 (Wolfram Research, USA) using the GEAR method. The prediction error is given as root mean square deviation (RMSD).

3.3.1.1.   Modelling of reactor

Modelling of photocatalytic reactor requires the inclusion of several sub-models to consider the physicochemical phenomena occurring inside the reactor. The model takes into account four aspects: (1) radiation emission, (2) radiation scattering, (3) mixing, and (4) reaction kinetics [196]. For the mathematical modelling of the reactor two conditions were assumed: (1) the photoreactor behaves like a completely mixed batch reactor and (2) the degradation of the contaminant is only due to the TiO$_2$ P25 photocatalytic activity (there is no direct photolysis). Cross-section and geometrical parameters of the photoreactor model is shown in Figure 7.
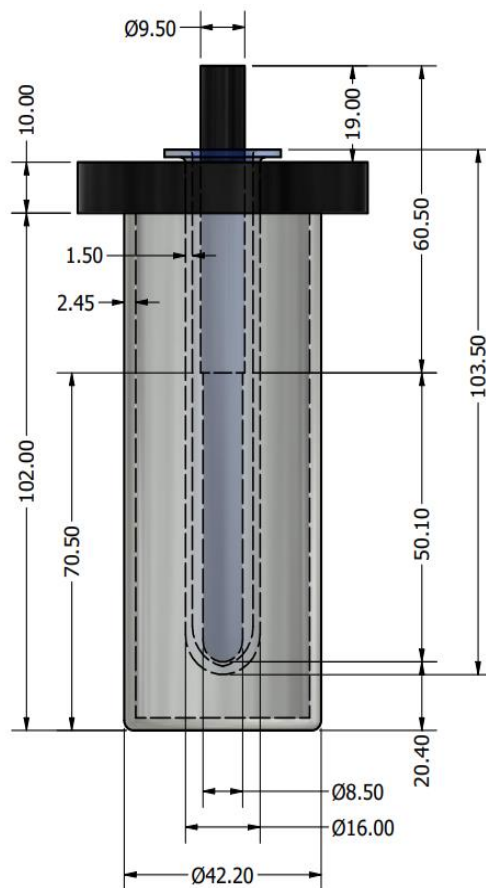
Figure 7 Cross-section and geometrical parameters of the photoreactor model.

The emission or radiation from UV-A lamp was modelled by means of the linear source spherical emission (LSSE) model by Jacob [197]. To determine the light irradiation intensity at every point

within the reactor it assumes that each point of the line emits radiation isotopically with the same intensity. If the electrical input power to the lamp is P_L, the length of the lamp discharge zone is L and the radiation efficiency is η, then the irradiance per unit length of the lamp, S_L, is as follows [169]:

$$S_L = \frac{\eta P_L}{L} \tag{33}$$

The irradiance on the surface of the lamp, I_w, with assumed that irradiance of the discharge is uniform along its length is calculate as follows:

$$I_w = \frac{S_L}{2\pi r_L} \tag{34}$$

where r_L is the radius of the lamp.

The radiation intensity $I(r, z)$ at the point in the annulus $R_1 < r < R_2$ and $0 < z < H$, as is shown at Figure 6, is calculated by integrating the contributions of the source points along the axis of the discharge zone:

$$I(r,z) = \int_{H_1}^{H_2} \left[\frac{S_L}{(4\pi(r^2+(z-x)^2))} \right] \tag{35}$$

where x is the axial coordinate of the emission point P', z is the axial coordinate of the irradiated point P, r is the radial coordinate of P.

The agglomeration of the photocatalyst has a strong impact on the design and operation of photocatalytic reactors. Furthermore, according to the experimentally obtained data, a linear dependence between radius of the agglomerates, R_A and different catalyst concentrations, D_o can be assumed, as shown by the following expression [169]:

$$R_A(D_o) = R_{A0} + B \cdot D_o \tag{36}$$

$\pm 1\ \mu m \cdot L \cdot g^{-1}$ (with a correlation coefficient greater than 0.96).

The distribution of the radiation in the volume of the photoreactor can be determined by the solution of numerous numerical equations, as it was presented in some papers [187, 188, 189]. Therefore, the extinction coefficient Λ, describes the light absorption and scattering phenomena by the catalyst

particles. It is related to the absorption and scattering phenomena by the catalyst particles and therefore can be considered proportional to the number of catalyst particles per unit volume and the effective cross section for the interaction with radiation, S_p [200]:

$$\Lambda = \frac{N_{aggl}S_p}{V} \tag{37}$$

where N_{aggl}/V is the number of agglomerates per unit volume. It follows that the effective cross section for the interaction with radiation, S_p, can be calculated as twice the geometric cross section:

$$S_p = 2\pi \, (R_{Ao} + B \cdot D_o)^2. \tag{38}$$

From the mentioned expression follows for the calculation of the extinction coefficient:

$$\Lambda = \frac{3D_o}{2\rho_{aggl}(R_{A0} + BD_o)} \tag{39}$$

where ρ_{aggl} is the apparent density of the catalyst in an agglomerate, that is assumed to be equal to the tapped density given by the manufacturer: 130 kg·m^{-3}.

Cid et al. [169] obtained an expression for radial distribution of the photon density per unit of volume in the reactor with cylindrical symmetry. Accordingly, the photon volume density (moles of photons per unit volume) inside the annulus, n_p, evaluated in a differential volume adjacent to the inner surface (R_1), is related to the intensity of the radiation entering the annulus through the inner surface, $I(R_1)$, as follows:

$$n_p(R_1) = \frac{I(R_1)N}{h\nu c N_A} \tag{40}$$

where N is the effective refractive index of the slurry, assumed to be close to that of water (1.332), c is the speed of light in vacuum (2.998·10^8, m·s^{-1}), N_A is the Avogadro constant (6.022·10^{23}, mol^{-1}) and the vacuum wavelength, λ, of the UV-A is 365 nm, h is Planck constant (6.626·10^{-34}, J·s), ν is vacuum lamp frequency ($\nu = c/\lambda$, s^{-1}) and $I(R_1)$ is calculated by eq. 35, based on measurements (32.7889 W·m^{-2}).

Finally, the expression for the determination of the photon density in the reactor is given by the following expression [169]:

$$n_{\mathrm{p}} = \frac{2\,n_{\mathrm{p}}(R_1)\,R_1}{(R_2^2 - R_1^2)\,\lambda}\left[1 - e^{-\Lambda(R_2 - R_1)}\right]. \tag{41}$$

The characteristic extinction coefficient, Λ, and the average photon density in the reactor, n_{p} from eq. (39 and 41), is calculated for different catalyst concentrations in the range of $0.4 - 2$ g·L⁻¹. The reactor parameters are those of the experimental setup: $R_1 = 0.008$ m, $R_2 = 0.01865$ m, and the slurry level was $H = 0.102$ m. Therefore, the density of photons at the inner radius is $n_{\mathrm{p}}(R_1)$ is obtained from eq. 40.

One of the important factors for modelling photocatalytic processes is the total amount, per unit volume, of available adsorption sites on the photocatalyst, S, is proportional to the is related to the catalyst concentration D_{o} through the proportionality constant k_{c} [169]:

$$S = k_{\mathrm{c}}\frac{D_{\mathrm{o}}}{(D_{\mathrm{oc}} + D_{\mathrm{o}})} \tag{42}$$

where k_{c} (mol·m⁻³) is a proportionality constant that is calculated from eq. 43:

$$k_{\mathrm{c}} = \frac{3k_0}{\rho_{\mathrm{aggl}}\,B} \tag{43}$$

while k_{o} (mol·m²) and B correlation coefficient are obtained from the linear mathematical dependence between radius of the agglomerates, R_{A} and different catalyst concentrations D_{o} (eq. 36). D_{oc} (g·L⁻¹) is defined as a characteristic catalyst concentration as follows:

$$D_{\mathrm{oc}} = \frac{R_{\mathrm{A}0}}{B}. \tag{44}$$

The mathematical dependence of n_{p} and S as a function of the different concentrations of the photocatalyst used was further used to solve differential equations to simulate the calculation of the holes and electrons generated as dominant species for the photocatalytic process.

3.3.1.2. Modelling of photocatalytic reactions

As already mentioned, the composition of the reaction mixture depends on time. The composition of the reaction mixture is the same at every point, so that mass balances can be established for the reactor as a whole. The general expression for the mass balance in a batch reactor at constant volume, constant temperature and ideal mixing is given by the expression:

$$\frac{dc_i}{dt} = -r_i \tag{45}$$

where c_i is the mean value of the concentration of chemical species i in the solution and r_i is the rate of its disappearance. For the development of photocatalytic mathematical – mechanistic models, degradation of coumarin was modelled first to confirm the generation of HO• within the studied system as well as to fine tune the system regarding the generation of HO•. Coumarin was used as a chemical probe because its degradation via HO• mediated mechanism yields the formation of the typical fluorescent intermediate 7-hydroxycoumarin. Since the superoxide radical is the second most important radical for pollutant degradation in the photocatalytic process, the degradation of BQ was also modelled to confirm the generation of superoxide radicals and fine tune reactions with its involvement. After defining the degradation mechanisms, the developed model was applied to simulate the degradation of IBP as a test compound with a 1.2 g·L⁻¹, concentration of TiO_2 P25 and the model was verified at other experimental concentrations of TiO_2 P25. In addition to the conversion of pollutant degradation, the percentage of mineralisation (i.e., the proportion of reduction in TOC indicators) was also monitored, taking into account the u and w coefficients calculated for IBP on the basis of knowledge acquired during modelling of photooxidation of CECs by combined mechanistic and QSA/PR modelling [170].The Table 4 shows the balance equations for pollutant degradation by the UV-A/TiO_2 P25 process and its reaction rate constants (k). The constant of reaction rates were obtained mostly from the literature or by the trial-and-error method by fitting the values to the model and comparing them to the experimental data, minimizing the root mean square deviation (RMSD) used as the accuracy criterion. The RMSD between experimentally obtained ($y_{exp,i}$) and data predicted by model ($y_{mod,i}$) was calculated using the equation:

$$RMSD = \sqrt{\frac{1}{N}\sum_{i=1}^{i=N}(y_{exp,i} - y_{mod,i})^2} \tag{46}$$

Table 4 Balance equations for the degradation of pollutants by the TiO₂ P25/UV-A process and its reaction rate constant:

#	Chemical reactions	Reaction rate constants	Literature
1	$h^+ + OH^- \rightarrow HO\bullet$	$k_1 = 2.4 \cdot 10^{11}$ (mol dm⁻³)⁻¹ s⁻¹	[201]
2	$e^- + O_2 \rightarrow O_2^{-\bullet}$	$k_2 = 1.38 \cdot 10^{12}$ (mol dm⁻³)⁻¹ s⁻¹	[202]
3	$h^+ + OxAc \rightarrow IP$	$k_3 = 5.29 \cdot 10^{-2}$ (mol dm⁻³)⁻¹ s⁻¹	This study

#	Bulk reactions	Reaction rate constants	Literature
4	$HO\bullet + H_2O_2 \rightarrow HO_2^{\bullet} + H_2O$	$k_4 = 2.7 \cdot 10^9$ (mol dm⁻³)⁻¹ s⁻¹	[8]
5	$HO\bullet + HO_2^- \rightarrow HO_2^{\bullet} + OH^-$	$k_5 = 4.5 \cdot 10^{11}$ (mol dm⁻³)⁻¹ s⁻¹	[8]
6	$HO_2^{\bullet} + H_2O_2 \rightarrow HO\bullet + H_2O + O_2$	$k_6 = 180$ (mol dm⁻³)⁻¹ s⁻¹	[8]
7	$O_2^{-\bullet} + H_2O_2 \rightarrow HO\bullet + O_2 + OH^-$	$k_7 = 7.8$ (mol dm⁻³)⁻¹ s⁻¹	[8]
8	$2HO\bullet \rightarrow H_2O_2$	$k_8 = 2.52 \cdot 10^{11}$ (mol dm⁻³)⁻¹ s⁻¹	[196, 197, 198]
9	$HO\bullet + HO_2^{\bullet} \rightarrow H_2O + O_2$	$k_9 = 3.96 \cdot 10^{11}$ (mol dm⁻³)⁻¹ s⁻¹	[196, 197, 198]
10	$HO_2^{\bullet} + HO_2^{\bullet} \rightarrow H_2O_2 + O_2$	$k_{10} = 4.98 \cdot 10^7$ (mol dm⁻³)⁻¹ s⁻¹	[196, 197]
11	$HO_2^{\bullet} + O_2^{-\bullet} \rightarrow HO_2^- + O_2$	$k_{11} = 5.82 \cdot 10^9$ (mol dm⁻³)⁻¹ s⁻¹	[8]
12	$HO\bullet + O_2^{-\bullet} \rightarrow O_2 + OH^-$	$k_{12} = 4.2 \cdot 10^{11}$ (mol dm⁻³)⁻¹ s⁻¹	[204]
13	$HO_2^{\bullet} \rightarrow O_2^{-\bullet} + H^+$	$k_{13} = 9.48 \cdot 10^6$ M	[8]
14	$O_2^{-\bullet} + H^+ \rightarrow HO_2^{\bullet}$	$k_{14} = 6 \cdot 10^{11}$ (mol dm⁻³)⁻¹ s⁻¹	[196, 197, 198]
15	$HO_2^- + H^+ \rightarrow H_2O_2$	$k_{15} = 1.56\ 10^{12}$ (mol dm⁻³)⁻¹ s⁻¹	[196, 197, 198]
16	$H_2O_2 \rightarrow HO_2^- + H^+$	$k_{16} = 2.22$ M	[185, 186, 187]
17	$HO\bullet + H_2O_2 \rightarrow O_2^{-\bullet} + H_2O$	$k_{17} = 1.62 \cdot 10^9$ (mol dm⁻³)⁻¹ s⁻¹	[8]

#	Pollutant reactions	Reaction rate constants	Literature
18A	Coum + HO •→ BP	$k_{18A} = 1.2 \cdot 10^{11}$ (mol dm^{-3})$^{-1}$ s^{-1}	[173]
18B	BQ + HO • → BP	$k_{18B} = 7.2 \cdot 10^{10}$ (mol dm^{-3})$^{-1}$ s^{-1}	[173]
18C	IBP + HO • → BP	$k_{18C} = 3.38 \cdot 10^{11}$ (mol dm^{-3})$^{-1}$ s^{-1}	[173]
19B	BQ + $O_2^{-•}$ → BP	$k_{19B} = 5.88 \cdot 10^{10}$ (mol dm^{-3})$^{-1}$ s^{-1}	[202]
19C	IBP + $O_2^{-•}$ → BP	$k_{19C} = u \cdot 6.01 \cdot 10^{2}$ (mol dm^{-3})$^{-1}$ s^{-1}	This study
20	BP+HO •→ IP+ OxAc	$k_{20} = u \cdot 6 \cdot 10^{10}$ (mol dm^{-3})$^{-1}$ s^{-1}	[206]
21	OxAc + HO • → IP	$k_{21} = 8.4 \cdot 10^{7}$ (mol dm^{-3})$^{-1}$ s^{-1}	[197, 198]

Kinetic models of chemical reactions derived from Table 4:

$$r_1 = c_{h^+} \cdot c_{OH^-} \tag{47}$$

$$r_2 = k_2 \cdot c_{e^-} \cdot c_{O_2} \tag{48}$$

$$r_3 = k_3 \cdot c_{h^+} \cdot c_{OxAc} \tag{49}$$

$$r_4 = k_4 \cdot c_{HO•} \cdot c_{H_2O_2} \tag{50}$$

$$r_5 = k_5 \cdot c_{OH•} \cdot c_{HO_2^-} \tag{51}$$

$$r_6 = k_6 \cdot c_{HO_2^•} \cdot c_{H_2O_2} \tag{52}$$

$$r_7 = k_7 \cdot c_{O_2^{-•}} \cdot c_{H_2O_2} \tag{53}$$

$$r_8 = k_8 \cdot c_{HO•}^2 \tag{54}$$

$$r_9 = k_9 \cdot c_{HO•} \cdot c_{HO_2^•} \tag{55}$$

$$r_{10} = k_{10} \cdot c_{HO_2^\bullet} \cdot c_{HO_2^\bullet} \tag{56}$$

$$r_{11} = k_{11} \cdot c_{HO_2^\bullet} \cdot c_{O_2^{-\bullet}} \tag{57}$$

$$r_{12} = k_{12} \cdot c_{HO^\bullet} \cdot c_{O_2^{-\bullet}} \tag{58}$$

$$r_{13} = k_{13} \cdot c_{HO_2^\bullet} \tag{59}$$

$$r_{14} = k_{14} \cdot c_{H^+} \cdot c_{O_2^{-\bullet}} \tag{60}$$

$$r_{15} = k_{15} \cdot c_{H^+} \cdot c_{HO_2^-} \tag{61}$$

$$r_{16} = k_{16} \cdot c_{H_2O_2} \tag{62}$$

$$r_{17} = k_{17} \cdot c_{HO^\bullet} \cdot c_{H_2O_2} \tag{63}$$

$$r_{18A} = k_{18A} \cdot c_{HO^\bullet} \cdot c_{Coum} \tag{64}$$

$$r_{18B} = k_{18B} \cdot c_{HO^\bullet} \cdot c_{BQ} \tag{65}$$

$$r_{18C} = k_{18C} \cdot c_{HO^\bullet} \cdot c_{IBP} \tag{66}$$

$$r_{19B} = k_{19B} \cdot c_{O_2^{-\bullet}} \cdot c_{BQ} \tag{67}$$

$$r_{19C} = k_{19C} \cdot c_{O_2^{-\bullet}} \cdot c_{IBP} \tag{68}$$

$$r_{20} = k_{20} \cdot c_{HO^\bullet} \cdot c_{BP} \tag{69}$$

$$r_{21} = k_{21} \cdot c_{HO^\bullet} \cdot c_{OxAc} \tag{70}$$

Differential equations:

    a) formation of electrons and holes:

$$\frac{dh^+}{dt} = Y_1 \cdot Y_2 \cdot Y_3 - r_1 \tag{71}$$

$$\frac{de^-}{dt} = Y_1 \cdot Y_2 \cdot Y_3 - r_2 \tag{72}$$

where Y_1, Y_2, Y_3 are mathematical functions determined for the dependence of parameters of reactor model (n_p, D_o) and recombination rate of photogenerated holes and electrons toward TiO$_2$ P25 loading.

b) conversion of coumarin and formation 7-hydroxycoumarin (BP):

$$\frac{dc_{\text{Coum}}}{dt} = -r_{18A} \tag{73}$$

$$\frac{dc_{\text{BP}}}{dt} = r_{18A} - r_{20} \tag{74}$$

c) conversion of BQ

$$\frac{dc_{\text{BQ}}}{dt} = -r_{18B} - r_{19B} \tag{75}$$

d) conversion and mineralisation (IP) of IBP:

$$\frac{dc_{\text{IBP}}}{dt} = -r_{19C} - r_{20C} \tag{76}$$

$$\frac{dc_{\text{IP}}}{dt} = r_3 + w \cdot r_{20} + r_{21} \tag{77}$$

$$\frac{dc_{\text{OxAc}}}{dt} = -r_3 + (1 - w) \cdot r_{20} - r_{21} \tag{78}$$

3.3.2. Response surface modelling and Design of experiments

The influence of the adsorption process parameters (initial pH and γ(TiO$_2$ P25)) on the removal of 30 studied organic compound was investigated using 3^2 FFD (Table 5) in combination with response surface modelling.

Table 5 Experimental Matrix for the applied 3^2 Full Factorial Design (FFD):

input variables				response
coded X_1	uncoded pH	coded X_2	uncoded γ(TiO$_2$ P25), mg·L^{-1}	Y, L·g^{-1}
-1	4	-1	0.4	K_1
0	7	-1	0.4	K_2
1	10	-1	0.4	K_3
-1	4	0	0.8	K_4
0	7	0	0.8	K_5
1	10	0	0.8	K_6
-1	4	1	1.2	K_7
0	7	1	1.2	K_8
1	10	1	1.2	K_9

The extent of adsorption was mathematically described for each of the 30 organics by quadratic polynomial eq. (79), i.e., RSM model including direct linear (X_1 and X_2) and quadratic ($X_1{}^2$ and $X_2{}^2$) as well as interactive ($X_1 \times X_2$) effects of both process parameters (initial pH and γ(TiO$_2$ P25)), with the adsorption coefficient (K, L·g^{-1}) selected as a response (Y).

$$Y = AX_1 + BX_1^2 + CX_2 + DX_2^2 + EX_1X_2 + F \tag{79}$$

In this case, the range of process parameters (initial pH and γ(TiO$_2$ P25)) was chosen according to the literature related to photocatalytic treatment of organics using TiO$_2$ P25 [163, 164, 165]. Their values were transferred into dimensionless coded values (X_1 and X_2) at levels according to the

chosen 3^2 FFD (Table 5). As response were used experimentally determined adsorption coefficient (K, L·g^{-1}), commonly used in studying adsorption of various pollutants onto vast array of adsorbents, which is calculated using eq. (80):

$$K = \frac{q_e}{c_e} \tag{80}$$

where c_e (mg·L^{-1}) is the average concentration of an organic compound in the aqueous phase at equilibrium, while q_e (mg·g^{-1}) is the amount of adsorbed organics at equilibrium on the surface of TiO$_2$ P25, which is calculated by eq. (81):

$$q_e = \frac{c_0 - c_e}{c_A} \tag{81}$$

where: c_0 (mg·L^{-1}) is the average concentration of organic compound in the samples of the control experiments; c_e (mg·L^{-1}) is the average concentration of organic compound in the liquid phase at the equilibrium; and c_A (g·L^{-1}) is the concentration of adsorbent [148, 180]. The adsorption coefficient depends on the equilibrium concentration whenever the adsorption isotherm is nonlinear in nature [212]. The experimental design, i.e., obtained results, were analysed with RSM and quadratic model (79) was constructed for each compound, using software packages Design Expert 7.1 (StatEase, USA) and STATISTICA 13.5 (StatSoft Inc., USA). Goodness-of-fit of RSM models was estimated based on coefficient of determination (R^2) and analysis of variance (ANOVA).

3.3.3. Development of the quantitative relationship between structure, activity/property

Generally, QSA/PR relates molecular structures with activity or its property. Following relations are established by the means of molecular descriptors:

1) relationship between the molecular structure and the coefficients from RSM modelling
2) relationship between the molecular structure and the reaction rate between HO•/O$_2$$^{-•}$ in photocatalytic processes.

QSA/PR modelling was performed in several steps:

1) Molecular structures of organic compounds studied were built using GaussView 6.0 software (Gaussian, Inc, USA).

2) Built molecular structures of organic compounds were optimized using chemical density functional theory (DFT) by method (B3LYP/6-311++G(d,p)) employing Gaussian16 (Gaussian Inc, Wallingford, CT, USA).

3) Empirical quantum chemical parameters, such as dipole moment (total μ, as well as its X, Y, and Z components), energy of the highest (E_{HOMO}) and the lowest occupied molecular orbital (E_{LUMO}) and the gap between (HLG), final heat of formation (ΔH_f), and ionization potential, were calculated using chemical density functional theory (DFT) methods (B3LYP/6-311++G(d,p)) employing Gaussian16 (Gaussian Inc, Wallingford, CT, USA).

4) The molecular descriptors were calculated by DRAGON 6.0 software (Milano Chemometrics and QSAR Research Group, TALETE, Italy) from optimized molecules. Overall, 3129 molecular descriptors were obtained capturing relevant structural features of compounds placed in the training and test sets encompassing chemical diversity of the studied organics.

5) The correlation between the QSA/PR responses, i.e., the coefficients from RSM modelling, reaction rate between $HO\bullet/O_2^{-\bullet}$ and the structure-related descriptors (DRAGON and DFT generated) was obtained using the variable selection Genetic Algorithm (GA) and Multiple Linear Regression Analysis (MLRA) methods. The combination of previous two techniques were applied for the selection of influential descriptors and constructions of 1 – 5 variable models using QSARINS 2.2.3 (QSAR Group, University of Insubria, Italy) [184]. GA variable selection technique started with following parameters: 200 random models, generation size of 2000 iterations, and the mutation probability specified as 20%.

6) Model selection and validation was performed by comparing the values of the common statistical parameters: R (the correlation coefficient of regression); R^2 (the model explained variance); Q^2 (the leave-one-out cross-validation coefficient); F (F-ratio between the variances of observed and calculated property); p (probability value for calculated F); s (standard error); and S_{PRESS} (standard error of the predictive residue of sum of squares). The validation of models selected as the best for each chosen response was also performed using Leave Many Out (LMO), external validation and "Y-scrambling" tests. The chemical applicability domain (AD) for obtained models was checked by the leverage approach to verify the prediction reliability [213]. William's plot was used to investigate the applicability domain (AD) of developed QSA/PR models. Such a plot of standardized

cross-validated residuals (RES) *vs*. leverage values (HAT) clearly depicts both the response outliers (Y outliers) and structurally influential compounds (X outliers) in the model [214].

4. RESULTS AND DISCUSSION

4.1. Modelling and simulation of photocatalytic reactor

In the photocatalytic reactor, the UV-A lamp is placed along the axis of the annulus. Figure 7 shows the coordinates of an emission point in the lamp, $P(0, x)$, and a point in the annulus, $P(r, z)$. Therefore, the distribution of irradiation intensity at the points in the annulus $R_1 < r < R_2$ and $0 < z < H$, are experimentally determined as shown at Figure 8.
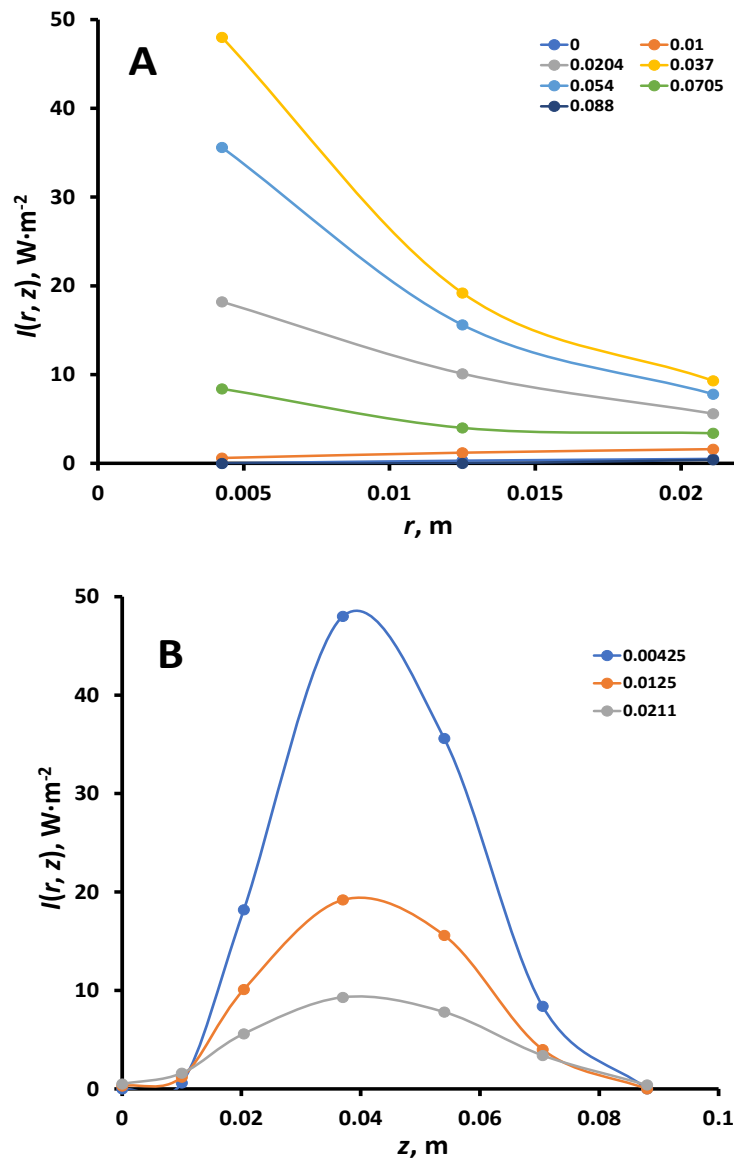
Figure 8 Irradiation intensity in photocatalytic reactor at the inner radius of the reactor annulus as a function of A) axial and B) radial measurement of irradiation of z and r points.

Figure 8 shows the irradiation intensity profiles I (W·m^{-2}) as a function of the axial coordinate z (A), calculated for different values of the annulus inner radius r (m). The bottom of the reactor is at $z = 0$ m and the measured zone of discharge of the lamp extends from $z = 0 - 0.088$ m. The maximum irradiation intensity was calculated on the surface of the quartz tube for $r = 0.00425$ m at a distance of $z = 0.038$ m that is 48.8 W·m^{-2}. The maximum of irradiation is almost half the length of the discharge zone, what was expected. The irradiance on the surface of the lamp is calculate by the eq. 34 and it is 32.78 W·m^{-2}, with assumed that irradiance of the discharge is uniform along its length. The irradiation intensity decreases with the distance from the surface of the quartz tube (where irradiation is the highest), i.e., with an increase in the value of r, as shown in Figure 8 B. Furthermore, the radiation intensity increases in all measurement cases from the distance from the bottom of the reactor $z = 0$ to $z = 0.038$ m, where the maximum radiation intensity was observed, after which the radiation intensity decreases and can be considered negligible at a distance greater $z = 0.0705$ m.

Figure 9, 3D diagram shows more clearly the determination of the maximum radiation intensity as a function of the position of the measurement points in the reactor: $z = 0, 0.010, 0.0204, 0.037, 0.054, 0.0705, 0.088$ m and $r = 0.00425, 0.0125, 0.0211$ m.
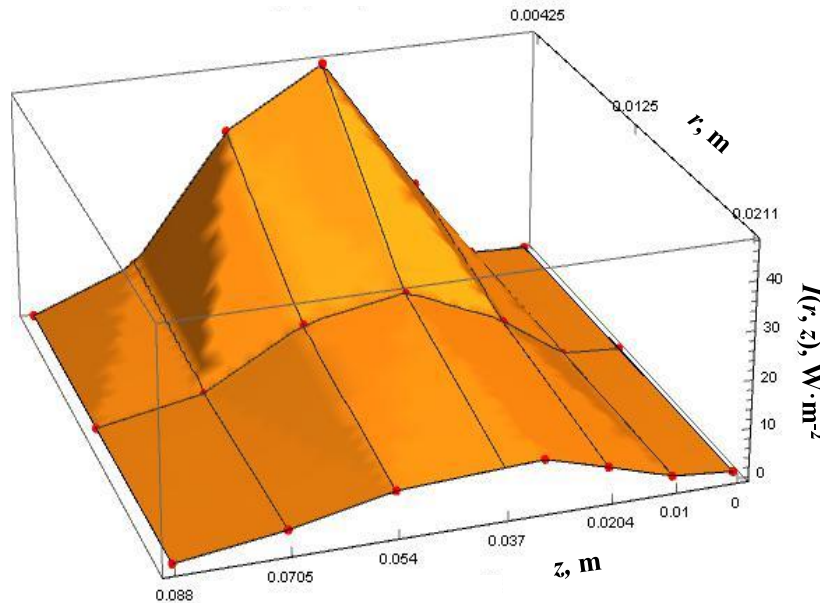
Figure 9 3D plot of irradiation intensity in photocatalytic reactor at the inner radius of the annulus for different values of r and z.

As mentioned before, agglomeration of the catalyst has significant implications for the design and operation of photocatalytic reactors. Close to neutral pH, the catalyst nanoparticles agglomerate, as shown by Li et al. [215]. For practical applications, operation close to pH 7 is desirable to avoid alkalization or acidification steps. In addition, TiO_2 nanoparticles are known to form agglomerates in close to neutral aqueous suspensions, as shown by Xu [216], with a radius on the order of microns, according to Li et al. [215]. Furthermore, based on the experimentally obtained data in this work, a linear dependence between the radius of the agglomerates, R_A, and different catalyst concentrations, D_o, was assumed, and modelled by eq. 36. Figure 10 and Table 6 show good agreement between experimentally obtained results and results calculated from established model that is confirmed by RMSD criterion (≤ 1). Average radius of agglomerates increases with increasing concentration of TiO_2 P25 what is expected.
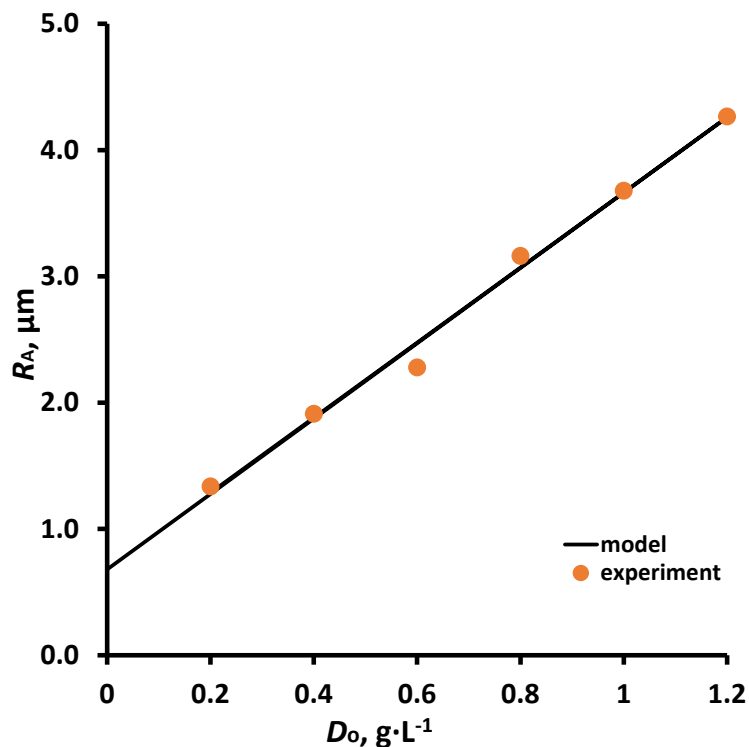
Figure 10 Linear dependence of average radius, R_A of TiO_2 P25 agglomerates and different catalyst concentration.

The extinction coefficient, Λ is related to the phenomena of absorption and scattering by catalyst particles and it is calculated via eq. 39. Results are presented in Table 6. The extinction coefficient

is a characteristic that determines how strongly a species absorbs or reflects radiation or light irradiation at a particular wavelength. As follows from results Λ, increase with concentration of TiO$_2$ P25.

The average photon density in the reactor, n_p, was calculated according to eq. 41 including the extinction coefficient and the reactor parameters. n_p decreases with higher concentration of photocatalyst.

Table 6 Experimentally and modelled values of average radius, R_A, of agglomerates TiO$_2$ P25 and RMSD values, calculated extinction coefficient, Λ, and the average photon density in the volume of the reactor, n_p and the total available adsorption sites on the catalyst, S:

D_o, g·L^{-1}	R_{Aexp}, μm	R_{Amodel}, μm	RMSD (R_{Aexp} vs. R_{Amodel})	Λ, m^{-1}	$n_p \cdot 10^{-15}$, mol·m^{-1}	S, mol·m^{-3}
0.2	1.34	1.29	0.092	1794.34	13.97	11.45
0.4	1.91	1.88		2454.29	10.21	16.74
0.6	2.28	2.48		2796.88	8.96	21.04
0.8	3.16	3.07		3006.88	8.33	22.09
1	3.68	3.66		3148.73	7.96	22.98
1.2	4.27	4.26		3250.97	7.71	23.96

Important parameters for photocatalytic processes are total available adsorption sites on the catalyst, S, that was calculated by eq. 42 and depend on TiO$_2$ P25 concentration (Table 6 and Figure 11). Mathematically dependence: available adsorption sites on the catalyst and concentration of TiO$_2$ P25, average photon density in the volume of the reactor and concentration of TiO$_2$ P25 and coefficient of recombination and concentration of TiO$_2$ P25 are described by equations $Y_1 - Y_2$ that are shown at Figure 11 and Table 7. The calculated mathematical dependencies are later used in the creation of differential equations for simulating the formation of holes and electrons pairs responsible for the generation of hydroxyl and superoxide radicals as dominant radicals in photocatalytic processes.
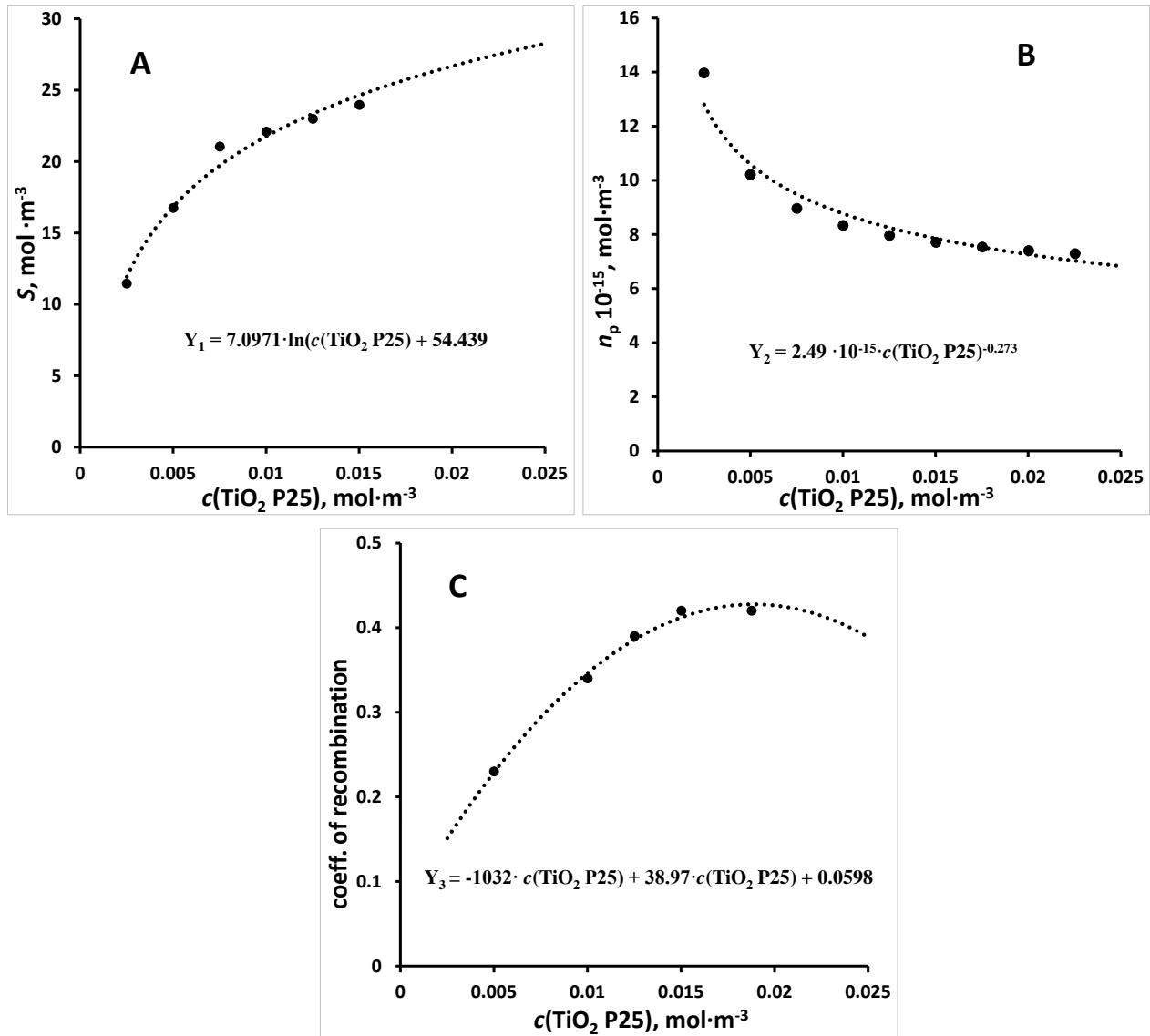
Figure 11 Mathematical dependence of A) available adsorption sites on the catalyst and the concentration of TiO_2 P25, B) average photon density in the volume of the reactor and concentration of TiO_2 P25, C) coefficient of recombination and concentration of TiO_2 P25.

Table 7 Mathematical dependence Y_1, S and $c(TiO_2 P25)$; Y_2, n_p and $c(TiO_2 P25)$; Y_3, coefficient of recombination and $c(TiO_2 P25)$ based on obtained empirical and calculation values during modelling of reactor:

Equations
$Y_1 = 7.0971 \cdot \ln(c(TiO_2 P25) + 54.439$
$Y_2 = 2.49\ 10^{-15} \cdot c(TiO_2 P25)^{-0.273}$
$Y_3 = -1032 \cdot c(TiO_2 P25) + 38.97 \cdot c(TiO_2 P25) + 0.0598$

4.2. Development of mathematical – mechanistic model for photocatalytic process

Heterogeneous photocatalytic processes are complex systems whose efficiency is influenced by the reactor system, the scattering effect due to the presence of solid particles in the system that cause shielding of the induced radiation, adsorption on the catalyst material, and the presence of additional reactive species. The part related to the scattering effect causing the shielding was solved based on the approach of Cid et al. [169], adapting the values for our reactor system and integrating them into a mathematical – mechanistic model that is set of differential equations for simulating pollutant degradation. Furthermore, first step for the development of photocatalytic mathematical – mechanistic model, was investigate and modelled degradation of coumarin and BQ to confirm generation $HO\bullet$ and $O_2^{-\bullet}$ and fine tune reactions with their involvement. After that, experimental results of photocatalytic degradation of IBP at initial conditions of pH 7, $c(IBP) = 0.05$ mM, and 1.2 $g \cdot L^{-1}$ concentration of TiO_2 P25 photocatalyst were used to develop the model. Furthermore, for the development of the model, the conversion and mineralisation of IBP were monitored. Mineralisation is defined as the reduced value of the ratio of total organic carbon at a certain reaction time (TOC) to total organic carbon at the beginning of the reaction (TOC_0) of 1 (or 100%) ($M = 1 - \frac{TOC}{TOC_0}$). The developed model was then verified on experimental results obtained at different loading of photocatalyst; 0.4, 0.8 and 2 $g \cdot L^{-1}$.

The formation of radical species such as HO• and $O_2^{-\bullet}$ plays an important role in a determination of photocatalytic pathways and as such their identification is important. The efficiency of HO• in photocatalytic reactions is predominantly based on their strong oxidising potential of 2.8 V (vs. NHE) [217]. The challenge in its determination lies in the non-selective nature and short lifetime of the radical, which restricts the possibility of direct quantification [218]. The use of a chemical probe to capture HO• is a potentially efficient method for measuring the radical due to the low cost, rapid analysis time, and reproducibility of the method. Coumarin was used as a quantitative probe for HO• formation and to assess the photocatalytic efficiency [201, 202, 203, 204]. Upon reaction with the HO•, coumarin produces several hydroxylated products of which one, 7-hydroxycoumarin, is strongly fluorescent. Hence, to confirm the formation of radicals, experiments on the degradation of coumarin and the formation of 7-hydroxycoumarin were performed with different concentrations of TiO$_2$ P25 $0.4 - 1.2$ g·L^{-1} and c(Coum) = 0.05 mM. An investigation on the photodegradation of coumarin and formation of 7-hydroxycoumarin at various concentrations TiO$_2$ P25 is presented at Figure 12. As it can be observed, higher concentrations of the photocatalyst generate more hydroxyl radicals so the rate of photocatalytic degradation is increased with increasing generation of HO•. During photocatalytic hydroxylation of coumarin over TiO$_2$ P25 under UV-A light, 7-hydroxycoumarin is formed, as also shown in Figure 12 which confirms the formation of the HO•.
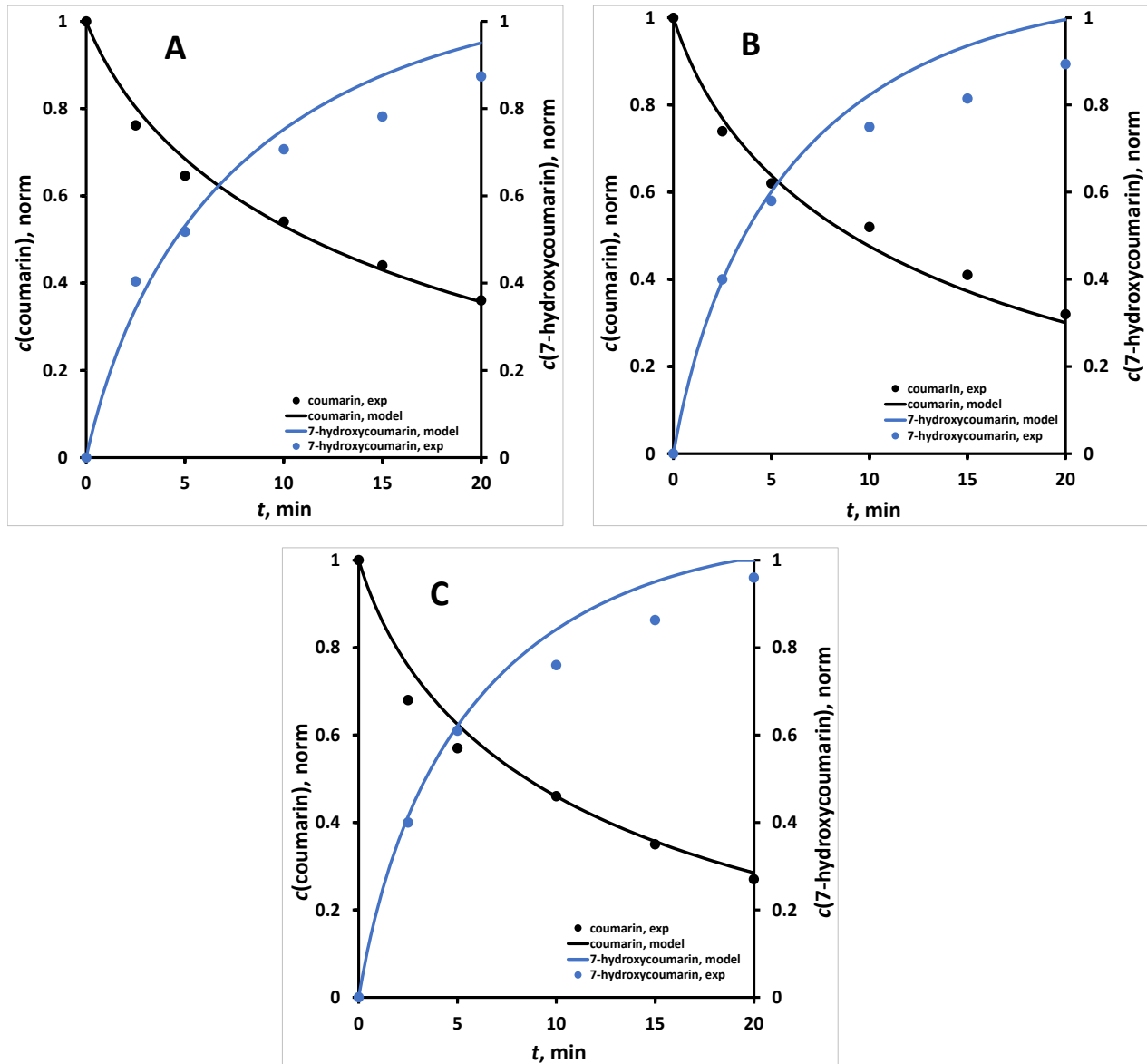
Figure 12 Graphical representation of the experimental and simulation results of photodegradation of coumarin and formation 7-hxdroxycoumarin by UV-A/TiO$_2$ P25 processes at different concentration of catalyst TiO$_2$ P25 A) 0.4 g·L^{-1}, B) 0.8 g·L^{-1}, C) 1.2 g·L^{-1}.

Figure 12 shows the production of 7-hydroxycoumarin but also the achievement of its maximal formation, especially at concentrations of 0.8 and 1.2 g·L^{-1} of TiO$_2$ P25 (Figure 12 (A and C)), which indirectly indicates the amount of HO• radicals formed. The concentration of 7-hydroxycoumarin reaches its maximum after 20 minutes of the process, after which the concentration drops. The decrease in 7-hydroxycoumarin concentration can also be attributed to

the presence of superoxide radicals, as reported by Czili and Horvath [219]. When comparing the results obtained experimentally and with the simulation model, slightly larger deviations were observed in the case of 7-hydroxycoumarin, especially at lower concentrations of TiO_2 P25 (Figure 12 (A and B)). In the case of coumarin, a relatively good agreement between the results obtained from the model and the experimental results is shown. In addition, Table 8 shows the calculated root mean square deviation values for each of the simulation model-experiment data pairs for coumarin and 7-hydroxycoumarin, as can be seen RMSD $\leq$ 1.0 is for all cases.

Table 8 Values of calculated root mean square deviation for each of simulation model-experiment data pairs: coumarin and 7-hydroxycoumarin:

Compound	RMSD		
γ (TiO$_2$ P25), g·L^{-1}	0.4	0.8	1.2
Coumarin	0.023	0.031	0.039
7-hydroxycoumarin	0.063	0.074	0.055

Figure 13 shows the photodegradation of BQ with experimental and simulation model results at different concentrations of TiO_2 P25. As mentioned earlier, BQ was used as a chemical probe to determine the formation of $O_2^{-\bullet}$ [221], the second most important radical for photocatalytic degradation. However, it should be noted that BQ reacts with HO• as well, even at considerably high reaction rate (Table 4, reaction 18B). Hence, its degradation is owned via both HO• and $O_2^{-\bullet}$. After almost 15 min of process, BQ is almost completely degraded, while according to the simulation model, the reaction is slightly faster and BQ is completely degraded after 5 min in the case of the 0.4 g·L^{-1} photocatalyst used. At higher concentrations of TiO_2 P25, even faster decomposition of BQ is observed. Therefore, a greater agreement between the experimental results and the model results is observed at higher concentrations of TiO_2 P25, which was confirmed by the RMSD calculation, and the results are shown in Table 9.
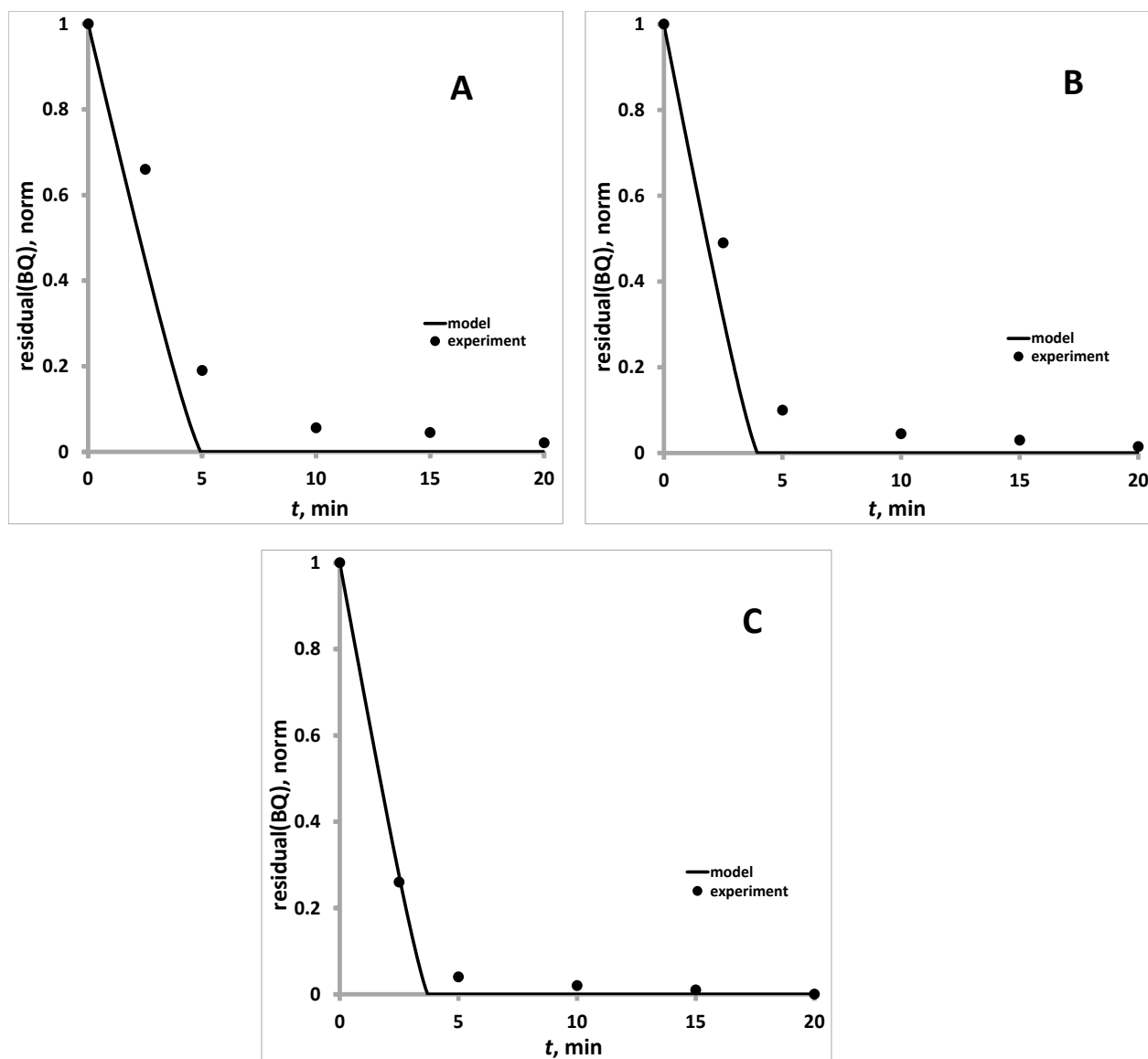
Figure 13 Graphical representation of the experimental and simulation results of photodegradation of BQ at different catalyst concentration of TiO_2 P25 by UV-A/TiO_2 P25 processes: A) 0.4 $g \cdot L^{-1}$, B) 0.8 $g \cdot L^{-1}$, C) 1.2 $g \cdot L^{-1}$.

Table 9 Values of calculated root mean square deviation for each of simulation model – experiment data pairs for BQ:

Compound	RMSD		
γ(TiO$_2$ P25), g·L^{-1}	0.4	0.8	1.2
BQ	0.116	0.089	0.023

After confirming the formation of the presented radical species in UV-A/TiO$_2$ P25 photocatalysis processes, as well as used reaction rate constants for the formation of both HO• and O$_2^{-•}$ via photogenerated holes and electrons, respectively comparing model predictions and obtained experimental results with rather high agreement, a mathematical – mechanistic model was tested in simulation of the photocatalytic degradation of IBP. The model was tested and fined tuned for the specific reactions in the case of IBP based on experimental results for 1.2 g·L^{-1} TiO$_2$ P25, and thereafter verified on other photocatalyst concentrations. It should be noted that two model parameters determined in our previous study; u and w, to be structure dependent, are calculated based on molecular descriptors of IBP. Parameter u is used as an empirical parameter corresponding to rates of degradation of formed by-products by determined radicals and w corresponding to the ratio of "fast" and "slow" mineralizing by-products formed by radicals driven mechanisms.

Figure 14 show the graphical representation of the simulation model for the conversion (Figure 14 A) and mineralisation (Figure 14 B) of IBP in correlation with experimental results at test catalyst concentrations 1.2 g·L^{-1}. The developed simulation model shows good agreement with the experimental results.
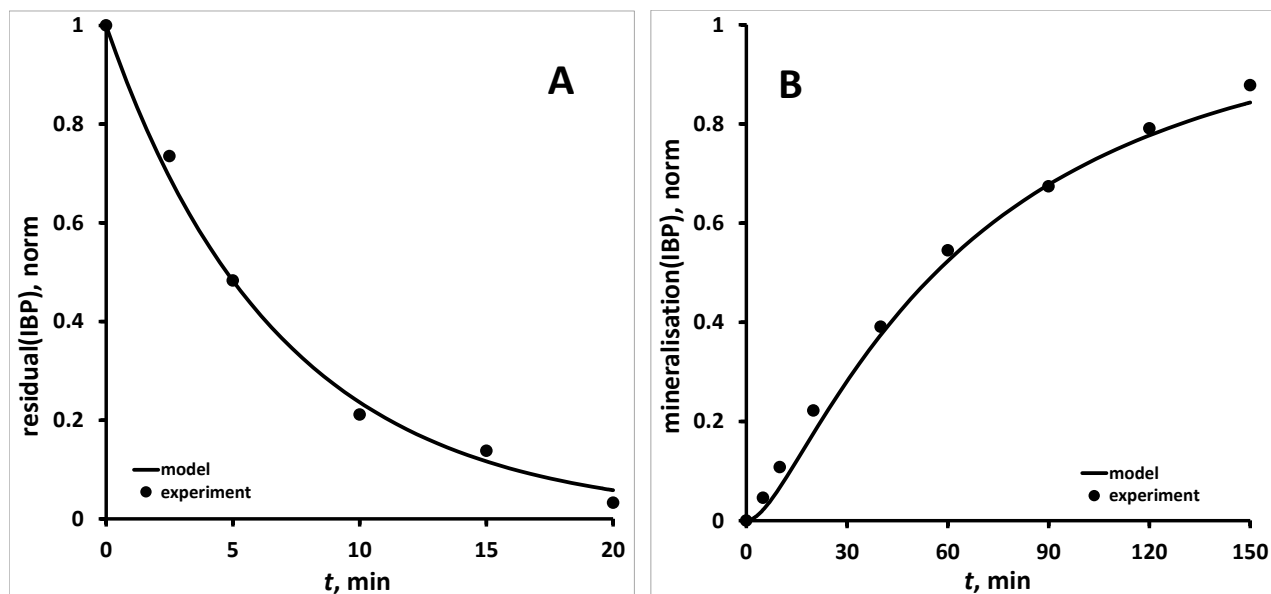
Figure 14 Graphical representation of the model simulation of photodegradation of IBP by UV-A/TiO$_2$ P25 process at 1.2 g·L^{-1} concentration of TiO$_2$ P25 A) conversion, B) mineralisation.

Good agreement between the simulation model and the experimental results is also shown by the values of the calculated RMSD for each pair of experimental/model data, which in the case of the simulation model for 1.2 g·L^{-1} TiO$_2$ P25 is ≤ 1, as shown in Table 10.

The observed small deviations between the model and the experimental results are probably a consequence of the simplicity of the model. The deviations of the model and the experimental results could be explained as the degradation of acidic degradation products resulting from the degradation of IBP. According to the literature, the influence of acidic degradation products on the behaviour of systems described by models can be easily illustrated by the formation and degradation of oxalic acid [222]. Oxalic acid is a known degradation product of various aromatic compounds [222] and has a relatively small reaction rate constant with HO•. Therefore, slow mineralizing degradation products such as oxalic acid determine the overall kinetics of the process. It is also important to note that "slow" mineralizing degradation products are not always represented by oxalic acid, but may also include other short-chain organic acids (e.g., formic acid, acetic acid, malonic acid) as well as non-acidic degradation products such as aldehydes and ketones [223].

The previously presented results indicate very good predictions of the simulation model, but the accuracy of the model needs to be verified against the experimental results of the UV-A/TiO$_2$ P25 process at other concentrations of the photocatalyst used. Therefore, the results of the model verification are presented in the following Figures 15 – 17. They show a graphical representation of the conversion and mineralisation using 0.4, 0.8, and 2.0 g·L^{-1} TiO$_2$ P25. As can be seen, slight discrepancies were observed mainly in the mineralisation processes at the lowest concentration of TiO$_2$ P25, while in other cases the agreement between the model and the experimental results is almost ideal, especially for IBP conversion. The better agreement of the model with the experimental results increases with increasing TiO$_2$ P25 concentration, where the degree of conversion and mineralisation is higher. Deviations from the model can be attributed to the fact that mathematical – mechanistic model does not consider the detailed degradation mechanisms of target pollutant. As previously mentioned, the degradation of CEC, as in the case of any aromatic water pollutant, would eventually lead to dearomatization producing ring-opened by-products, mainly aliphatic acids and/or aldehydes [224].
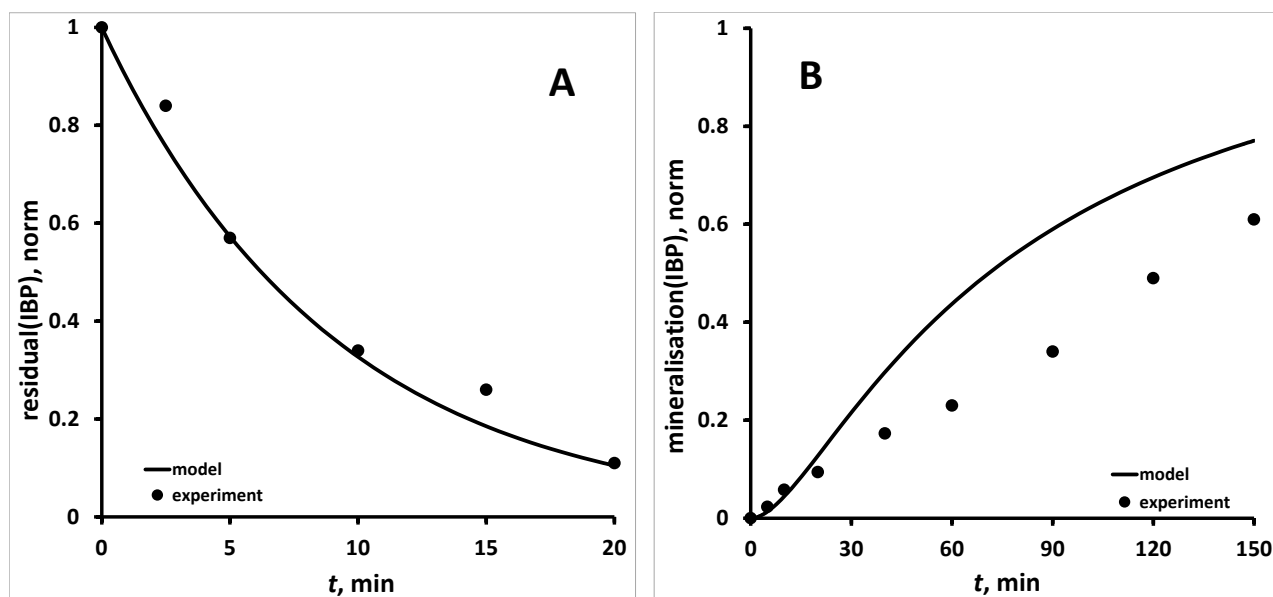
Figure 15 Graphical representation of the model simulation of photodegradation of IBP by UV-A/TiO$_2$ P25 process at 0.4 g·L^{-1} concentration of TiO$_2$ P25 A) conversion, B) mineralisation.
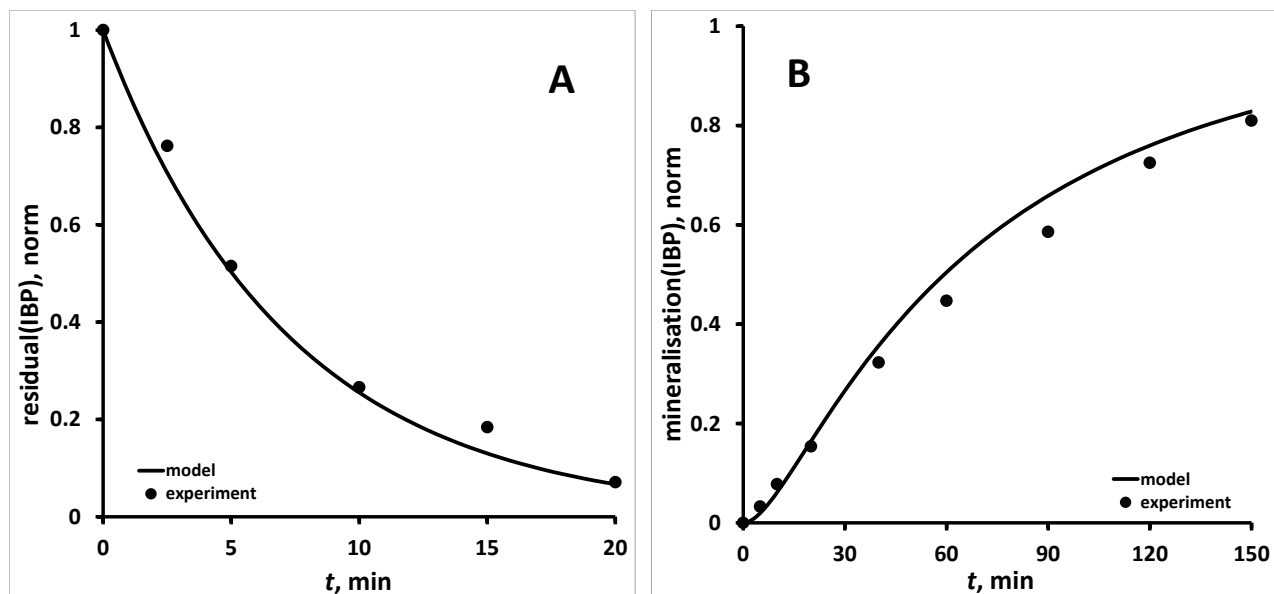
Figure 16 Graphical representation of the model simulation of photodegradation of IBP by UV-A/TiO$_2$ P25 process at 0.8 g·L^{-1} concentration of TiO$_2$ P25 A) conversion, B) mineralisation.
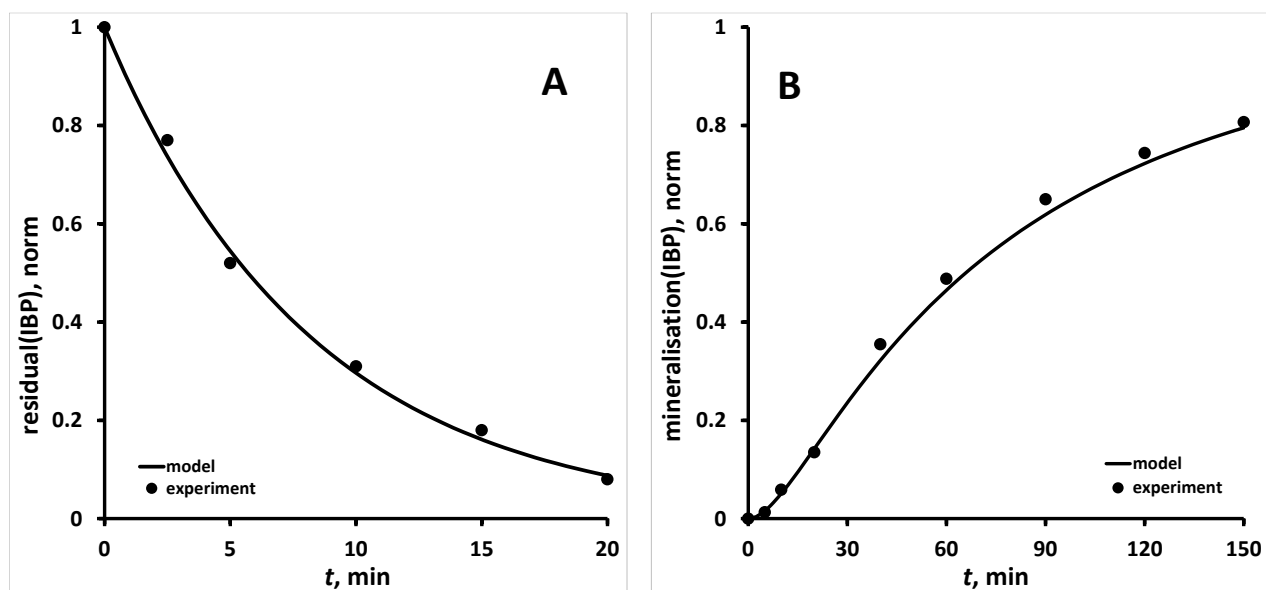
Figure 17 Graphical representation of the model simulation of photodegradation of IBP by UV-A/TiO$_2$ P25 process at 2.0 g·L^{-1} concentration of TiO$_2$ P25 A) conversion, B) mineralisation.

From Table 10 and the RSMD criteria, there is good agreement between the conversion and mineralisation data, with all results are ≤ 1.

Table 10 Values of calculated root mean square deviation for each of simulation model-experiment data pairs: ibuprofen conversion and mineralisation:

Compound	RMSD			
γ(TiO$_2$ P25), g·L^{-1}	0.4	0.8	1.2	2.0
conversion (IBP)	0.046	0.033	0.023	0.016
mineralisation (IBP)	0.145	0.037	0.025	0.019

Although the developed mathematical – mechanistic model predicts conversion and mineralisation very well, with the exception of the experiment of mineralisation at 0.4 g·L^{-1} of TiO$_2$ P25, additional experiments are required to collect data to fit the model to the range of pollutants studied. To achieve robustness of the developed mathematical – mechanistic model according to adsorption processes as a preliminary step of photocatalytic processes, and the distribution of degradation mechanisms using the two dominant radicals HO• and $O_2^{-•}$ the quantitative structure activity/property relationship methodology was applied in further step as described in sections 4.3. and 4.4.

4.3. Structural features of organic compounds promoting adsorption onto TiO₂ P25

The mathematical – mechanistic model previously developed for the photocatalytic degradation of ibuprofen is valid for the description of the mentioned process/pollutant system, but to be robust it should incorporate the structural features of the pollutant that influence the adsorption phenomenon, which is the main preliminary step in the photocatalysis process. For this purpose, a study influence of the structural features of organic compounds that promote adsorption onto TiO₂ P25 was carried out.

In the first step, RSM approach was used to study the influence of key adsorption process parameters on the extent of removal of 30 selected organic compounds given in Table 1. The extent of adsorption was described mathematically for each of the 30 organics by a quadratic polynomial eq. (79), with the adsorption coefficients K, L·g^{-1} selected as response Y. Experimentally determined K coefficients according to 3^2 FFD and calculated by eq. (80) are given in Table A1 and Table A2 in Appendix. The coefficients A, B, C, D, E and F (Table 11) obtained from quadratic polynomial equation for each compound were later used as the response in QSA/PR modelling. Therefore, with the aim of achieving the maximum accuracy of the models, as well as the highest possible similarity between them due to the transfer of obtained data in QSA/PR modelling, several transformations of original response Y (K, L·g^{-1}) were tested. The square root transformation function $Y' = \sqrt{Y}$ was selected as the best one. ANOVA was used to test all 30 RSM models for significance and model adequacy, while the accuracy was estimated using the determination coefficient R^2 and results are presented in Table A3 in Appendix. Briefly, obtained values of $0.9524 < R^2 < 0.9975$ and $0.0004 < p < 0.0338$ indicate that all models are accurate and significant.

Besides, the model terms whose coefficients are targeted as responses in QSA/PR modelling were tested for significance using F and p values obtained by ANOVA, along with values of coefficients A, B, C, D, E and F. It should be noted that the model and constituent model terms are considered significant if $p < 0.05$ [147, 169].

Table 11 The values of coefficients (A, B, C, D, E and F) and the significance of accompanied model terms in derived RSM models in a form of quadratic polynomial equations for 30 studied organics compounds using 3^2 FFD with square root transformation of the response ($Y' = \sqrt{Y}$):

Abbreviation	A (X_1)	p<0.05	B (X_1^2)	p<0.05	C (X_2)	p<0.05	D (X_2^2)	p<0.05	E (X_1*X_2)	p<0.05	F
ALC	0.008	0.342	0.117	0.002	-0.041	0.009	0.002	0.849	0.011	0.261	0.514
o-aminoBenzAc	0.095	0.004	-0.092	0.022	-0.020	0.998	0.000	0.188	0.002	0.914	0.657
AMX	0.118	0.004	0.280	0.002	-0.003	0.849	-0.026	0.382	-0.092	0.014	1.448
AZN	0.183	0.002	0.218	0.005	-0.072	0.022	0.026	0.428	-0.030	0.233	0.435
BenzAc	-0.256	0.010	0.275	0.035	-0.057	0.274	0.088	0.324	-0.147	0.068	0.303
BPA	-0.024	0.861	0.529	0.094	-0.721	0.011	-0.079	0.742	-0.782	0.015	2.804
CIP	-1.566	0.000	-0.493	0.009	0.120	0.081	-0.127	0.212	-0.022	0.720	2.665
DSL	0.197	0.013	0.377	0.010	-0.172	0.018	0.043	0.548	-0.170	0.032	0.969
DVF	0.887	0.002	0.945	0.007	-0.123	0.233	0.111	0.496	-0.229	0.109	0.238
DCP	0.039	0.074	0.007	0.795	0.103	0.006	-0.141	0.011	-0.019	0.363	0.523
DCF	-2.440	0.001	1.887	0.006	0.182	0.324	0.057	0.845	-0.202	0.365	1.021
1,4-DMB	-0.094	0.046	0.291	0.010	0.144	0.015	0.053	0.363	-0.187	0.013	0.544
2,6-DMP	0.037	0.044	0.136	0.006	-0.045	0.027	0.028	0.244	-0.014	0.363	0.329
DIU	-0.009	0.613	0.240	0.004	-0.042	0.083	0.056	0.142	-0.162	0.004	0.604
DPH	-0.133	0.001	0.048	0.093	-0.162	0.001	0.058	0.059	0.029	0.130	0.952
EE2	-0.291	0.002	0.294	0.009	-0.199	0.006	0.111	0.104	0.050	0.241	0.731
ETD	-0.709	0.001	0.394	0.029	-0.257	0.021	0.162	0.203	0.413	0.010	1.742
HCTZ	-0.329	0.003	0.350	0.010	0.095	0.071	0.077	0.290	-0.191	0.020	0.259
IBP	-0.329	0.004	0.247	0.040	0.005	0.906	0.039	0.624	0.109	0.119	0.606
p-MP	0.020	0.054	-0.089	0.004	0.016	0.084	-0.008	0.508	0.007	0.420	0.325
m-NP	-0.152	0.001	0.078	0.028	-0.151	0.001	0.028	0.242	0.062	0.021	0.601
p-NP	-0.025	0.060	-0.050	0.041	0.055	0.007	0.040	0.070	0.036	0.038	0.309
OMP	-0.223	0.013	0.044	0.588	-0.065	0.219	0.178	0.091	0.427	0.004	1.866
OXY	-0.638	0.001	-0.413	0.011	0.085	0.136	0.029	0.716	0.189	0.036	2.421
Ph	-0.008	0.057	0.013	0.069	-0.003	0.289	0.009	0.155	0.025	0.005	0.184
SalAc	-0.667	0.002	0.176	0.195	0.165	0.074	-0.053	0.649	-0.143	0.153	1.013
SZM	0.093	0.002	0.072	0.002	-0.101	0.008	0.034	0.019	-0.071	0.115	0.633
SA	0.029	0.019	-0.054	0.016	-0.107	0.000	0.026	0.102	0.047	0.009	0.736
TB	0.037	0.306	-0.433	0.004	-0.369	0.001	0.141	0.072	-0.065	0.173	2.037
VZD	0.283	0.010	0.242	0.062	-0.260	0.012	0.084	0.386	-0.021	0.747	1.335

The simultaneous influence of initial pH and γ(TiO$_2$ P25) parameters on the observed adsorption coefficients are represented graphically via 3D surface and contour plots in Figure 18 and Figure 19 for all 30 studied organic compound. In most RSM models, both process parameters are highly influential either through direct linear, direct quadratic or interaction effects, according to pertaining p values in Table A3, that is consequently reflected in the layout of 3D surface. However, there are some exceptions as can be seen from the Figure 18 and 19. For example, adsorption of p-MP and o-aminoBenzAc onto TiO$_2$ P25 is highly dependent on the initial pH value, while TiO$_2$ P25 loading has minor role. Although one could conclude the same for OXY, however TiO$_2$ P25 loading has been shown to be an important parameter over interaction model term. On the other hand, in the case of DCP, its adsorption strongly depends on TiO$_2$ P25 loading, while the initial pH value plays minor role in the process. Although no clear pattern can be discerned at first glance, it is clear that the structural features of the studied organics play a significant role in their adsorption onto TiO$_2$ P25, which is further investigates employing QSA/PR modelling on RSM coefficients A, B, C, D, E, and F.
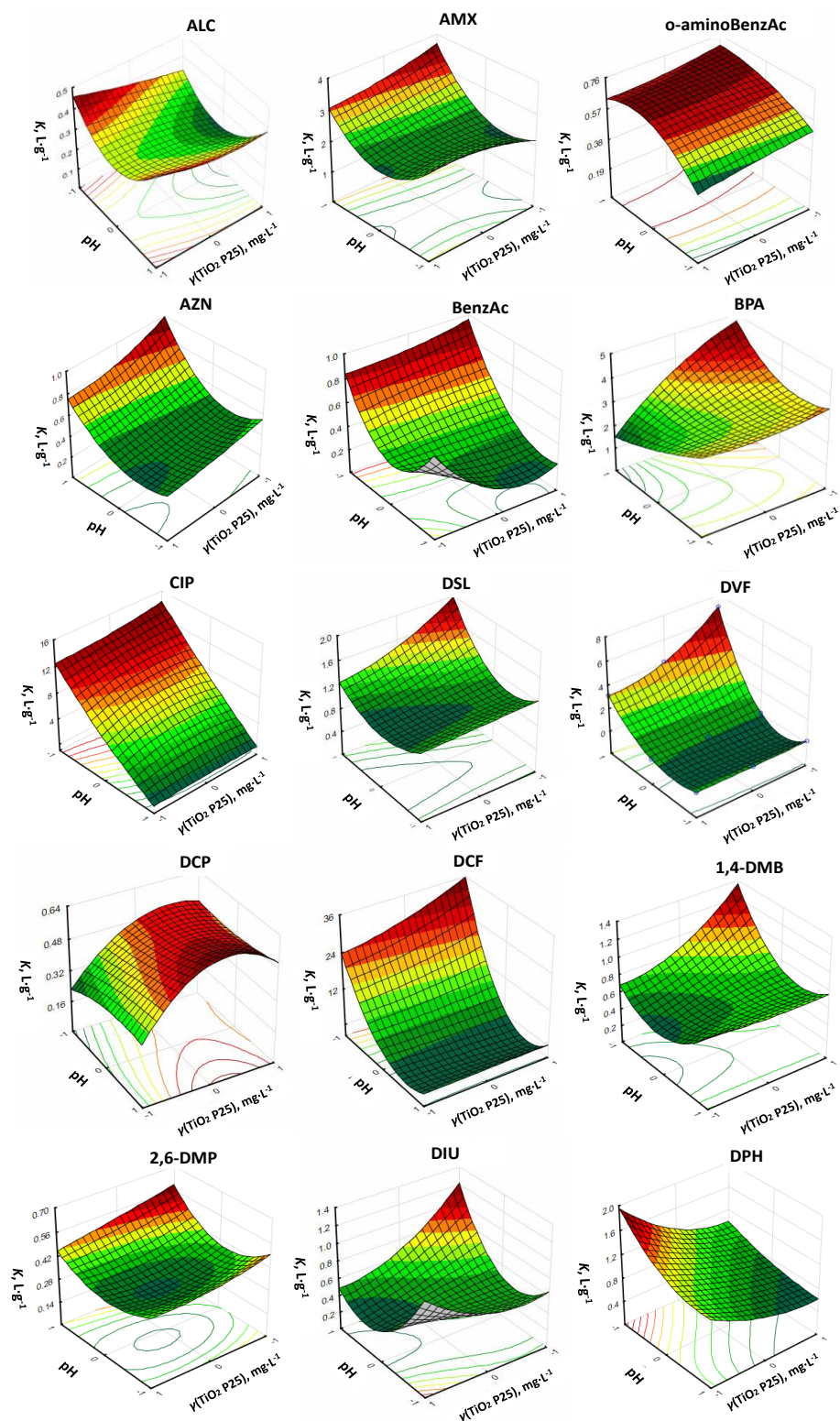
Figure 18 3D surface and contour diagrams showing the effect of mutual interactions between initial pH values (X_1) and TiO$_2$ P25 loading (X_2) on the response, adsorption constant (K, L·g^{-1}), for organic compounds (Table A3).
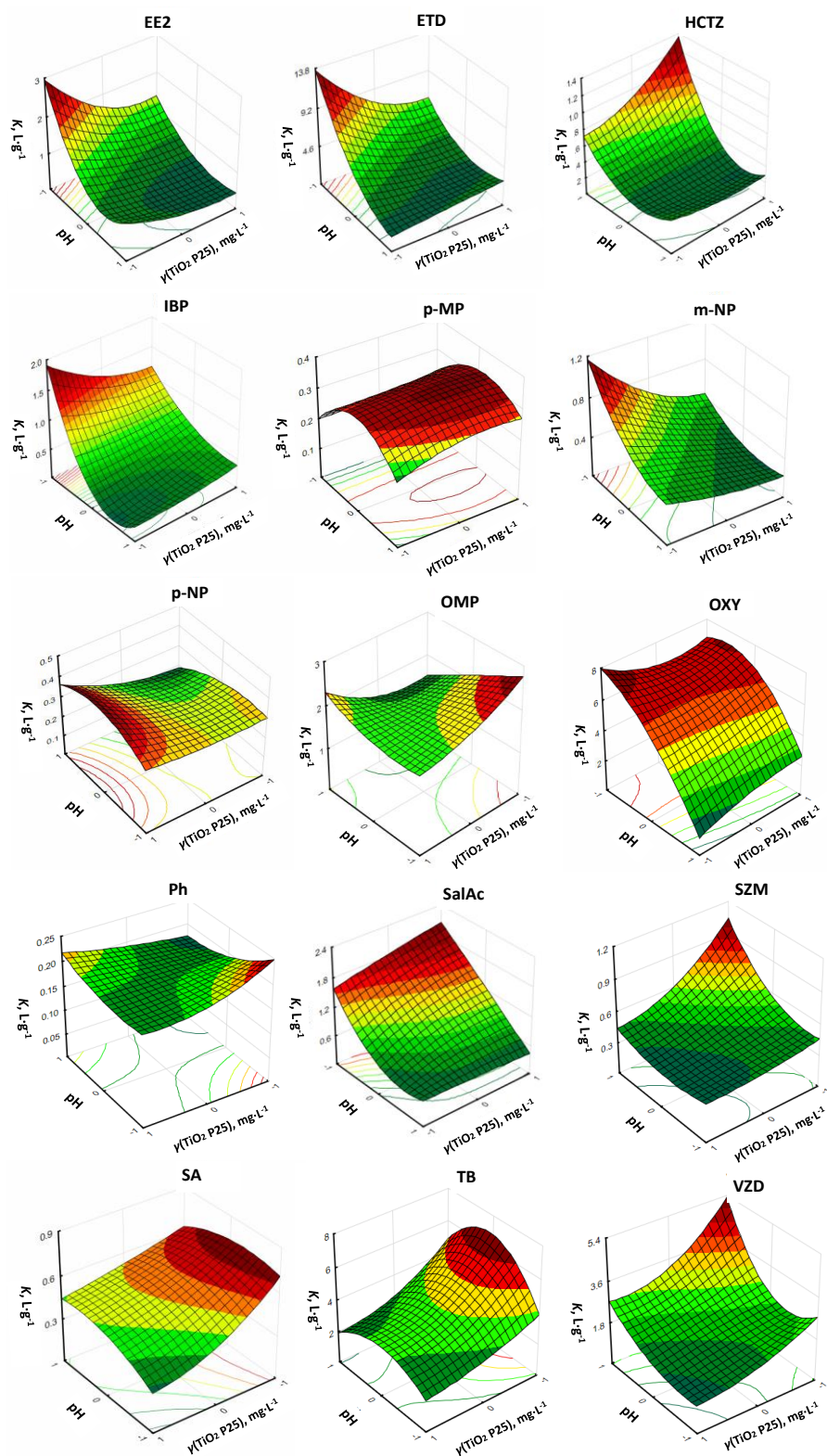
Figure 19 3D surface and contour diagrams showing the effect of mutual interactions between initial pH values (X_1) and TiO$_2$ P25 loading (X_2) on the response, adsorption constant (K, L·g^{-1}), for organic compounds (Table A3).

4.3.1. Modelling of RSM coefficients using QSA/PR methodology

QSA/PR methodology was applied in correlation of A, B, C, D, E and F coefficients obtained by RSM modelling with the structural characteristics of 30 studied organics. Firstly, the set of 30 organics was divided into a training set and test set, containing 25 and 5 compounds, respectively (Table 12). Then, QSA/PR modelling was performed for each RSM coefficient by building models with 1 to 5 variables for the training set to obtain the highest accuracy possible (according to R^2) whilst keeping the linearity of derived models. Accordingly, the descriptors included in the selected models for the training set must not to be cross-correlated (correlation coefficient $R_{ij} \leq 0.7$). The models with a higher number of variables were not considered due to the "rule of thumb"; the ratio of more than 1:5 between the number of variables included into the model vs. number of compounds included in the set for developing the model (i.e. training set) is not desirable [168, 185]. Preliminary modelling showed rather high accuracy in predicting almost all RSM coefficients; the exception was coefficient C. Accordingly, several transformations of the C value employing simple mathematical operations such as square root, log, ln, power of base 10, power of base e, etc. were tested. In general, the transformations are used to narrow the range of responses, which results with improved correlation upon modelling [227]. According to the results after the applied transformations, the highest accuracy was obtained in the case of 10^C transformation, thus, it was kept in the further modelling.

Table 12 Original and transformed values of coefficients of RSM models and splitting of studied organics into training and test set for QSA/PR modelling:

Compound	abbreviation	shifted and transformed values					
		A	B	10^C	D	E	F
training set: 25 compounds							
Alachlor	ALC	0.008	0.117	0.910	0.002	0.011	0.514
o-Aminobenzoic acid	*o*-aminoBenzAc	0.095	-0.092	0.955	0.000	0.002	0.657
Amoxicillin	AMX	0.118	0.280	0.993	-0.026	-0.092	1.448
Atrazine	AZN	0.183	0.218	0.847	0.026	-0.030	1.448
Benzoic acid	BenzAc	-0.256	0.275	0.877	0.088	-0.147	0.303
Bisphenol A	BPA	-0.024	0.529	0.190	-0.079	-0.782	2.804
Ciprofloxacin	CIP	-1.566	-0.493	1.318	-0.127	-0.022	2.665
Desvenlafaxine	DVF	0.887	0.945	0.753	0.111	-0.229	0.238
2,4-Dichlorophenol	DCP	0.039	0.007	1.268	-0.141	-0.019	0.523
Diclofenac	DCF	-2.440	1.887	1.521	0.057	-0.202	1.021
1,4-Dimethoxybenzene	1,4-DMB	-0.094	0.290	1.390	0.050	-0.190	0.544
2,6-Dimethoxyphenol	2,6-DMP	0.037	0.136	0.902	0.028	-0.014	0.329
Diuron	DIU	-0.009	0.240	0.908	0.056	-0.162	0.604
17α-Ethinylestradiol	EE2	-0.152	0.294	0.632	0.111	0.050	0.731
Etodolac	ETD	-0.709	0.394	0.553	0.162	0.413	1.742
p-Methoxyphenol	*p*-MP	0.020	-0.089	1.038	-0.008	0.007	0.325
m-Nitrophenol	*m*-NP	-0.223	0.078	0.706	0.178	0.062	0.601
p-Nitrophenol	*p*-NP	-0.025	-0.050	1.135	0.040	0.036	0.309
Omeprazole HCl	OMP	0.283	0.044	0.861	0.028	0.427	1.866
Oxytetracycline	OXY	-0.638	-0.413	1.216	0.029	0.189	2.421
Phenol	Ph	-0.008	0.013	0.993	0.009	0.025	0.184
Salicylic acid	SalAc	-0.667	0.176	1.462	-0.053	-0.143	1.013
Sulfanilic acid	SA	0.029	-0.054	0.782	0.026	0.047	0.736
Tobramycin	TB	0.037	-0.433	0.428	0.141	-0.065	2.037
Vilazodone HCl	VZD	-0.291	0.242	0.550	0.084	-0.021	1.335
test set: 5 compounds							
Desloratadine	DSL	-0.133	0.048	0.689	0.058	0.029	0.952
Donepezil HCl	DPH	0.197	0.377	0.673	0.043	-0.170	0.969
Hydrochlorothiazide	HCTZ	0.093	0.072	0.793	0.034	-0.071	0.633
Ibuprofen	IBP	-0.329	0.247	1.012	0.039	0.109	0.606
Simazine	SZM	-0.329	0.350	1.245	0.077	-0.191	0.259

The values of the statistical parameters R^2, Q^2, F, p, s and S_{PRESS} determining the performance of the selected 1-, 2-, 3-, 4- and 5- variable QSA/PR models for all responses (A, B, 10^C, D, E, and F) divided into the training and test sets are summarized in Table 13.

Table 13 Statistical evaluation of QSA/PR models for predicting coefficients of RSM models (A, B, C, D, E and F) derived for training set (25 compounds) and applied on test set (5 compounds):

Model	\multicolumn{6}{c}{Training set}	\multicolumn{3}{c}{Test set}
	n	R^2	Q^2	F	p	s	S_{PRESS}	n	R^2	F	s
A coefficient
1-variabe		0.050	0.602	1.216	0.281	0.635	0.211		0.069	4.298	0.351
2-variable		0.620	0.513	17.888	< 0.0001	0.411	0.465		0.111	4.498	0.413
3-variable	25	0.767	0.376	23.136	< 0.0001	0.329	0.539	5	0.478	7.660	0.308
4-variable		0.884	0.808	37.689	< 0.0001	0.239	0.306		0.536	4.623	0.263
5-variable		0.894	0.836	32.673	< 0.0001	0.231	0.290		0.181	4.889	0.415
B coefficient
1-variabe		0.306	0.113	10.153	0.0041	0.398	0.450		0.019	4.077	0.110
2-variable		0.794	0.736	42.436	< 0.0001	0.222	0.251		0.006	4.024	0.100
3-variable	25	0.885	0.857	53.795	< 0.0001	0.170	0.189	5	0.030	4.124	0.214
4-variable		0.941	0.913	80.041	< 0.0001	0.124	0.151		0.132	4.610	0.602
5-variable		0.966	0.743	42.282	< 0.0001	0.151	0.266		0.053	5.557	0.063
Transformed C coefficient; 10^C
1-variabe		0.327	0.245	11.188	0.0028	0.273	0.289		0.500	8.006	0.078
2-variable		0.388	0.269	6.975	0.0045	0.266	0.291		0.500	8.006	0.082
3-variable	25	0.576	0.444	9.525	0.0004	0.227	0.260	5	0.003	4.012	0.114
4-variable		0.674	0.577	10.345	0.0001	0.204	0.232		0.122	4.553	0.386
5-variable		0.751	0.566	11.342	< 0.0001	0.184	0.241		0.676	12.340	0.088
D coefficient
1-variabe		0.334	0.225	11.529	0.0025	0.066	0.072		0.181	4.884	0.013
2-variable		0.450	0.347	9.006	0.0014	0.062	0.067		0.181	4.884	0.105
3-variable	25	0.629	0.477	11.850	0.0001	0.052	0.062	5	0.538	4.658	0.028
4-variable		0.797	0.730	20.386	< 0.0001	0.039	0.045		0.682	16.220	0.056
5-variable		0.893	0.797	31.519	< 0.0001	0.029	0.040		0.810	9.995	0.051
E coefficient
1-variabe		0.240	0.063	7.268	0.0129	0.199	0.221		0.826	22.959	0.033
2-variable		0.386	0.207	6.919	0.0047	0.183	0.207		0.146	4.686	0.090
3-variable	25	0.695	0.557	16.007	< 0.0001	0.132	0.159	5	0.236	5.234	0.405
4-variable		0.714	0.679	12.514	< 0.0001	0.131	0.138		0.627	10.714	0.077
5-variable		0.813	0.389	14.180	< 0.0001	0.115	0.196		0.670	19.507	0.029
F coefficient
1-variabe		0.712	0.654	57.013	0.0001	0.436	0.479		0.036	4.147	0.248
2-variable		0.830	0.757	53.850	< 0.0001	0.343	0.410		0.277	5.535	0.240
3-variable	25	0.878	0.767	50.699	< 0.0001	0.297	0.411	5	0.346	6.114	0.146
4-variable		0.933	0.902	70.421	< 0.0001	0.225	0.273		0.293	5.657	0.212
5-variable		0.953	0.943	77.907	< 0.0001	0.193	0.214		0.284	5.585	0.166

Furthermore, a comparative study of the *R* values (correlation coefficient of regression) for the training and test sets *vs*. the number of variables in selected QSA/PR models are shown in Figure 20.
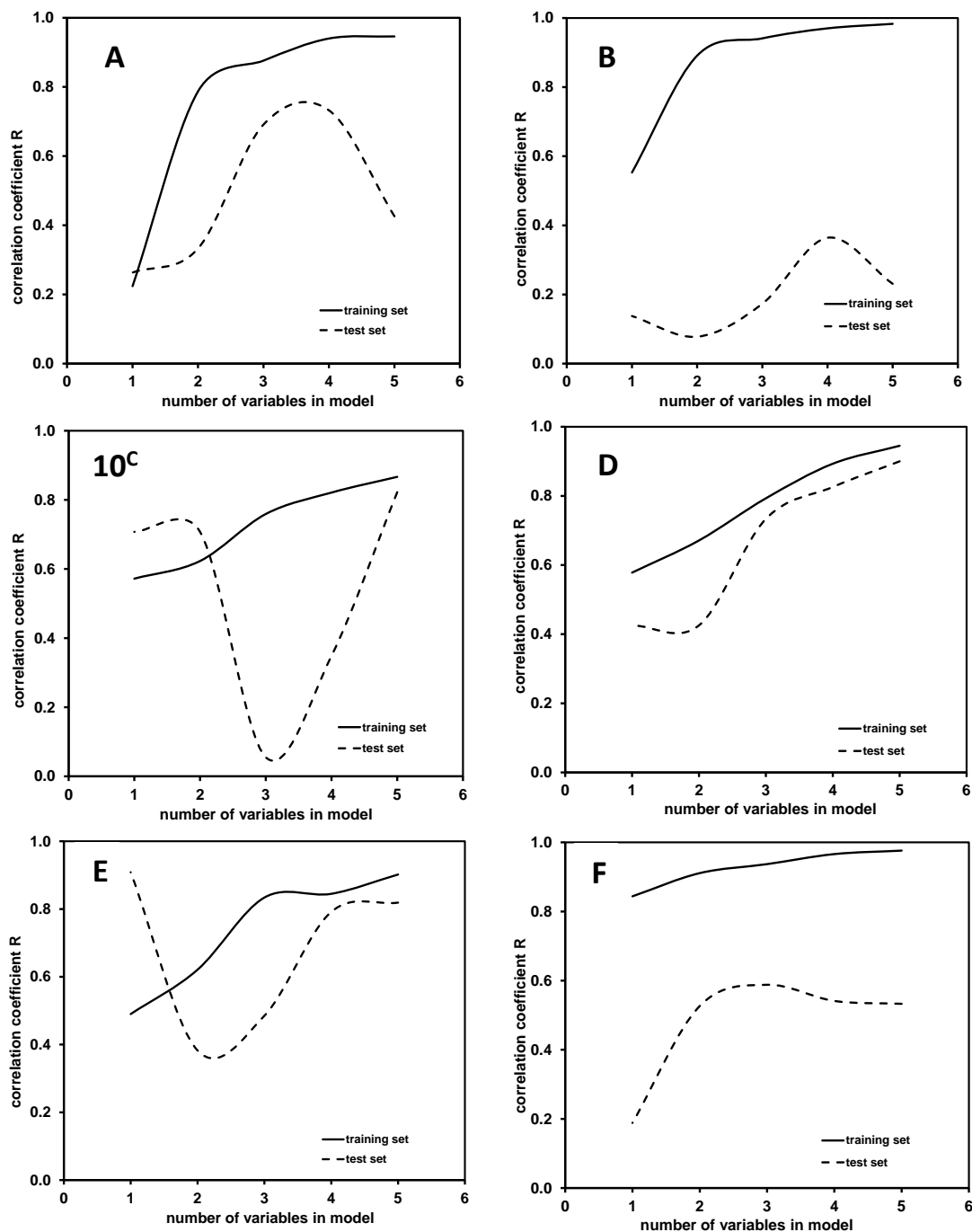
Figure 20 Comparison of correlation coefficients obtained for training and test set by 1 – 5 variable models for modelling of A, B, C, D, E and F coefficients of the RSM models.

As can be seen from the results presented in Figure 20 the R values for the models developed for the training set increase with the model enlargement, i.e., inclusion of new variables. A similar trend can be mostly observed for the R values for the test set, however, up to the certain number of variables, where levelling off occurs as higher dimension models are overfitted across this number of variables. Thus, in the case of coefficients A and B, 4-variable models were selected as the best, while for coefficients C (i.e., their value is transformed into 10^C), D and E, 5-variables were selected as the best. There is a possibility that higher dimensional models (over 5 variables) might show better predictability in the cases of those three responses, however, due to the "rule of thumb" that is not tested. Finally, in the case of the F coefficient, the 3-variable model was selected as the best. These selected models were further validated over the Leave-Many-Out (LMO) technique [185, 187] and "Y-scrambling" test [188, 189]; graphical representations of those two tests for coefficients A, B, C (i.e. 10^C), D, E and F of RSM model (79) are provided Figures 21 – 26.
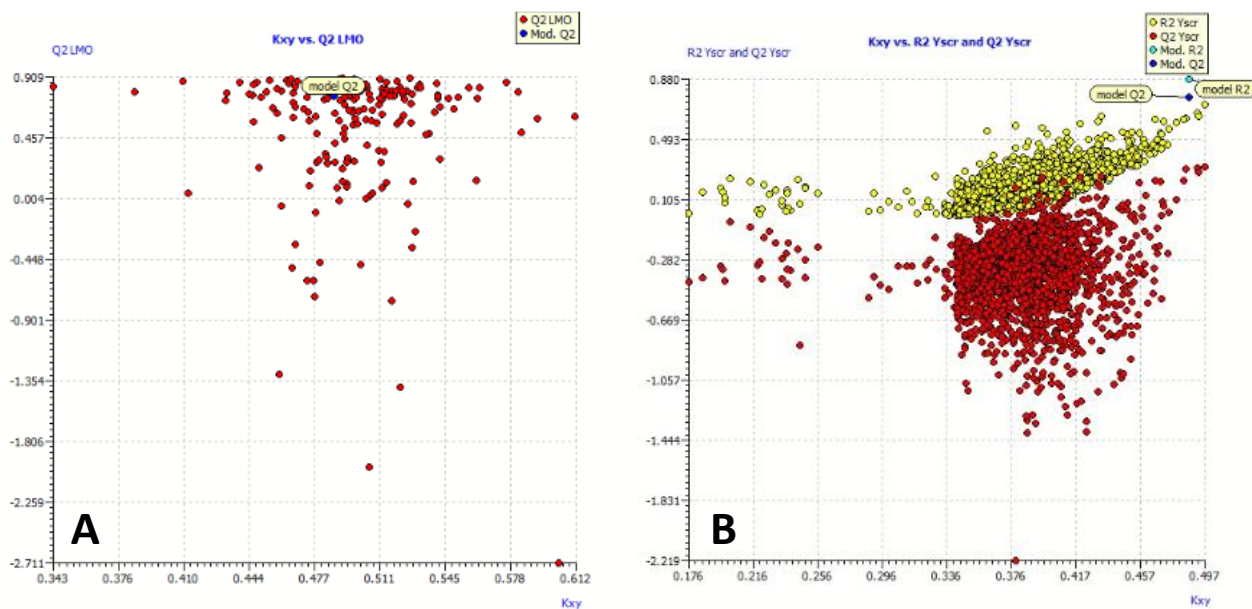
Figure 21 Scatter plots of LMO (A) and Y-scrambling (B) model compared to the QSA/PR models; 4-variable model predicting coefficient A from RSM model (79).
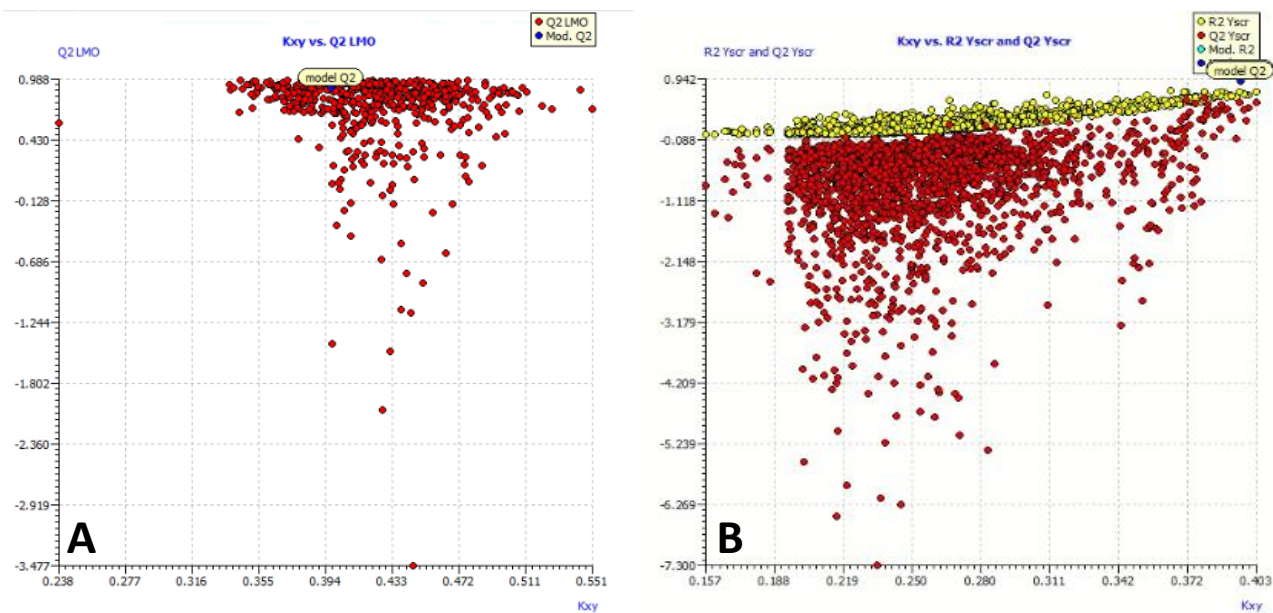
Figure 22 Scatter plots of LMO (A) and Y-scrambling (B) model compared to the QSA/PR models; 4-variable model predicting coefficient B from RSM model (79).
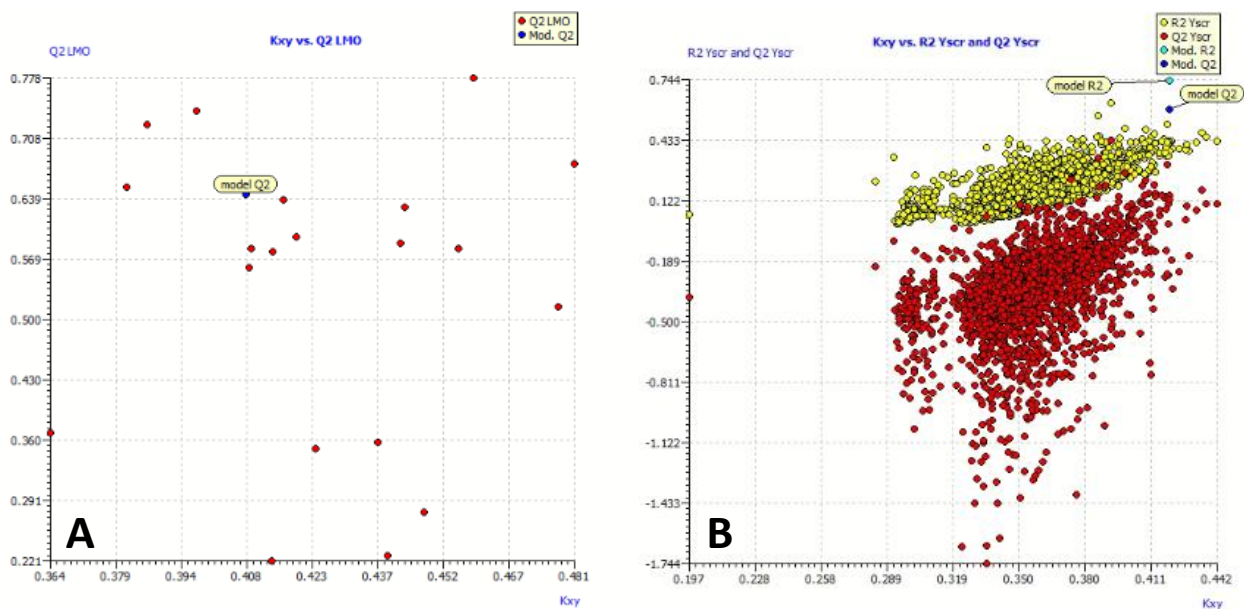
Figure 23 Scatter plots of LMO (A) and Y-scrambling (B) model compared to the QSA/PR models; 5-variable model predicting coefficient C (i.e., its transformed value 10^C) from RSM model (79).
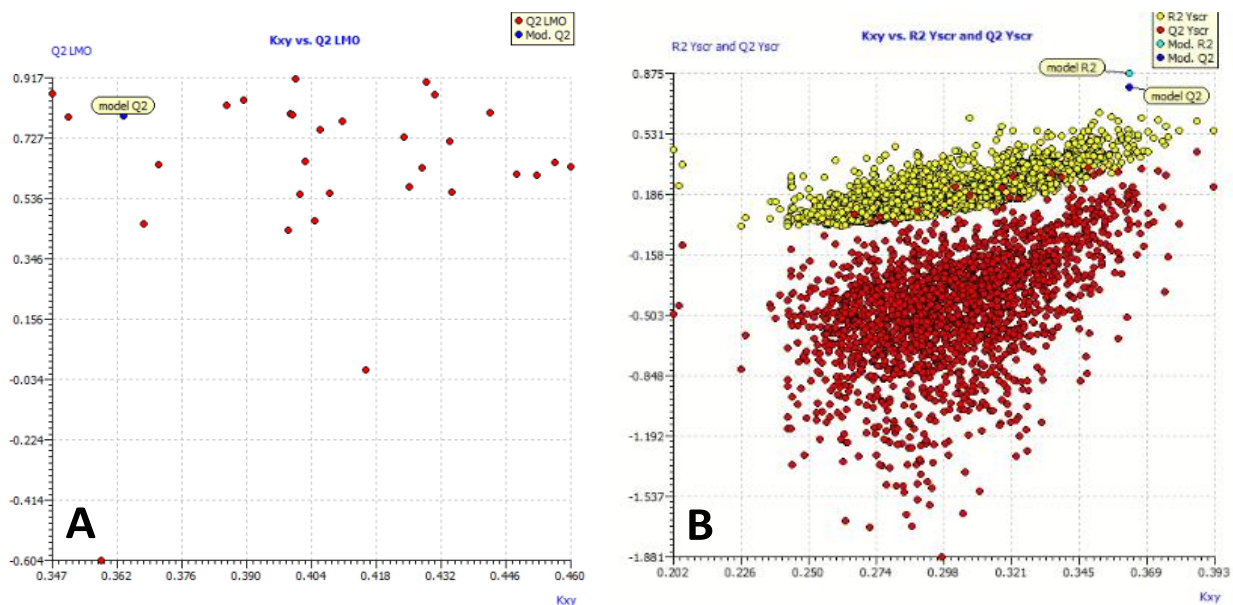
Figure 24 Scatter plots of LMO (A) and Y-scrambling (B) model compared to the QSA/PR models; 5-variable model predicting coefficient D from RSM model (79).
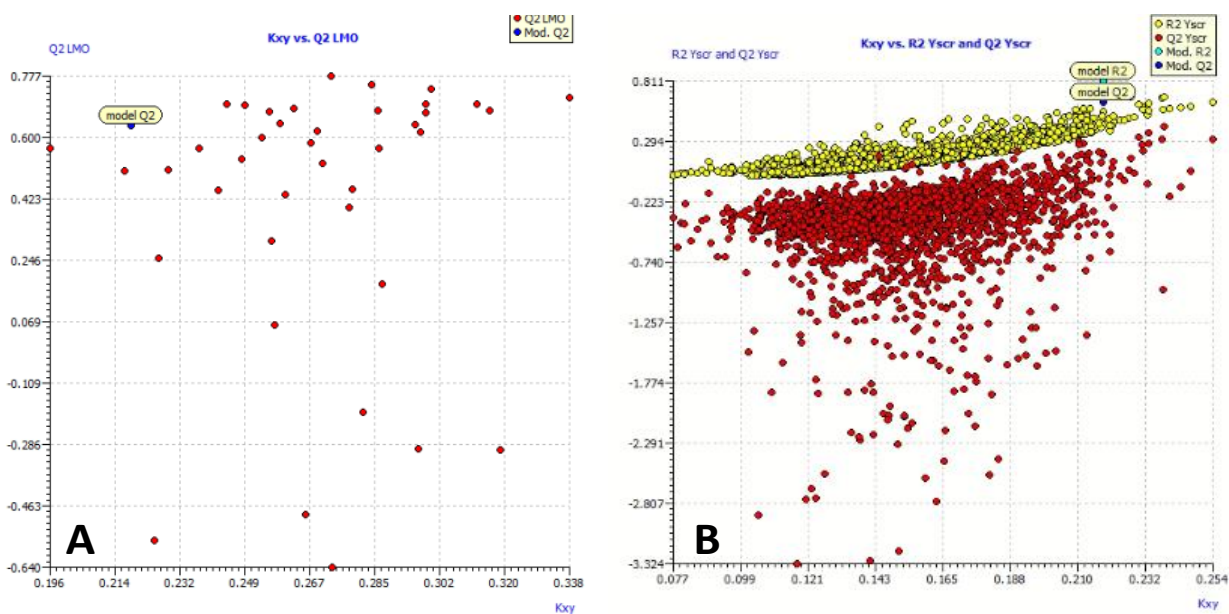
Figure 25 Scatter plots of LMO (A) and Y-scrambling (B) model compared to the QSA/PR models; 5-variable model predicting coefficient E from RSM model (79).
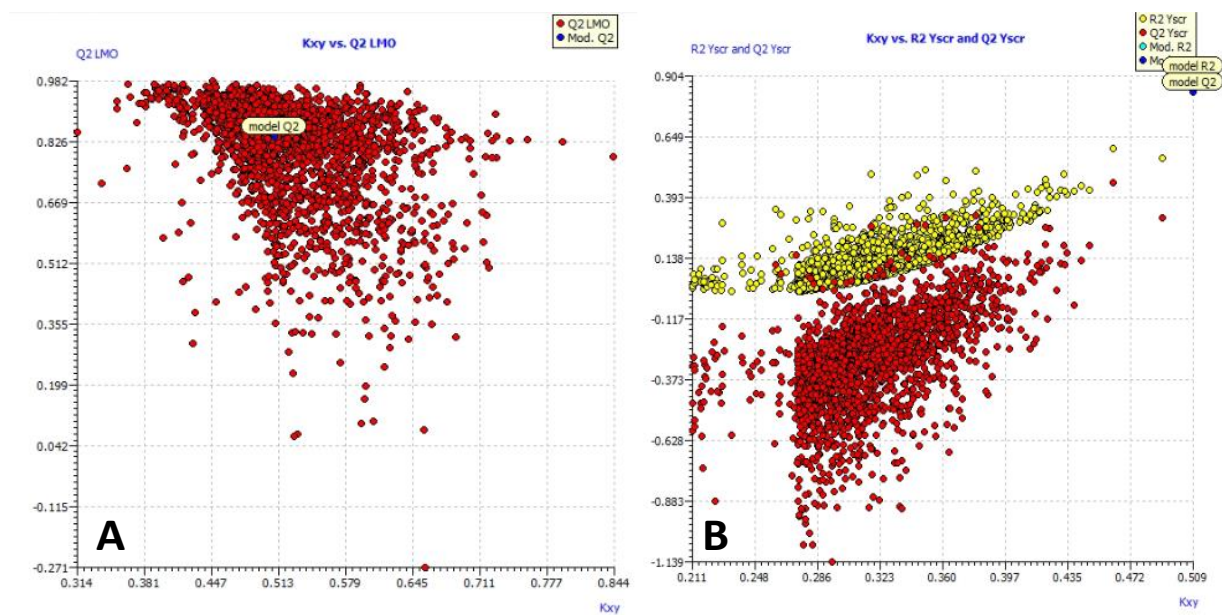
Figure 26 Scatter plots of LMO (A) and Y-scrambling (B) model compared to the QSA/PR models; 3-variable model predicting coefficient F from RSM model (79).

As can be seen from the scatter plots Figures 21 – 26 the Q^2_{LMO} values are close to Q^2_{LOO} values of selected models for coefficients A, B and F, and in these cases, the Q^2_{LMO} values are not widely scattered, which indicates on the validity of derived QSA/PR models. However, for the other three chosen responses: 10^C, D and F this is not the case; Q^2_{LMO} values are rather scattered. On the other hand, the results of the "Y-scrambling" test, in which the R^2 and Q^2_{LOO} values obtained from the selected models are significantly higher than the calculated $R^2_{Y-SCRAMBLING}$ and $Q^2_{Y-SCRAMBLING}$ values, support the validity of all selected model. All fitting and internal validation criteria values for all QSA/PR models selected as the best for each of responses (A, B, 10^C, D, E and F) are summarized in Table 14.

Table 14 Values of fitting and internal validation criteria of selected best models predicting A, B, 10^C, D, E and F responses:

Fitting criteria	A 4 variable model	B 4 variable model	10^C 5 variable model	D 5 variable model	E 5 variable model	F 3 variable model
R^2	0.865	0.940	0.744	0.875	0.811	0.904
R^2_{adj}	0.843	0.928	0.691	0.843	0.772	0.890
R^2-R^2_{adj}	0.022	0.012	0.053	0.033	0.039	0.014
LOF	0.084	0.027	0.054	0.002	0.018	0.101
$RMSE_{tr}$	0.213	0.112	0.155	0.028	0.089	0.242
MAE_{tr}	0.156	0.088	0.126	0.023	0.067	0.201
CCC_{tr}	0.928	0.969	0.853	0.934	0.896	0.950
Internal validation criteria						
Q^2_{loo}	0.825	0.910	0.630	0.798	0.636	0.841
R^2-Q^2_{loo}	0.040	0.029	0.149	0.077	0.175	0.063
Q^2_{LMO}	0.769	0.790	0.519	0.708	0.569	0.818
$PRESS_{cv}$	1.765	0.469	1.133	0.031	0.460	2.428
$RMSE_{cv}$	0.243	0.137	0.194	0.035	0.124	0.312
MAE_{cv}	0.187	0.111	0.161	0.030	0.088	0.251
CCC_{cv}	0.900	0.957	0.763	0.894	0.804	0.916
R^2Y_{scr}	0.135	0.166	0.171	0.206	0.172	0.124
Q^2Y_{scr}	-0.497	-0.902	-0.359	-0.462	-0.422	-0.288

The performance of the models selected as the best for each of targeted responses, when applied for all 30 organic compounds selected, is shown in Figure 27, while the model layouts are presented via equations (82) – (87), along with the values of corresponding statistical parameters determining their accuracy and significance.

A = -5.914(±3.277)×**SpMax_B(i)**-2.174(±0.489)×**H8m**-1.076(±0.420)×**CATS2D_05_NL**+
1.152(±0.392)×**F04[C-N]**+5.344(±3.033)   (82)

$(n = 30; R^2 = 0.875; s = 0.225; F = 43.496; p < 0.0001; Q^2 = 0.830; S_{PRESS} = 0.261)$

B = 0.594(±0.451)×**GATS2s**+0.595(±0.258)×**Mor16i**+1.753(±0.345)×**R8m**+0.435(±0.314)×
CATS2D_08_DA-0.319(±0.251)   (83)

$(n = 30; R^2 = 0.874; s = 0.164; F = 43.460; p < 0.0001; Q^2 = 0.791; S_{PRESS} = 0.211)$

10^C = 0.999(±0.375)×**RDF055m**-0.217(±0.165)×**Mor29m**+0.444(±0.303)×**Mor17v** -
1.019(±0.770)×**H1e**+0.464(±0.333)× **cRo5** +1.150(±0.623)   (84)

$(n = 30; R^2 = 0.743; s = 0.173; F = 13.940; p < 0.0001; Q^2 = 0.595; S_{PRESS} = 0.217)$

D = -0.014(±0.096)×**SpMaxA_AEA(ri)**+0.129(± 0.060)×**Mor19s**-0.026(±0.069) ×
CATS2D_06_DL-0.099(± 0.070)×**B03[N-N]**-0.109(±0.079)×**F03[O-Cl]**+0.040(±0.066)   (85)

$(n = 30; R^2 = 0.598; s = 0.051; F = 7.144; p = 0.0003; Q^2 = 0.305; S_{PRESS} = 0.067)$

E=-0.222(±0.158)×**CIC4**-0.171(±0.099)×**JGI7**-0.370(±0.154)×**C-024**+0.535(±0.173)×
CATS2D_07_AA+0.550(±0.197)×**CATS2D_06_NL**+0.221(±0.104)   (86)

$(n = 30; R^2 = 0.810; s = 0.100; F = 20.375; p < 0.0001; Q^2 = 0.633; S_{PRESS} = 0.139)$

F=-0.879(±0.516)×**Mor04p**+2.142(±0.535)×**CATS2D_06_DL**+0.615(±0.308)×**B08[C-N]**+
0.377(±0.173)   (87)

$(n = 30; R^2 = 0.820; s = 0.335; F = 39.395; p < 0.0001; Q^2 = 0.746; S_{PRESS} = 0.397)$

The descriptive statistical data of the coefficients included in QSA/PR models (82) – (87) were assessed it as well (Table 15) can be clearly seen that all included model terms are significant (p_T < 0.05). The correlation matrices for all 6 models are provided (Table 16) and clearly show that none of the descriptor pairs has $R_{ij} > 0.7$, i.e., the models are linear.

Table 15 Descriptive statistical data of coefficients included in best QSA/PR models predicting A, B, C (i.e., transformed value 10^C), D, E and F for entire set of organic compounds:

Response / model	descriptor	Coef.	Stdev	95% Conf	t-ratio	*p**
A 4-variable	Constant	5.348	1.473	3.034	3.632	0.001
	SpMax_B(i)	-5.918	1.591	3.278	-3.720	0.001
	H8m	-2.174	0.237	0.489	-9.161	0.000
	CATS2D_05_NL	-1.076	0.204	0.420	-5.281	0.000
	F04[C-N]	1.152	0.191	0.392	6.049	0.000
B 4-variable	Constant	-0.318	0.121	0.250	-2.616	0.014
	GATS2s	0.445	0.164	0.338	2.710	0.011
	Mor16i	0.416	0.087	0.180	4.752	0.0001
	R8m+	10.191	0.973	2.006	10.464	0.000
	CATS2D_08_DA	-0.217	0.076	0.157	-2.847	0.008
10^C 5-variable	Constant	1.528	0.256	0.527	5.981	0.000
	RDF055m	1.026	0.175	0.361	5.871	0.000
	Mor29m	-0.306	0.119	0.246	-2.563	0.017
	Mor17v	-0.367	0.122	0.252	-2.998	0.006
	H1e	-1.241	0.301	0.620	-4.129	0.000
	cRo5	0.297	0.147	0.304	2.015	0.049
D 5-variable	Constant	0.165	0.044	0.091	3.736	0.001
	SpMaxA_AEA(ri)	-0.410	0.114	0.235	-3.603	0.001
	Mor19s	0.091	0.039	0.080	2.353	0.027
	CATS2D_06_DL	-0.095	0.037	0.076	-2.595	0.016
	B03[N-N]	-0.134	0.029	0.061	-4.555	0.000
	F03[O-Cl]	-0.128	0.033	0.068	-3.903	0.001
E 5-variable	Constant	0.221	0.050	0.104	4.399	0.000
	CIC4	-0.119	0.041	0.084	-2.899	0.008
	JGI7	-7.133	2.004	4.136	-3.560	0.002
	C-024	-0.046	0.009	0.019	-4.955	0.000
	CATS2D_07_AA	0.268	0.042	0.087	6.382	0.000
	CATS2D_06_NL	0.275	0.048	0.099	5.764	0.000
F 3-variable	Constant	0.377	0.084	0.173	4.483	0.000
	Mor04p	-0.340	0.097	0.200	-3.499	0.002
	CATS2D_06_DL	0.357	0.043	0.089	8.227	0.000
	B08[C-N]	0.615	0.150	0.308	4.106	0.000

Table 16 Correlation matrix of descriptors included in best QSA/PR models predicting A, B, C (i.e., transformed value 10^C), D, E and F for entire set of organic compounds (cross-correlation R_{ij} < 0.7):

A coefficient / 4-variable model			
	SpMax_B(i)	H8m	CATS2D_05_NL	F04[C-N]
SpMax_B(i)	1	0.039	0.311	0.464
H8m	0.039	1	0.207	0.348
CATS2D_05_NL	0.311	0.207	1	0.033
F04[C-N]	0.464	0.348	0.033	1

B coefficient / 4-variable model			
	GATS2s	Mor16i	R8m+	CATS2D_08_DA
GATS2s	1	0.557	0.142	0.123
Mor16i	0.557	1	0.101	0.471
R8m+	0.142	0.101	1	0.006
CATS2D_08_DA	0.123	0.471	0.006	1

C coefficient (over transformed value 10^C) / 5-variable model				
	RDF055m	Mor29m	Mor17v	H1e	cRo5
RDF055m	1	0.106	0.190	0.664	0.470
Mor29m	0.106	1	0.127	0.184	0.033
Mor17v	0.190	0.127	1	0.454	0.013
H1e	0.664	0.184	0.454	1	0.386
cRo5	0.470	0.033	0.013	0.386	1

D coefficient / 5-variable model				
	SpMaxA_AEA(ri)	Mor19s	CATS2D_06_DL	B03[N-N]	F03[O-Cl]
SpMaxA_AEA(ri)	1	0.408	0.559	0.393	0.127
Mor19s	0.408	1	0.061	0.199	0.026
CATS2D_06_DL	0.559	0.061	1	0.134	0.200
B03[N-N]	0.393	0.199	0.134	1	0.089
F03[O-Cl]	0.127	0.026	0.200	0.089	1

E coefficient / 5-variable model				
	CIC4	JGI7	C-024	CATS2D_07_AA	CATS2D_06_NL
CIC4	1	0.109	0.066	0.088	0.029
JGI7	0.109	1	0.066	0.108	0.213
C-024	0.066	0.066	1	0.183	0.034
CATS2D_07_AA	0.088	0.108	0.183	1	0.093
CATS2D_06_NL	0.029	0.213	0.034	0.093	1

F coefficient / 3-variable model		
	Mor04p	CATS2D_06_DL	B08[C-N]
Mor04p	1	0.535	0.277
CATS2D_06_DL	0.535	1	0.374
B08[C-N]	0.277	0.374	1

As can be seen in Figure 27 that presents observed and predicted values of RSM coefficients, the points or point clusters in all six diagrams are in good agreement to the regressed diagonal lines, suggesting the rather high accuracy of derived QSA/PR models.
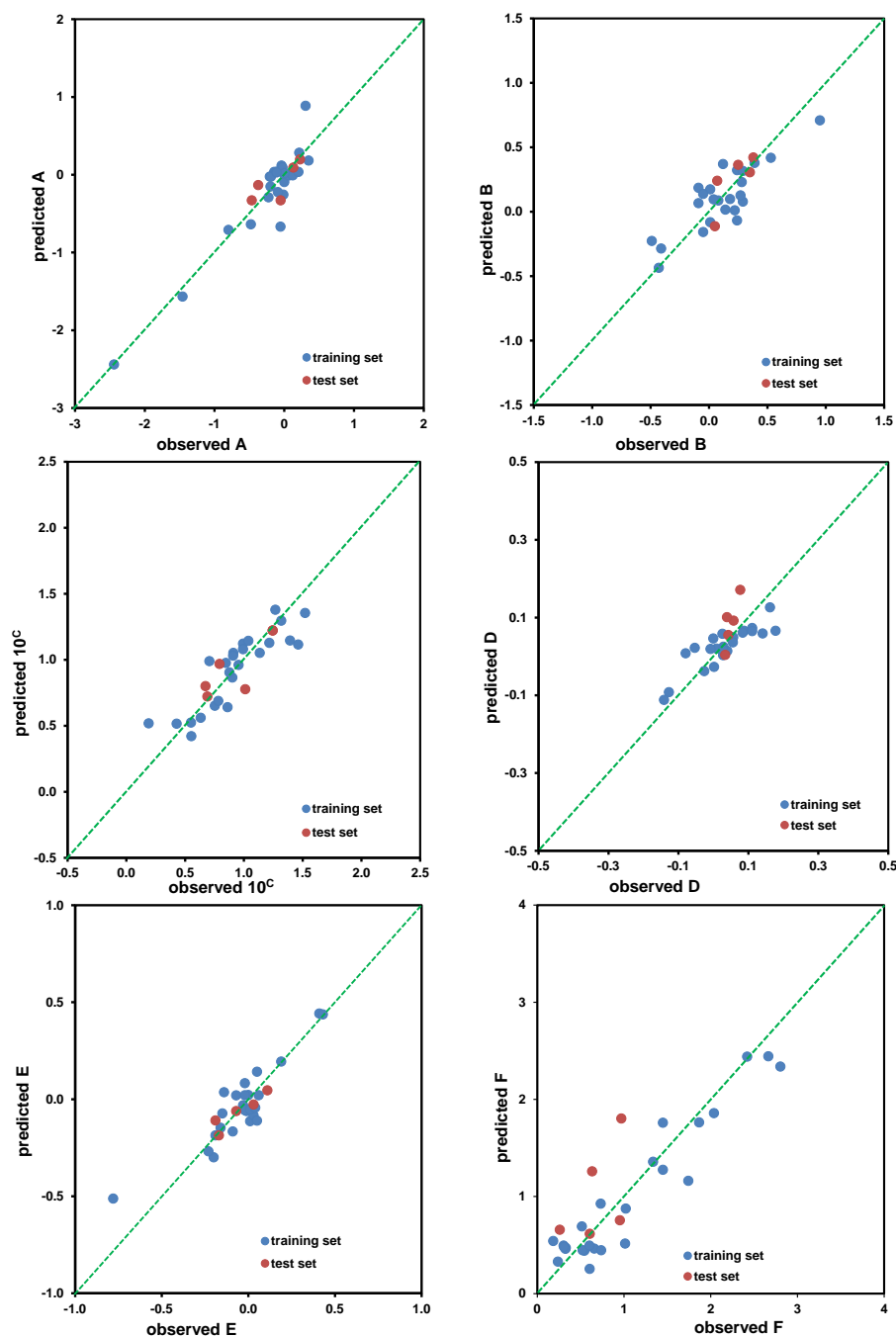
Figure 27 The observed vs. predicted values for A, B, C (in transformed 10^C form), D, E and F coefficients of RSM model for the entire set (30 compounds) calculated by corresponding QSA/PR models (82 – 87).

Williams plot was used to investigate the applicability domain (AD) of developed QSA/PR models (Figure 28). Such a leveraged approach allows simultaneous detection of the highly structurally influential chemicals and response outliers. The limit at X axis (h_{ii}), calculated based on $h_{ii} = 3(m+1)/n$ where m and n represent number of variables in the model and number of compounds in the training set, respectively, determines the structurally influential chemicals according to their HAT values. The limits on the Y axis represent standardized RES values over $\pm 3.0\sigma$, and determine the response outliers, which could also be also associated with experimental error [188, 190]. As can be seen from Figure 28, there are no outliers (none of std. RES values exceed the $\pm 3.0\sigma$ limits) in the models predicting coefficients A, B and C (over its transformed value 10^C) of the RSM model, which strongly suggests high predictivity, validity and accuracy of the developed QSA/PR models (82), (83) and (84). However, the Williams plots for the QSA/PR models predicting the other three coefficients exhibit few outliers: two in the case of D coefficient and per one in the cases of E and F coefficients. As mentioned above, these can be associated with experimental errors, i.e., in our case with experimental and computational errors transferred from RSM into QSA/PR. It should be noted that several structurally influenced compounds can be observed in Williams plots; DCF for A and B coefficients, and CIP, ETD and EE2 for A, E and F coefficients, respectively. However, considering the overall results, it can be generally concluded that derived models are accurate.
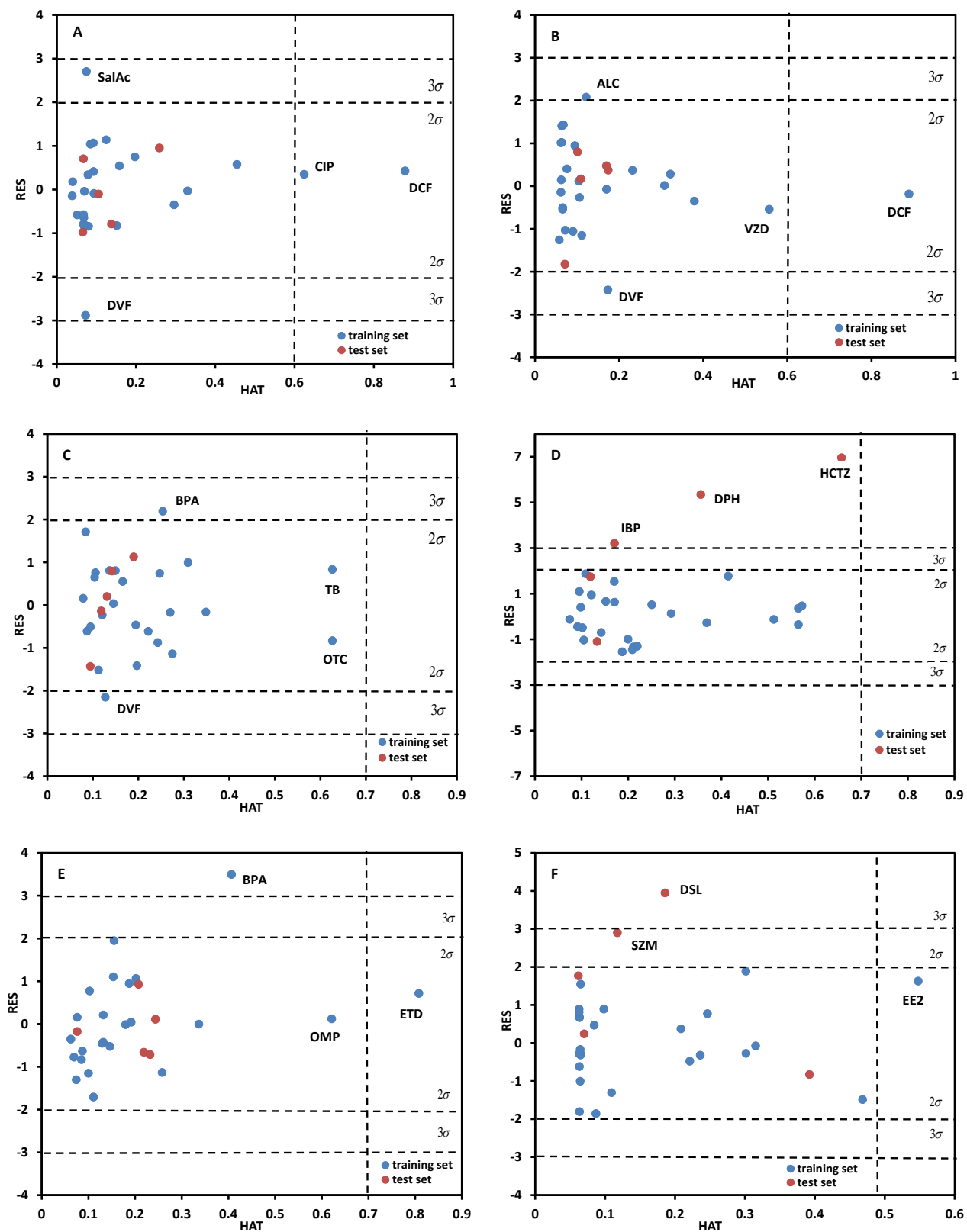
Figure 28 Determination of applicability domain for best models predicting A, B, C (in transformed 10^C form), D, E and F coefficients of RSM model for the 30 organic compounds.

The list of descriptors included in the selected models 82 – 87 and its definition is summarized in Table 17.

Table 17 Definitions of descriptors included in three-, four- and five- variable models for prediction of coefficients A, B, C, D, E and F:

Response / model		descriptor name	descriptor definition	descriptor type
A	4-variable	SpMax_B(i)	leading eigenvalue from Burden matrix weighted by ionization potential	2D matrix-based
		H8m	H autocorrelation of lag 8 / weighted by mass	GETAWAY
		CATS2D_05_NL	CATS2D Negative-Lipophilic at lag 05	CATS 2D
		F04[C−N]	Frequency of C − N at topological distance 4	2D Atom Pairs
B	4-variable	GATS2s	Geary autocorrelation of lag 2 weighted by I-state	2D autocorrelations
		Mor16i	signal 16 / weighted by ionization potential	3D-MoRSE
		R8m+	R maximal autocorrelation of lag 8 / weighted by mass	GETAWAY
		CATS2D_08_DA	CATS2D Donor-Acceptor at lag 08	CATS 2D
10^C	5-variable	RDF055m	Radial Distribution Function − 055 / weighted by mass	RDF
		Mor29m	signal 29 / weighted by mass	3D-MoRSE
		Mor17v	signal 17 / weighted by van der Waals volume	3D-MoRSE
		H1e	H autocorrelation of lag 1 / weighted by Sanderson electronegativity	GETAWAY
		cRo5	Complementary Lipinski Alert index	Drug-like indices
D	5-variable	SpMaxA_AEA(ri)	normalized leading eigenvalue from augmented edge adjacency mat. weighted by resonance integral	Edge adjacency indices
		Mor19s	signal 19 / weighted by I-state	3D-MoRSE
		CATS2D_06_DL	CATS2D Donor-Lipophilic at lag 06	CATS 2D
		B03[N−N]	Presence/absence of N − N at topological distance 3	2D Atom Pairs
		F03[O−Cl]	Frequency of O − Cl at topological distance 3	2D Atom Pairs
E	5-variable	CIC4	Complementary Information Content index (neighborhood symmetry of 4-order)	Information indices
		JGI7	mean topological charge index of order 7	2D autocorrelations
		C-024	R--CH--R	Atom-cantered fragments
		CATS2D_07_AA	CATS2D Acceptor-Acceptor at lag 07	CATS 2D
		CATS2D_06_NL	CATS2D Negative-Lipophilic at lag 06	CATS 2D
F	3-variable	Mor04p	signal 04 / weighted by polarizability	3D-MoRSE
		CATS2D_06_DL	CATS2D Donor-Lipophilic at lag 06	CATS 2D
		B08[C−N]	Presence/absence of C − N at topological distance 8	2D Atom Pairs

As can be seen, descriptors pertain to several classes that are calculated by rather complex schemes: GETAWAY, 2D autocorrelations, 3D-MoRSE, RDF, CATS 2D, Information indices, Edge adjacency indices, and Drug-like indices.

GETAWAY (Geometry, Topology, and Atom-Weights AssemblY) descriptors are derived from Molecular Influence Matrix (MIM), representing the molecular structure through particular output developed [232], and are divided into two groups: (i) descriptors computed using traditional matrix operators and information theory concepts onto MIM and influence/distance matrix R, and (ii) descriptors derived using the spatial autocorrelation formulas that weight the molecule atoms simultaneously accounting for properties such as atomic mass, polarizability, van der Waals volume, and electronegativity together with 3D information encoded by the elements of MIM and R. Descriptors in both groups can weighted with some property associated with the atoms; e.g. *m* (relative atomic mass), *p* (polarizability), *e* (Sanderson electronegativity), *v* (Van der Waals volume), *i* (ionization potential) and *s* (I-state; electrotopological states) [232].

2D-autocorrelations include descriptors computed using molecular graphs and Broto-Moreau (AST), Geary (GATS) and Moran (MATS) algorithms and are classified by term "the lag" with pertaining number and particular weighting scheme (*m*, *p*, *e*, *v*, *i* and *s*) [232]. The "lags" are calculated by summing the products of atomic weights of the terminal atoms of all paths of the considered path length.

3D-MoRSE class (3D Molecule Representation of Structures based on Electron diffraction) include descriptors that are computed by summing atom weights viewed by different angular scattering function and are tagged as Mor*sw*; *s* is in range from 1 to 32, while *w* denotes particular weighting scheme (*m*, *p*, *e*, *v*, *i* and *s*) explained above [232].

RDF descriptor types are based on the distance distribution in the molecule. Generally, the radial distribution function of an ensemble of *n* atoms can be interpreted as the probability distribution of finding an atom in a spherical volume of radius *R* and are typically denoted as RDF*sw*, where $10 \leq s \leq 155$ in five unit steps, while *w* stands for weighting scheme; by atomic properties *m*, *p*, *e*, and *v*, or can be unweighted (*u*) [177].

CATS2D comprehend topological pharmacophore descriptors based on auto- and cross-correlation of pharmacophoric atom types [233]. Atoms are represented as five different pharmacophore types: H-bond donor (D), H-bond acceptor (A), positively charged (P), negatively charged (N), and lipophilic (L) [234]. Any atom of the molecule can be assigned to none, one, or two atom types,

resulting in 15 possible atom pairs. CATS2D are calculated on a topological distance varying from 0 to 9 resulting into a vector of 150 frequencies.

2D matrix-based descriptors are topological indices calculated by applying a set of basic algebraic operators to different graph-theoretical matrices representing an H-depleted molecular graph of molecules [235].

Information indices are molecular descriptors that are calculated to provide information content (e.g. mean, structural, complementary, bonding) included in molecular structure represented from the molecular graph taking into account set of atoms and bonds in the molecule [236].

Edge adjacency indices is group of topological molecular descriptors derived from the edge adjacency matrix [237], which encodes the connectivity between graph edges.

Among descriptor groups with quite specific calculation procedures are also like **drug-like indices**, which present dummy variables taking value equal to 1 when all the criteria of the consensus definition of a drug-like molecule are satisfied, and 0 otherwise, including various specific filters to extract good drug candidates from large collections of compounds [238]. Since almost half of compounds studied are pharmaceuticals, it is not surprising that drug-like indices are included in QSPR models. Descriptors with more straightforward meaning are also included in QSA/PR models eq. 82 – 87 such as **Atom-cantered fragments** (denoting exact fragments in the molecules) and **2D Atom Pairs** (representing occurrence of exact atom pairs at certain topological distance in the molecules).

Nevertheless, the influence and contribution of structural properties of studied organics on their adsorption onto TiO_2 P25, which is represented throughout coefficients of RSM model (79) mimicking the influence of key operating parameters (initial pH and TiO_2 P25 loading), is provided based on the descriptors meaning (and weighting scheme where appropriate), along with the pertaining coefficients in QSA/PR models eq. 82 – 87. Hence, the coefficient F in RSM model (79) can be considered as a mean value of adsorption coefficient (K), while other coefficients provide fine-tuning based on the parameters influence; initial pH *via* A and B and TiO_2 P25 loading over C and D for linear and quadratic corresponding models terms, respectively, while E represents their mutual interaction effect. Accordingly, **CATS2D_06_DL** (QSA/PR model (87)) has the far highest contribution to the adsorption ability of organics onto TiO_2 P25 and provides a synergistic effect through its positive index. The other two included descriptors have much lower absolute values of coefficients: approx. 40% (**Mor04p**) and 30% (**B08[C-N]**) of that of **CATS2D_06_DL**. However,

these possess different contribution to endpoints; **B08[C-N]** has positive directly contributing to F, while **Mor04p** has negative index, providing antagonistic effects. **CATS2D_06_DL** denotes a preferred topological distance (6 bonds) between lipophilic and H-bond donor centres; such property also correlates with polarity and adsorption affinity. According to its positive index in the model (87), the compounds characterized by a higher value, i.e., less polar and consequently with more lipophilic centres overs H-donor centres, show higher affinity to be adsorbed at TiO_2 P25 surface; among studied, BPA, OXY, CIP, TB and EE2 exhibit the highest values. The lipophilic centres can be also considered as hydrophobic centres in our case; as is well known that hydrophilic centres tend to remain in bulk, thus hydrophobic compounds shield themselves from the aqueous medium by adsorption onto a to solid (i.e. TiO_2 P25 in this case) within the solid/liquid interface[172]. **Mor04p**, providing opposite effect than **CATS2D_06_DL** to end-point of interest (F), uses polarizability as weighting scheme. It should be noted that the highest values for **Mor04p** are calculated again for compounds with the highest **CATS2D_06_DL** values (not in the same decreasing order, and without CIP within). Hence, the polarity of molecule is one the key molecular property determining its affinity to be adsorbed onto TiO_2 P25 surface. The third descriptor included in model (87), **B08[C-N]**, corresponds to the presence/absence of the C – N bond at a topological distance 8 (DRAGON 6.0, library), there by taking into account compounds that have N as a heteroatom in their molecular structure, but at a specific position. Hence, the highest absolute value of that descriptor among compounds studied is 1 (computed for 8 compounds), regardless of the overall number of N-atoms present in their structures, e.g., TB has even 5 N-atoms, but its value of **B08[C-N]** is still 1. Additionally, since the topological distance between C and N atoms in this descriptor is rather large, all smaller molecules with a N heteroatom (e.g., SA, DIU) are not counted in this descriptor; thus, they are considered as without N-atoms present in molecular structure as their **B08[C-N]** value equals zero.

The influence of initial pH on adsorption of organics is represented by direct linear (X_1) and quadratic (X_1^2) model terms with coefficients A and B, respectively. The highest contribution to A is found to be over **SpMax_B(i)**, which has a negative index, thus providing antagonistic effects toward end-points. Other three descriptors contribute to a lesser extent according to absolute values of their coefficients: approx. 37% (**H8m**), 19% (**F04[C-N]**) and 18% (**CATS2D_05_NL**) of that **SpMax_B(i).** Interestingly, only **F04[C-N],** which corresponds to the frequency of C – N at topological distance 4, has a positive index that gives a synergistic effect to the end-points. This

descriptor takes into accounts the C atoms at a given position with respect to the N-atoms present within the molecular structure. Since the topological distance used for the calculation is much smaller than in the case of the 2D atom-pair descriptor in model (87) described above, all compounds with N as a heteroatom in the molecular structure are represented here. Hence, the higher value of **F04[C-N]** means that the compound has a higher affinity toward adsorption on TiO$_2$ P25. Descriptors with negative indices in model (82): **SpMax_B(i), H8m**, and **CATS2D_05_NL**, correspond to: leading eigenvalue from Burden matrix weighted by ionization potential, H autocorrelation of lag 8 / weighted by mass, and CATS 2D Negative-Lipophilic at lag 05, respectively. Considering the weighting schemes of the first two descriptors, it is clear that adsorption, facilitated by the direct influence of the initial pH, depends on the ionization potential, molecular mass and the number of negatively charged and lipophilic centres in the molecular structure. In addition, the initial pH also influences adsorption also over quadratic model term, accompanied with B coefficient. The largest contributor to B is indicated by **R8m+,** a GETAWAY descriptor corresponding to the maximum R autocorrelation of lag 8 / weighted by mass, providing synergistic effects toward end-points. The other three descriptors are contributed less, according to absolute values of their coefficients: approx. 34% (both **GATS2s** and **Mor16i**) and 25% (**CATS2D_08_DA**). The latter descriptor provides an antagonistic contribution to end-points and denotes the preferred topological distance (8) of the H-bond donor and acceptor centres. The other two descriptors have positive indices and thus provide a synergistic contribution to B coefficient prediction based on the molecular structures of studied compounds. **GATS2s** corresponds to I-state weighted Geary autocorrelation of lag 2, while **Mor16i** pertains to 3D-MoRSE descriptors and corresponds to signal 16 / weighted by ionization potential. Electrotopological state atom (I-state) indices are developed to better indicate the important topological features and molecular fragments mediating a particular response, combining electronic and topological characteristics of atoms/molecules [185, 192].

The influence of TiO$_2$ P25 loading onto K as a measure of adsorption ability of the studied organics is generally lower than that of initial pH; for almost half of the studied compounds the direct linear (X_2) terms are found to be not significant, while in the case of the quadratic (X_2^2) model terms their significance is an exception (only in the case of DCP and SZM). Thus, in these cases those model terms (and their associated coefficients) play a minor role in predicting adsorption to TiO$_2$ P25. In the case of coefficient C (together with the X_2 model term), the highest contributions in model (84)

were found to be by two descriptors with opposite indices; **RDF055m**, corresponding to Radial Distribution Function – 055 / weighted by mass, which has a positive index, and **H1e**, corresponding to H autocorrelation of lag 1 / weighted by Sanderson electronegativity, which has a negative index. There are also two 3D-MoRSE descriptors with different weighting schemes that contribution differently to end-points; one weighted by mass has a negative index, while another weighted by volume has a positive index. The fifth descriptor included, **cRo5**, corresponds to Complementary Lipinski Alert index. As it can be seen, all indices in model (87) point out on the rather low values of the D coefficient which, as mentioned above, possessing quite low influence in predicting adsorption of studied organics onto TiO_2 P25. However, several readily explainable descriptors are included: **CATS2D_06_DL**, explained above in the case of the contribution of model (87), as well as **B03[N-N]** and **F03[O-Cl],** which correspond to the presence of N – N and the abundance of O – Cl at topological distances 3, respectively. These descriptors are rather rarely present in the studied set and represent particular molecular features among the included organics that promote the influence of TiO_2 P25 loading as a parameter of the adsorption process. Finally, the E coefficient, which is accompanied with the interaction model term in the RSM model (86), is strongly influenced by the CATS2D descriptors: **CATS2D_07_AA** and **CATS2D_06_NL**, which have a similar positive influence on end-points and denote the preferable topological distances (7 and 6 bonds, respectively) between H-bond acceptor and acceptor centres and between negative and lipophilic centres, respectively. Since the topological distances (i.e., bonds) between such centres in the molecule taken into calculation are rather large, these descriptors are rather uncommon in the studied set; there occur in only 4 and 2 molecules, respectively. Therefore, in prediction of E coefficients, these can be considered as measure to correct under-calculation based on other three included descriptors in model (86). Atom centre fragment descriptor, C-024, which corresponds to the number of -CH= centres in the molecule, has negative contribution to the end point, implying that compounds with more such centres are more likely to remain in the bulk than adsorb on the TiO_2 P25 surface. Furthermore, **JGI7**, corresponding to the mean topological charge index of order 7, also has a negative index, which has an antagonistic effect toward end-points. Interestingly, single-benzene ring compounds in the set have a zero value for this descriptor, which means that simpler structured compounds can be more easily adsorbed on the TiO_2 P25 surface. Considering all mentioned above, in addition to the main key process parameters such as initial pH and TiO_2 P25 loading, the adsorption on the TiO_2 P25 surface is also influenced by structural

features such as molecular mass and volume, polarity and charge, ionization potential, as well as more or less specific molecular fragments such as –CH= centres, number of C atoms at a certain distance from neighbouring N-atoms or between two heteroatoms (O and Cl). Adsorption usually combines all three mechanisms: chemisorption, ionic and physical adsorption, which is particularly valid in our case as a wide range of pH values was covered (4 – 10), including the range below and above the TiO_2 P25 point of zero change value ($6.5 < pH_{PZC} < 6.7$, [240] as well as the presence of the studied compounds in their protonated and deprotonated forms. Thus, both the TiO_2 P25 surface charge as well as ionization states of molecule, dictating prevalence of ionic adsorption, were considered within modelling over various descriptors, mostly over their weighting schemes (e.g., I-state). The chemisorption come forth over CATS2D descriptors including topological distances between donor and acceptor centres, as well as 2D Atom Pairs denoting indirectly existence and directly positions of withdrawing and donating groups.

4.4. Structural features promoting photocatalytic degradation of organic compounds

In order for the developed mathematical – mechanistic model for the photocatalytic degradation of IBP by the UV-A/TiO$_2$ P25 process to be robust, the phenomena of the degradation of various organic compounds via the most important HO• and $O_2^{-\bullet}$ species must be included in the model depending on the structural features of the organics. Therefore, in the next step, photocatalytic degradation rates of various organic compounds were investigated to determine the distribution of degradation mechanisms by two dominant radicals, but also to determine the influence of the structural features of the investigated compounds on the mentioned process using the QSA/PR methodology.

4.4.1. Photocatalytic degradation of organic compounds

The photocatalytic degradation of organic compounds can undergo two mechanisms: (i) direct, occurring at the photocatalyst surface by photogenerated holes (h^+) and electrons (e^-), and (ii) indirect, occurring in the bulk by reactive oxygen species (ROS), primarily HO• and $O_2^{-\bullet}$ that are generated as products of reactions of HO^- (as water dissociates) and O_2 (dissolved) with photogenerated h^+ and e^-, respectively [241]. In this study, focus was only on the indirect degradation by ROS, and in that purpose, experiments with DMSO and BQ as effective scavenging agents for HO• and $O_2^{-\bullet}$, respectively, [194, 195, 196]. Experiments were performed with the same organic compounds used in adsorption experiments that are present in Table 1. The tendency of studied organics to be adsorbed onto TiO$_2$ P25 surface were tested and in such sorption process be removed from the reaction solution what is explain in previous section. Most of studied organics, even 17 compounds, showed very low adsorption (between 0 and 2%) in a case of the adsorption at applied photocatalytic process conditions (pH 7 and TiO$_2$ P25 loading of 0.8 g·L^{-1}) that are used in this part of research. Furthermore, low adsorption (between 3 to 5% removal) was recorded for 5 compounds (EE2, DSL, DCF, DPH and SalAc), while higher removal values are recorded for following organics: AMX and VZD (11%), ETD (15%), OMP (17%), TB (21%), OXY (27%) and BPA and CIP (31%) (Table 18).

In order to investigate the potential for the direct degradation (by photogenerated h^+ and e^-) of compounds with high adsorbed amount at the catalyst surface, additional experiments with addition of both ROS scavenging agents (DMSO and BQ) were performed in order to suppress bulk reactions. After that, desorption tests to determine remained concentration adsorbed at the catalyst surface were performed. In all cases desorbed concentration corresponded to the values established as adsorbed at the catalyst surface during initial dark period (within mentioned experimental error). Accordingly, it can be concluded that direct oxidation/reduction of studied organics is not favourable, and that majority of degradation occurs in the bulk. Hence, degradation extents in tests with scavenging agents to those without were compared, deducting the adsorbed amount from the overall concentration of targeted compound, and accordingly, to establish the portion in overall degradation extent of each organic compound which pertained to photocatalytic degradation meditated by HO• and $O_2^{-•}$. The results for selected organics are summarized in Table 18 and Figure A1 and A2 in Appendix. Such relative values were then brought into correlation by creating K coefficient which denotes ratio of organics degraded by HO• ($M_{HO•}$) *vs.* that driven by $O_2^{-•}$ ($M_{O_2^{-•}}$) (eq. (88)):

$$K = \frac{M_{HO•}}{M_{O_2^{-•}}} \tag{88}$$

where $M_{HO•}$ is the relative removal mediated by HO• expressed in % and $M_{O_2^{-•}}$ is the relative removal mediated by $O_2^{-•}$ expressed in %. The calculated values for K coefficient are provided in Table 18. In such manner, bulk degradation mechanism can be presented by single value enabling easier QSA/PR modelling to establish structural characteristics or organic pollutants that are more susceptible to HO• degradation ($K \gg 1$) from those undergoing preferable reduction reactions via $O_2^{-•}$ ($K \ll 1$).

Table 18 Experimental results of the removal and degradation of studied organic compounds by UV-A/TiO$_2$ P25 process (pH 7 and TiO$_2$ P25 loading of 0.8 g·L^{-1}):

#	Abbreviation	Overall removal, %	Removal due to adsorption, %	Removal due to degradation, %	k_{obs}, s^{-1} (×10^{-2})	Relative removal mediated by HO•, %	$k(HO•)_{obs}$, s^{-1} (×10^{-2})	Relative removal mediated by O$_2^{-•}$, %	$k(O_2^{-•})_{obs}$, s^{-1} (×10^2)	K	$\dfrac{1}{\sqrt{(K+1)}}$
1	ALC	90.68	1.55	89.13	11.98	72.60	5.28	26.67	1.41	2.722	0.518
2	*o*-aminoBenzAc	77.50	1.99	75.51	7.63	7.31	0.03	92.42	6.34	0.079	0.963
3	AMX	69.05	11.00	58.05	5.35	8.58	0.31	90.57	4.44	0.095	0.956
4	AZN	45.72	1.19	44.35	2.90	79.74	2.24	19.85	0.47	4.017	0.446
5	BenzAc	80.86	0.59	80.27	8.28	27.16	1.23	72.56	4.40	0.374	0.853
6	BPA	67.17	31.54	35.63	3.79	60.87	1.92	38.52	1.14	1.580	0.623
7	CIP	98.00	30.71	67.29	17.34	30.50	1.69	68.96	5.66	0.852	0.735
8	DSL	74.89	4.89	70.00	6.81	58.91	2.95	40.85	1.67	1.442	0.640
9	DVF	70.27	0.36	69.91	5.94	30.77	1.20	69.14	3.43	0.445	0.832
10	DCP	59.05	1.79	57.26	4.41	76.76	3.03	22.86	0.74	3.358	0.479
11	DCF	78.81	5.00	73.81	7.89	31.28	1.45	68.49	3.94	0.457	0.829
12	1,4-DMB	90.89	1.73	89.16	11.99	28.51	1.49	71.25	5.22	0.400	0.845
13	2,6-DMP	99.54	0.71	98.84	15.23	5.04	0.27	94.51	13.15	0.053	0.974
14	DIU	78.67	1.99	76.68	7.52	88.60	5.84	10.60	0.45	8.358	0.327
15	DPH	63.31	5.39	57.91	4.70	78.77	3.33	21.04	0.69	1.404	0.645
16	EE2	56.08	3.21	52.87	3.96	64.56	2.19	35.21	1.07	1.833	0.594
17	ETD	94.92	15.27	79.65	13.98	6.29	0.03	93.55	10.61	0.067	0.968
18	HCTZ	58.23	0.62	57.61	4.44	65.58	2.42	33.80	1.11	1.940	0.583
19	IBP	95.86	1.80	94.16	16.40	28.67	1.68	71.26	6.04	0.402	0.844
20	*p*-MP	91.83	0.63	91.19	12.19	23.31	1.22	76.46	6.28	0.305	0.875
21	*m*-NP	47.42	2.07	45.35	3.15	65.81	1.84	33.48	0.84	1.965	0.581
22	*p*-NP	46.76	0.64	46.12	3.15	58.89	1.64	40.97	1.09	1.437	0.641
23	OMP	74.40	17.41	56.99	5.88	23.15	0.09	76.55	3.75	0.302	0.876
24	OXY	81.24	27.16	54.08	6.96	65.08	3.27	33.97	1.43	1.916	0.586
25	Ph	56.46	0.24	56.22	4.17	74.96	2.77	24.43	0.76	3.069	0.496
26	SalAc	85.26	4.20	81.06	9.73	31.22	1.61	68.58	4.57	0.455	0.829
27	SZM	88.53	1.93	86.60	10.54	68.27	4.74	31.45	1.66	2.171	0.562
28	SA	53.90	1.95	51.95	3.91	40.43	1.24	59.25	1.96	0.682	0.771
29	TB	78.28	21.00	57.28	6.51	71.91	3.72	27.51	1.12	2.614	0.526
30	VZD	67.45	10.74	56.71	5.14	51.73	1.98	47.73	1.90	1.084	0.693

4.4.2.   Modelling the ratio of the radical contribution coefficient

Experimentally determined by photocatalytic experiments and calculated K coefficients (eq. 88 and Table 18) for 30 studied organic compound, was applied in next step of modelling, correlations of coefficients with their structural characteristics by QSA/PR. Firstly, the set of 30 organics was divided into a training set and test set, containing 25 and 5 compounds (AMX, CIP, 1,4-DMB, p-MP, SZM), respectively. Then, QSA/PR modelling was performed in step-wise fashion, by building models with 1 to 5 variables (i.e. descriptors) for the training set to obtain the highest accuracy possible (according to R^2) whilst keeping the linearity of derived models. Furthermore, the same procedure and methodology for developing QSA/PR models were applied as in previous chapter.

The very high ratio of maximum and minimum value of K coefficients calculated for the selected organics (~158) indicated on the need of certain transformation function to improve modelling results. In general, the transformations are used to narrow the range of responses, which results with improved correlation upon modelling [145, 186]. Accordingly, several transformations of K coefficients were tested employing simple mathematical operations such as square root, log, ln, power of base 10, power of base e, etc. According to the results of preliminary modelling actions after the applied transformations, the highest accuracy was obtained in the case of $\frac{1}{\sqrt{(K+1)}}$ transformation, thus, it was kept in the further modeling. By using such a transformation another benefit was obtained; it is not possible that model would predict some of very small K coefficient values as negative, which does not have practical and physical meaning.

The values of the statistical parameters (R^2, Q^2, F, p, s, S_{PRESS}) determining the performance of the selected 1-, 2-, 3-, 4- and 5-variable QSA/PR models divided into the training and test sets are summarized in Table 19 while a comparative study of R values (correlation coefficient of regression) for the training and test sets *vs.* the number of variables in selected QSA/PR model is shown in Figure 29.

Table 19 Statistical evaluation of QSA/PR models for training set (25 compounds) and test set (5 compounds):

Model	Training set						Test set			
	n	R^2	Q^2	F	p	s	S_{PRESS}	n	R^2	F	s
1-variable		0.367	0.274	13.372	0.0013	0.145	0.156		0.313	1.825	0.064
2-variable		0.629	0.546	18.639	p<0.0001	0.114	0.126		0.121	0.548	0.081
3-variable	25	0.740	0.637	19.911	p<0.0001	0.097	0.115	5	0.147	0.684	0.144
4-variable		0.808	0.731	20.971	p<0.0001	0.086	0.101		0.252	1.349	0.075
5-variable		0.902	0.841	35.004	p<0.0001	0.063	0.080		0.541	4.716	0.044
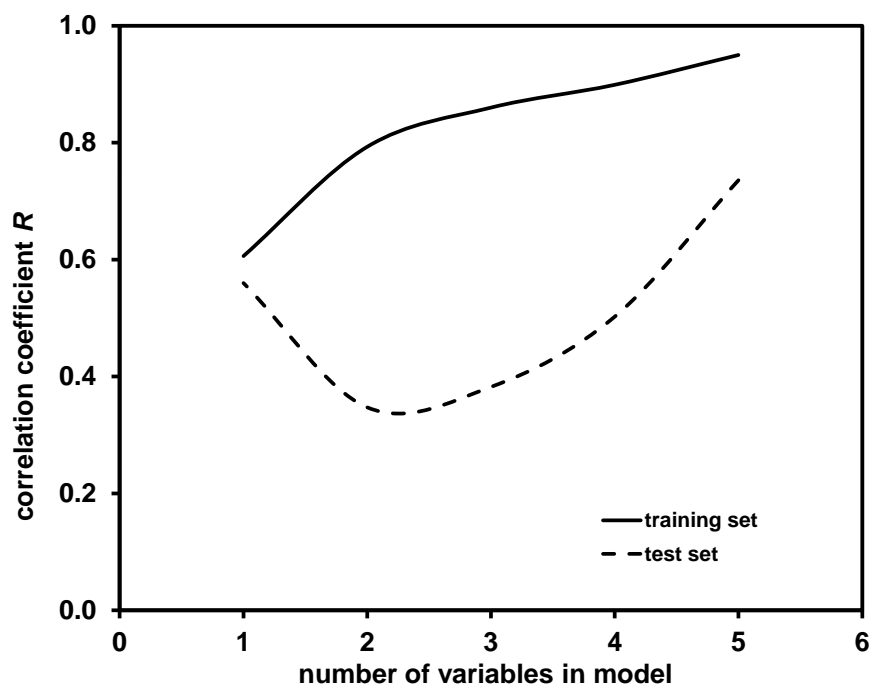
Figure 29 Comparison of correlation coefficients obtained for training and test set by $1 - 5$ variable models for modelling of K coefficient.

As can be seen from the results presented in Figure 29, R values for the model developed for the training set increase with the model enlargement, i.e., inclusion of new variables. A similar trend

can be observed for the R values for the test set; the exception was 1-variable which possessed higher R value than those of 2- and 3-variable models. Hence, the highest accuracy for the test set was obtained by 5-variable model. There is a possibility that higher dimensional models (over 5 variables) might show better predictability, however, due to the "rule of thumb" that was not tested. This 5-variable model was further validated over the Leave-Many-Out (LMO) technique [228] and "Y-scrambling" test [230]; graphical representations of those two tests are provided in Figure 30, respectively. As can be seen from the scatter plots (Figure 30 A), the Q^2_{LMO} values are close to Q^2_{LOO} value of selected 5-variable models and Q^2_{LMO} values are not widely scattered, which indicates on the validity of derived QSA/PR model.
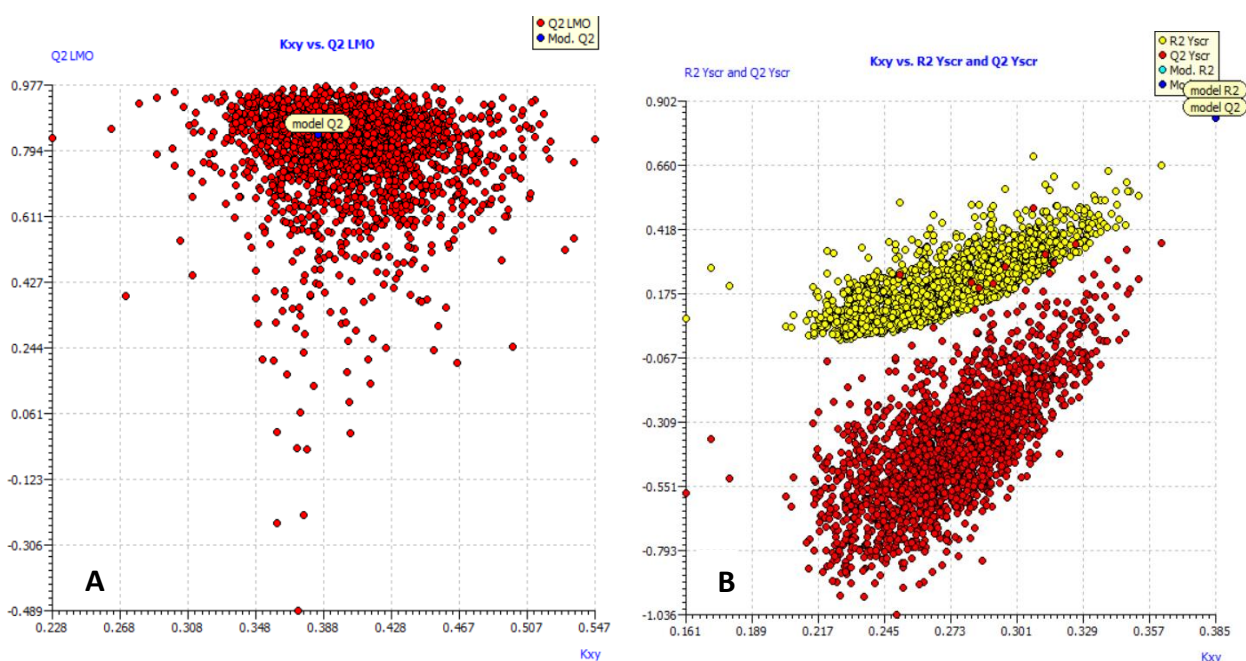
Figure 30 Scatter plots of LMO (A) and Y-scrambling model (B) compared to the 5-variable QSA/PR model.

The results of the "Y-scrambling" test, in which the R^2 and Q^2_{LOO} values obtained from the selected model are significantly higher than the calculated $R^2_{Y-SCRAMBLING}$ and $Q^2_{Y-SCRAMBLING}$ values (Figure 30 B), supporting the validity of selected model. All fitting, internal and external validation criteria values for selected 5-variable model are summarized in Table 20.

Table 20 Values of fitting, internal and external validation criteria of selected best 5-variable model:

Fitting criteria		Internal validation criteria		External validation criteria	
R^2	0.902	Q^2_{loo}	0.841	R^2_{ext}	0.541
R^2_{adj}	0.876	R^2-Q^2_{loo}	0.060	Q^2F_1	0.719
R^2-R^2_{adj}	0.026	Q^2_{LMO}	0.818	Q^2F_2	0.537
LOF	0.008	PRESS$_{cv}$	0.121	Q^2F_3	0.719
RMSE$_{tr}$	0.055	RMSE$_{cv}$	0.070	PRESS$_{ext}$	0.043
MAE$_{tr}$	0.045	MAE$_{cv}$	0.059	RMSE$_{ext}$	0.093
CCC$_{tr}$	0.948	CCC$_{cv}$	0.917	MAE$_{ext}$	0.081
		R^2Y_{scr}	0.206	CCC$_{ext}$	0.714
		Q^2Y_{scr}	-0.399	R^2_{ext}	0.541

The performance of the model selected as the best (5-variable), when applied for the entire studied set (i.e., all 30 organic compounds selected), is shown in Figure 31 while the model equation is presented below (89), along with the values of corresponding statistical parameters determining their accuracy and significance.

$$Y(\frac{1}{\sqrt{(K+1)}}) = -0.327(\pm 0.086) \times \textbf{MATS4v} -$$

$0.245(\pm 0.086) \times$**Mor10u**$+0.165(\pm 0.061) \times$**CATS2D_01_DN** $- 0.176(\pm 0.076) \times$**B04[C-Cl]**

$+ 0.151(\pm 0.067) \times$**B08[C-O]** $+ 0.533(\pm 0.053)$ (89)

($n = 30$; $R^2 = 0.876$; $s = 0.069$; $F = 33.665$; $p < 0.0001$; $Q^2 = 0.816$; $S_{PRESS} = 0.084$; $S_{DEP} = 0.076$)
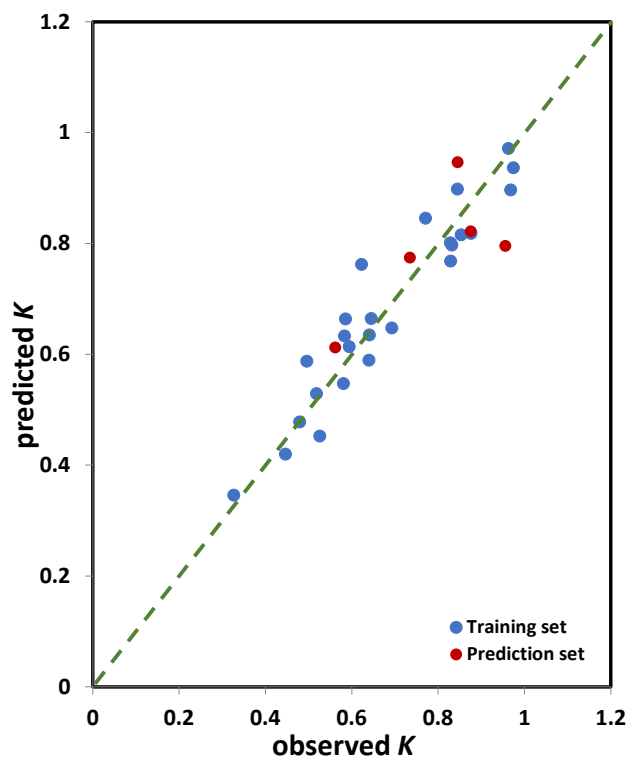
Figure 31 The observed *vs.* predicted values for *K* coefficient (in transformed $\frac{1}{\sqrt{(K+1)}}$ form), for the entire set (30 compounds) calculated by 5 variable model.

As can be seen in Figure 31 the points or point clusters are in good agreement to the regression diagonal line, suggesting the rather high accuracy of derived QSA/PR model (89). The descriptive statistical data of the coefficients included in model (89) were assessed as well (Table 21).

Table 21 Descriptive statistical data included in the best 5-variable model:

predictor	Coef.	Stdev	95% Conf	t-ratio	*p**
Constant	0.533	0.026	0.053	20.727	0
MATS4v	-0.294	0.037	0.077	-7.862	0
Mor10u	-0.245	0.042	0.086	-5.854	0
CATS2D_01_DN	0.165	0.030	0.061	5.545	0
B04[C-Cl]	-0.176	0.033	0.076	-4.789	0.0001
B08[C-O]	0.151	0.033	0.067	4.648	0.0001

*p < 0.05 is significance limit

114

It can be clearly seen that all included model terms are significant ($p_T < 0.05$). Furthermore, the correlation matrix for model is provided (Table 22), clearly showing that none of the descriptor pairs has $R_{ij} > 0.6$, i.e., the model is linear.

Table 22 Correlation matrix of descriptors included in best 5 variable model for entire set of compounds (cross-correlation $R_{ij} < 0.6$):

	MATS4v	Mor10u	CATS2D_01_DN	B04[C-Cl]	B08[C-O]
MATS4v	1	0.076	0.016	0.187	0.184
Mor10u	0.076	1	0.025	0.49	0.542
CATS2D_01_DN	0.016	0.025	1	0.113	0.233
B04[C-Cl]	0.187	0.49	0.113	1	0.269
B08[C-O]	0.184	0.542	0.233	0.269	1

In this research it was also assessed the applicability domain test over Williams plot (Figure 32). Such a leveraged approach allows simultaneous detection of the highly structurally influential chemicals and response outliers. The limits on the Y axis represent standardized RES values over $\pm 3.0\sigma$, and determine the response outliers, which could also be associated with experimental error [231]. As can be seen, there are no outliers (none of std. RES values exceed the $\pm 3.0 \sigma$ limits), which strongly suggests high predictivity, validity and accuracy of the developed QSA/PR model (89).
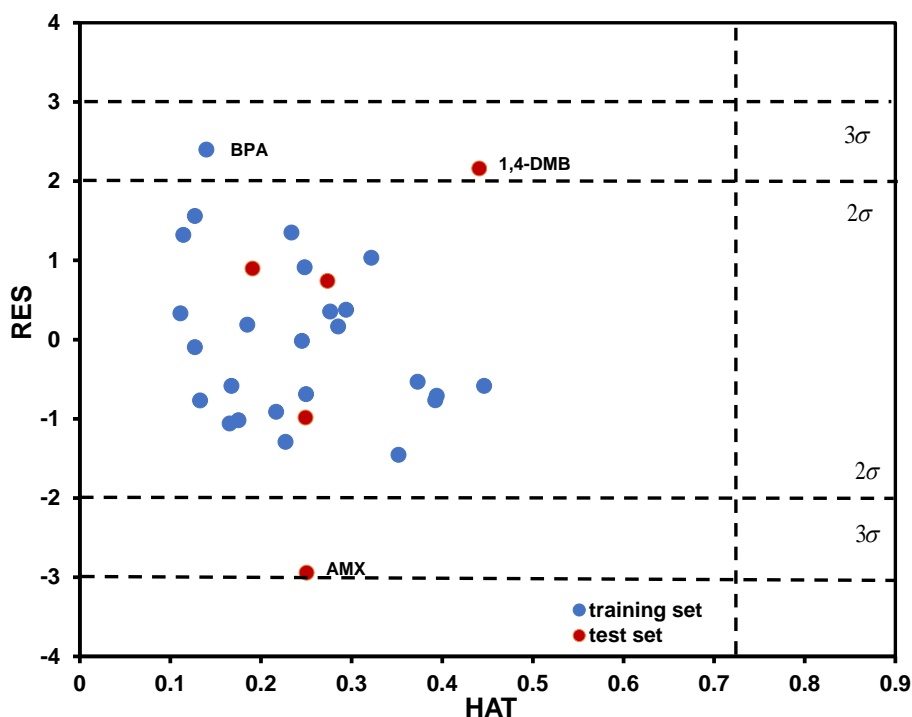
Figure 32 Determination of applicability domain (AD) for the 5-variable model, selected as the best among tested, through Williams plot.

It should be noted that there are also no X outliers, i.e., structurally influenced compounds, indicating on the model robustness regarding the molecular structures of organics. The list of descriptors included in the selected model (89) is summarized in Table 23 Descriptors included in model selected as the best, 5-variable model (89), pertain to following classes: 2D autocorrelations, 3D-MoRSE, CATS2D and 2D Atom Pairs and are described in section 4.3.

Table 23 Definitions of descriptors included in 5 variable model for prediction of *K* coefficient:

descriptor name	descriptor definition	descriptor type
MATS4v	Moran autocorrelation of lag 4 weighted by van der Waals volume	2D autocorrelations
Mor10u	signal 10 / unweighted	3D-MoRSE
CATS2D_01_DN	CATS2D Donor-Negative at lag 01	CATS 2D
B04[C-Cl]	Presence/absence of C – Cl at topological distance 4	2D Atom Pairs
B08[C-O]	Presence/absence of C – O at topological distance 8	2D Atom Pairs

Taking into account the values of indexes of descriptors included in model (89), the contribution of molecular features preferring degradation via HO• or $O_2^{-•}$ can be established. The highest contribution to the response was showed by **MATS4v** and due to the negative index of its coefficient, such contribution is antagonistic. However, it should be noted that we used transformed value of K coefficient in a form $\frac{1}{\sqrt{(K+1)}}$; thus, as lower the value of transformed K, the higher is original K value. Accordingly, what has antagonistic effect toward transformed K, it has synergistic effect toward original K, meaning the higher K coefficient, the higher is portion of organic compound degraded by HO• and *vice versa* for $O_2^{-•}$. The other four included descriptors have lower absolute values of coefficients: approx. 25% (**Mor10u**), 46% **(B04[C-Cl]),** 50% (**CATS2D_01_DN**) and 54% **(B08[C-O])**. Mor10u and **B04[C-Cl]** have negative indexes of coefficients, providing antagonistic effects toward transformed K, but synergistic to original K values (i.e. denoting structural features that promote degradation via HO•). On the other hand, indexes of **CATS2D_01_DN** and **B08[C-O]** coefficients are positive, contributing eventually negatively to original K values (i.e. denoting structural characteristics more susceptible to degradation via reductive reaction by $O_2^{-•}$). Although several descriptors are obtained with the rather complex calculations, their weighting schemes may indicate on the structural features more clearly. However, **Mor10u** is unweighted. On the other hand, v as weighting scheme in 2D-autocorrelation descriptor **MATS4v** indicate on the importance of Van der Waals volume, also called molecular volume and denoting volume "occupied" by a molecule, as a general structural characteristic of a molecule attacked more preferably by either HO• or $O_2^{-•}$. Thus, it can be concluded that size matters. Other three included descriptors provide more straightforward correlation of structural characteristics promoting HO• driven degradation over that by $O_2^{-•}$. Hence, **CATS2D_01_DN** denotes a preferred topological distance (1 bond) between H-bond donor and negative centres. In the studied set is characteristic for several compounds and amounts either 1 (possessing of such descriptor; compounds possessing carboxylic group (-COOH)) or 0 (compounds without that feature). Since **CATS2D_01_DN** has positive index in model (89), negatively contributing to K value, compounds with carboxylic group are preferably degraded by $O_2^{-•}$. The same influence to K has **B08[C-O]**, which corresponds to the presence/absence of the C–O bond at a topological distance 8. Such structural feature is characteristics for the most of CECs in the studied set, while smaller single-benzene ring compounds are discarded due to the maximal number of C atoms either in molecule in general or C atom at too far distance from O atom. Hence,

117

compounds possessing O as heteroatom at such topological distance from C atom represents preferable structural feature promoting reductive degradation via $O_2^{-\bullet}$. As possessing negative index in model (87), **B04[C-Cl]**, which denotes the presence/absence of the C–Cl bond at a topological distance 4, represents structural feature preferring HO• oxidative degradation over reduction via $O_2^{-\bullet}$. It should be noted that such structural feature is correlated with the most of studied organics possessing Cl as heteroatom. Exception is AZN; although has Cl, it is not counted within **B04[C-Cl]** descriptor because topological distance between C and Cl atoms is lower than 4. The importance of such structural feature for favouring HO• reactions can be correlated with known degradation pathways upon attack HO•. Namely, there are three main pathways: (i) H-abstraction (which is followed by subsequent hydroxylation), (ii) single electron transfer (SEC) and (iii) radical addition (RA) [229]. It was established that H-abstraction is the most preferable [229] [243]. Hence, in a case a halide atom (e.g. Cl) is bonded to aromatic ring, H-abstraction pathway would comprehend breaking of next C–H, followed by hydroxylation at the same position in the structure. Such action is more preferable than Cl atom release due to reduction reaction, which are actually mediated by $O_2^{-\bullet}$ [144, 201, 202].

5. CONCLUSION

This research presents the development of a mathematical – mechanistic model for the photocatalytic degradation and mineralisation of pharmaceutical by UV-A/TiO$_2$ P25, including the specifications of the photocatalytic reactor and photocatalyst.

1) The maximum irradiation intensity was found on the surface of the quartz tube for $r = 0.00425$ m at a distance of $z = 0.038$ m (48.8 W·m^{-2}) which corresponds to almost half the lamp inside the reactor. The irradiation intensity decreases with distance from the surface of the quartz tube (where the irradiation is highest), i.e., with an increase in the value of r. Furthermore, the radiation intensity increases in all measurement cases, from the distance from the bottom of the reactor $z = 0$ to $z = 0.038$ m, where the maximum radiation intensity was observed, after which the radiation intensity decreases and can be considered negligible at a distance greater than $z = 0.0705$ m.

2) The average radius of the agglomerates increases with increasing concentration of TiO$_2$ P25 and shows a linear dependence, but also a good agreement between experimental and predicted results.

3) The developed simulation models confirm the formation of HO• and O$_2^{-•}$ responsible for the photocatalytic process and show a good agreement (RMSD values are in the range: 0.023 – 0.074) between the experimental and predicted result, especially when using a higher concentration of the photocatalyst γ(TiO$_2$ P25) = 1.2 g·L^{-1}.

4) The developed simulation model describes very well the conversion and mineralisation of IBP by the UV-A/TiO$_2$ P25 process, especially at higher concentrations of TiO$_2$ P25 such as 1.2 and 2 g·L^{-1}. The good agreement between the predicted and experimental results is confirmed by the calculation of the RMSD, which is less than 1 in all cases studied. Moreover, the accuracy of the model, i.e., the agreement of the predicted with the experimental results, increases with increasing concentration of TiO$_2$ P25.

5) QSA/PR modelling combined with RSM yielded very good prediction and optimization of adsorption of organic compound with the more complex molecular structure.
The results of combined modelling present coefficient F in RSM model as a mean value of adsorption coefficient. Furthermore, the descriptors obtained by the corresponding models show that adsorption onto TiO$_2$ P25 surface is influenced by besides key process parameters such as

initial pH and TiO$_2$ P25 loading, structural features organics such as molecular mass and volume, polarity charge, ionization potential, as well as more and less specific molecular fragments such as –CH= centres, number of C atoms at certain distance of neighbouring N-atoms, or between two heteroatoms as O and Cl. Thus, compounds with more lipophilic centres over H-donor centres, show a higher tendency to be adsorbed at the TiO$_2$ P25 surface, so adsorption is positively correlated with hydrophobicity that favours organics adsorptions onto TiO$_2$ P25 surface.

6) The results of final QSA/PR modelling revealed that structural feature such as size of molecule, represented by MATS4v descriptor, influence the degradation rate in general. Furthermore, the presence/absence of molecular fragments such as C – O represented by CATS2D_01_DN and B08[C–O] descriptors, and C – Cl bonds, represented by the B04[C–Cl] descriptor, dictate the preferable degradation pathway of organic compound by photocatalytic degradation; the later favours HO• driven reaction, while former reductive pathway by O$_2^{-\bullet}$. QSA/PR successfully captured relevant structural features determining degradation kinetics of studied organic compound.

7) Developed mathematical – mechanistic model shows that the predicted results agree satisfactorily with the experimental data. Furthermore, the model is simple and robust and can be applied to the design and scaling of photocatalytic reactors and photocatalytic processes. Developed QSA/PR model can be considered as robust predictive tools for adsorption of organic compound and evaluating distribution between degradation mechanisms occurring in photocatalytic process UV-A/TiO$_2$ P25.

6. REFERENCES

[1]   O. Golovko, S. Örn, M. Sörengård, K. Frieberg, W. Nassazzi, F.Y. Lai, L. Ahrens, Occurrence and removal of chemicals of emerging concern in wastewater treatment plants and their impact on receiving water systems, Sci. Total Environ. 754 (2021) 1–27.

[2]   N. Patel, Z.A. Khan, S. Shahane, D. Rai, D. Chauhan, C. Kant, V.K. Chaudhary, Emerging pollutants in aquatic environment: Source, effect, and challenges in biomonitoring and bioremediation-A review, Pollution 6 (2020) 99–113.

[3]   J.P. Fernandes, C.M.R. Almeida, M.A. Salgado, M.F. Carvalho, A.P. Mucha, Pharmaceutical compounds in aquatic environments— occurrence, fate and bioremediation prospective, Toxics 9 (2021) 1–26.

[4]   M.J. Martínez Bueno, M.G. Valverde, M.M. Gómez-Ramos, J.A.S. Andújar, D. Barceló, A.R. Fernández-Alba, Fate, modeling, and human health risk of organic contaminants present in tomato plants irrigated with reclaimed water under real-world field conditions, Sci. Total Environ. 806 (2022) 1–17.

[5]   A.D. McEachran, M.L. Hedgespeth, S.R. Newton, R. McMahen, M. Strynar, D. Shea, E.G. Nichols, Comparison of emerging contaminants in receiving waters downstream of a conventional wastewater treatment plant and a forest-water reuse system, Environ. Sci. Pollut. Res. 25 (2018) 12451–12463.

[6]   D. Juretic, H. Kusic, D.D. Dionysiou, B. Rasulev, A. Loncaric Bozic, Modeling of photooxidative degradation of aromatics in water matrix combination of mechanistic and structural-relationship approach, Chem. Eng. J. 257 (2014) 229–241.

[7]   M. Salimi, A. Esrafili, M. Gholami, A. Jonidi Jafari, R. Rezaei Kalantary, M. Farzadkia, M. Kermani, H.R. Sobhi, Contaminants of emerging concern: a review of new approach in AOP technologies, Environ. Monit. Assess. 189 (2017) 1–22.

[8]   V. Brlenic, H. Kusic, D. Juretic, A.L. Bozic, Comparative study on photooxidative treatment of diclofenac: Response surface and mechanistic modeling, J. Water Process Eng. 10 (2016) 78–88.

[9]   A. Gissi, O. Nicolotti, A. Carotti, D. Gadaleta, A. Lombardo, E. Benfenati, Integration of QSAR models for bioconcentration suitable for REACH, Sci. Total Environ. 456–457 (2013) 325–332.

[10]   L. Patrolecco, S. Capri, N. Ademollo, Occurrence of selected pharmaceuticals in the principal sewage treatment plants in Rome (Italy) and in the receiving surface waters, Env. Sci. Pollut. Res. 8 (2014) 5864–5876.

[11]   J. Rivera-Utrilla, M. Sánchez-Polo, M.Á. Ferro-García, G. Prados-Joya, R. Ocampo-Pérez, Pharmaceuticals as emerging contaminants and their removal from water. A review, Chemosphere. 93 (2013) 1268–1287.

[12]   P. Grenni, V. Ancona, A. Barra Caracciolo, Ecological effects of antibiotics on natural ecosystems: A review, Microchem. J. 136 (2018) 25–39.

[13]   P.A. Blackwell, A.B.A. Boxall, P. Kay, H. Noble, Evaluation of a lower tier exposure assessment model for veterinary medicines, J. Agric. Food Chem. 53 (2005) 2192–2201.

[14]   L. Ge, J. Chen, Aquatic Photochemistry of Fluoroquinolone Antibiotics : Kinetics , Pathways , and Multivariate Effects of Main Water Constituents, Environ. Sci. Technol. 44 (2010) 2400–2405.

[15]   S. Zhou, C. Di Paolo, X. Wu, Y. Shao, T.B. Seiler, H. Hollert, Optimization of screening-level risk assessment and priority selection of emerging pollutants – The case of pharmaceuticals in European surface waters, Environ. Int. 128 (2019) 1–10.

[16]   D. O'Flynn, J. Lawler, A. Yusuf, A. Parle-Mcdermott, D. Harold, T. Mc Cloughlin, L. Holland, F. Regan, B. White, A review of pharmaceutical occurrence and pathways in the aquatic environment in the context of a changing climate and the COVID-19 pandemic, Anal. Methods. 13 (2021) 575–594.

[17]   S. Esteban, L. Moreno-Merino, R. Matellanes, M. Catalá, M. Gorga, M. Petrovic, M. López de Alda, D. Barceló, J.J. Durán, J. López-Martínez, Y. Valcárcel, Y. Valcárcel, Presence of endocrine disruptors in freshwater in the northern Antarctic Peninsula region, Environ. Res. 147 (2016) 179–192.

[18]   T. aus der Beek, F.A. Weber, A. Bergmann, S. Hickmann, I. Ebert, A. Hein, A. Küster, Pharmaceuticals in the environment-Global occurrences and perspectives, Environ. Toxicol. Chem. 35 (2016) 823–835.

[19]   A.J. Ebele, M. Abou-Elwafa Abdallah, S. Harrad, Pharmaceuticals and personal care products (PPCPs) in the freshwater aquatic environment, Emerg. Contam. 3 (2017) 1–16.

[20]   R.N. Coimbra, C. Escapa, M. Otero, Removal of pharmaceuticals from water: Conventional and alternative treatments, Water (Switzerland) 13 (2021) 1–6.

[21]   W. Chen, J. Xu, S. Lu, W. Jiao, L. Wu, A.C. Chang, Fates and transport of PPCPs in soil receiving reclaimed water irrigation, Chemosphere 93 (2013) 2621–2630.

[22]   J. Fick, H. Söderström, R.H. Lindberg, C. Phan, M. Tysklind, D.G.J. Larsson, Contamination of surface, ground, and drinking water from pharmaceutical production, Environ. Toxicol. Chem. 28 (2009) 2522–2527.

[23]   M. Patel, R. Kumar, K. Kishor, T. Mlsna, C.U. Pittman, D. Mohan, Pharmaceuticals of emerging concern in aquatic systems: Chemistry, occurrence, effects, and removal methods, Chem. Rev. 119 (2019) 3510–3673.

[24]   A.J. Paszczynski, Emerging Contaminants in Water: Detection, Treatment, and Regulation, Enzyme Microb. Technol. 13 (2012) 57–74.

[25]   G. Rhodes, G. Huys, J. Swings, P.M.C. Gann, M. Hiney, P. Smith, R.W. Pickup, Distribution of Oxytetracycline Resistance Plasmids between Aeromonads in Hospital and Aquaculture Environments : Implication of Tn1721 in Dissemination of the Tetracycline Resistance Determinant Tet A, Appl. Environ. Microbiol. 66 (2000) 3883–3890.

[26]   Y. Li, Y. Ma, L. Yang, S. Duan, F. Zhou, J. Chen, Y. Liu, B. Zhang, Ecotoxicology and Environmental Safety Effects of azithromycin on feeding behavior and nutrition accumulation of Daphnia magna under the different exposure pathways, Ecotoxicol. Environ. Saf. 197 (2020) 1–7.

[27]   S.K. Khetan, T.J. Collins, Human pharmaceuticals in the aquatic environment: A challenge to green chemisty, Chem. Rev. 107 (2007) 2319–2364.

[28] K. Fent, A.A. Weston, D. Caminada, Ecotoxicology of human pharmaceuticals, Aquat. Toxicol. 76 (2006) 122–159.

[29] D. Awfa, M. Ateia, M. Fujii, M.S. Johnson, Photodegradation of pharmaceuticals and personal care products in water treatment using carbonaceous-TiO$_2$ composites : A critical review of recent literature, Water Res. 142 (2018) 26–45.

[30] S. Wales, B. Kasprzyk-hordern, R.M. Dinsdale, A.J. Guwy, The occurrence of pharmaceuticals, personal care products, endocrine disruptors and illicit drugs in surface water in, Water Res. 42 (2008) 3498–3518.

[31] A. Pal, K.Y.H. Gin, A.Y.C. Lin, M. Reinhard, Impacts of emerging organic contaminants on freshwater resources: Review of recent occurrences, sources, fate and effects, Sci. Total Environ. 408 (2010) 6062–6069.

[32] D.J. Lapworth, N. Baran, M.E. Stuart, R.S. Ward, Emerging organic contaminants in groundwater: A review of sources, fate and occurrence, Environ. Pollut. 163 (2012) 287–303.

[33] S. Chiron, C. Minero, D. Vione, Photodegradation processes of the antiepileptic drug carbamazepine, relevant to estuarine waters, Environ. Sci. Technol. 40 (2006) 5977–5983.

[34] S. Wiegel, A. Aulinger, R. Brockmeyer, H. Harms, J. Löffler, H. Reincke, R. Schmidt, B. Stachel, W. Von Tümpling, A. Wanke, Pharmaceuticals in the river Elbe and its tributaries, Chemosphere 57 (2004) 107–126.

[35] H. Yamamoto, Y. Nakamura, S. Moriguchi, Y. Nakamura, Y. Honda, I. Tamura, Y. Hirata, A. Hayashi, J. Sekizawa, Persistence and partitioning of eight selected pharmaceuticals in the aquatic environment: Laboratory photolysis, biodegradation, and sorption experiments, Water Res. 43 (2009) 351–362.

[36] J. Radjenovic, M. Petrovic, D. Barceló, Analysis of pharmaceuticals in wastewater and removal using a membrane bioreactor, Anal. Bioanal. Chem. 387 (2007) 1365–1377.

[37] A. Joss, E. Keller, A.C. Alder, A. Göbel, C.S. McArdell, T. Ternes, H. Siegrist, Removal of pharmaceuticals and fragrances in biological wastewater treatment, Water Res. 39 (2005)

3139–3152.

[38] B. Kasprzyk-Hordern, Pharmacologically active compounds in the environment and their chirality, Chem. Soc. Rev. 39 (2010) 4466–4503.

[39] H. Hühnerfuss, M.R. Shah, Enantioselective chromatography-A powerful tool for the discrimination of biotic and abiotic transformation processes of chiral environmental pollutants, J. Chromatogr. A. 1216 (2009) 481–502.

[40] N.H. Hashim, L.D. Nghiem, R.M. Stuetz, S.J. Khan, Enantiospecific fate of ibuprofen, ketoprofen and naproxen in a laboratory-scale membrane bioreactor, Water Res. 45 (2011) 6249–6258.

[41] W.C. Li, Occurrence, sources, and fate of pharmaceuticals in aquatic environment and soil, Environ. Pollut. 187 (2014) 193–201.

[42] G. Huschek, P.D. Hansen, H.H. Maurer, D. Krengel, A. Kayser, Environmental risk assesssment of medicinal products for human use according to European Commission recommendations, Environ. Toxicol. 19 (2004) 226–240.

[43] U. Kunkel, M. Radke, Fate of pharmaceuticals in rivers: Deriving a benchmark dataset at favorable attenuation conditions, Water Res. 46 (2012) 5551–5565.

[44] D. Fatta-kassinos, S. Meric, A. Nikolaou, Pharmaceutical residues in environmental waters and wastewater: current state of knowledge and future research, Anal. Bioanal. Chem. 399 (2011) 251–275.

[45] A. Yu-Chen Lin, M. Reinhard, Photodegradation of common environmental pharmaceuticals and estrogens in river water, Environ. Chem. 24 (2005) 1303–1309.

[46] B. Petrie, R. Barden, B. Kasprzyk-Hordern, A review on emerging contaminants in wastewaters and the environment: Current knowledge, understudied areas and recommendations for future monitoring, Water Res. 72 (2015) 3–27.

[47] B. Henrique, L.A. Kristofco, C. Mara, R. De Oliveira, B.W. Brooks, Global review and analysis of erythromycin in the environment : Occurrence, bioaccumulation and antibiotic

resistance hazards, Environ. Pollut. 238 (2018) 440–451.

[48]   C.E. West, S.J. Rowland, Aqueous Phototransformation of Diazepam and Related Human Metabolites under Simulated Sunlight, Environ. Sci. Technol. 46 (2012) 4749−4756.

[49]   E. Koumaki, D. Mamais, C. Noutsopoulos, M.C. Nika, A.A. Bletsou, N.S. Thomaidis, A. Eftaxias, G. Stratogianni, Degradation of emerging contaminants from water under natural sunlight: The effect of season, pH, humic acids and nitrate and identification of photodegradation by-products, Chemosphere 138 (2015) 675–681.

[50]   R. Andreozzi, Pharmaceuticals in STP Effluents and Their Solar Photodegradation in Pharmaceuticals in STP effluents and their solar photodegradation in aquatic environment, Chemosphere 6535 (2017) 1–14.

[51]   L. Fu, T. Huang, S. Wang, X. Wang, L. Su, C. Li, Y. Zhao, Toxicity of 13 different antibiotics towards freshwater green algae Pseudokirchneriella subcapitata and their modes of action, Chemosphere 168 (2017) 217–222.

[52]   P. Kovalakova, L. Cizmas, T.J. Mcdonald, B. Marsalek, M. Feng, V.K. Sharma, Occurrence and toxicity of antibiotics in the aquatic environment : A review, Chemosphere 251 (2020) 1–15

[53]   S. Stolte, J. Arning, U. Uebers, A. Böschen, P. Stepnowski, A. Białk-bielin, M. Matzke, Ecotoxicity evaluation of selected sulfonamides, Chemosphere 85 (2011) 928–933.

[54]   R. Jijie, G. Mihalache, I. Balmus, S. Strungaru, E.S. Baltag, A. Ciobica, M. Nicoara, C. Faggio, Zebrafish as a Screening Model to Study the Single and Joint Effects of Antibiotics, Pharmaceuticals 14 (2021) 1–26.

[55]   A. Munch, B. Markussen, A. Baun, B. Halling-sørensen, Probabilistic environmental risk characterization of pharmaceuticals in sewage treatment plant discharges, Chemosphere 77 (2009) 351–358.

[56]   N. Martins, R. Pereira, N. Abrantes, J. Pereira, F. Gonc, C.R. Marques, Ecotoxicological effects of ciprofloxacin on freshwater species : data integration and derivation of toxicity thresholds for risk assessment, Ecotoxicology 21 (2012) 1167–1176.

[57]   N.H. Tran, M. Reinhard, K.Y.H. Gin, Occurrence and fate of emerging contaminants in municipal wastewater treatment plants from different geographical regions-a review, Water Res. 133 (2018) 182–207.

[58]   V. Homem, L. Santos, Degradation and removal methods of antibiotics from aqueous matrices - A review, J. Environ. Manage. 92 (2011) 2304–2347.

[59]   E. Zuccato, S. Castiglioni, R. Bagnati, M. Melis, R. Fanelli, Source, occurrence and fate of antibiotics in the Italian aquatic environment, J. Hazard. Mater. 179 (2010) 1042–1048.

[60]   R. Andreozzi, R. Marotta, N. Paxéus, Pharmaceuticals in STP effluents and their solar photodegradation in aquatic environment, Chemosphere 50 (2003) 1319–1330.

[61]   L. Lonappan, S.K. Brar, R.K. Das, M. Verma, R.Y. Surampalli, Diclofenac and its transformation products: Environmental occurrence and toxicity - A review, Environ. Int. 96 (2016) 127–138.

[62]   M. Parolini, Toxicity of the Non-Steroidal Anti-inflammatory Drugs (NSAIDs) acetylsalicylic acid, paracetamol, diclofenac, ibuprofen and naproxen towards freshwater invertebrates: a review, Sci. Total Environ. 740 (2020) 1–54.

[63]   Y. Zhang, J. Guo, T. Yao, Y. Zhang, X. Zhou, H. Chu, The influence of four pharmaceuticals on Chlorellapyrenoidosa culture, Sci. Rep. 9 (2019) 1–10.

[64]   J. Lee, K. Ji, Y. Lim, P. Kim, K. Choi, Ecotoxicology and Environmental Safety Chronic exposure to diclofenac on two freshwater cladocerans and Japanese medaka, Ecotoxicol. Environ. Saf. 74 (2011) 1216–1225.

[65]   U. Memmert, A. Peither, R. Burri, K. Weber, T. Schmidt, J.P. Sumpter, A.Hartmann, Diclofenac: New data on chronic toxicity and bioconcentration in fish, Environ. Toxicol. Chem. 32 (2013) 442–452.

[66]   E. Commission, Communication from the Commission to the European Parliament, the Council, and the European Economic and Social Committee, EU Commision. 128 (2019) 13.

[67] N. Milić, M. Milanović, N.G. Letić, M.T. Sekulić, J. Radonić, I. Mihajlović, M.V. Miloradov, Occurrence of antibiotics as emerging contaminant substances in aquatic environment, Int. J. Environ. Health Res. 23 (2013) 296–310.

[68] T.B. Minh, H.W. Leung, I.H. Loi, W.H. Chan, M.K. So, J.Q. Mao, D. Choi, J.C.W. Lam, G. Zheng, M. Martin, J.H.W. Lee, P.K.S. Lam, B.J. Richardson, Antibiotics in the Hong Kong metropolitan area: Ubiquitous distribution and fate in Victoria Harbour, Mar. Pollut. Bull. 58 (2009) 1052–1062.

[69] J. Żur, A. Piński, A. Marchlewicz, K. Hupert-Kocurek, D. Wojcieszyńska, U. Guzik, Organic micropollutants paracetamol and ibuprofen—toxicity, biodegradation, and genetic background of their utilization by bacteria, Environ. Sci. Pollut. Res. 25 (2018) 21498–21524.

[70] I. Georgaki, E. Vasilaki, N. Katsarakis, A Study on the Degradation of Carbamazepine and Ibuprofen by TiO_2 & ZnO Photocatalysis upon UV/Visible-Light Irradiation, Am. J. Anal. Chem. 5 (2014) 518–534.

[71] B.G. Zheng, Z. Zheng, J.B. Zhang, X.Z. Luo, J.Q. Wang, Q. Liu, L.H. Wang, Degradation of the emerging contaminant ibuprofen in aqueous solution by gamma irradiation, Desalination 276 (2011) 379–385.

[72] S.C. Reed, R.W. Crites, Natural systems for waste management and treatment, McGraw-Hill, Inc., New York, SAD, 1995.

[73] S. Han, K. Choi, J. Kim, K. Ji, S. Kim, B. Ahn, J. Yun, K. Choi, J.S. Khim, X. Zhang, J.P. Giesy, Endocrine disruption and consequences of chronic exposure to ibuprofen in Japanese medaka (Oryzias latipes) and freshwater cladocerans Daphnia magna and Moina macrocopa, Aquat. Toxicol. 98 (2010) 256–264.

[74] R. Loos, D. Marinov, I. Sanseverino, D. Napierska, T. Lettieri, Review of the 1st Watch List under the Water Framework Directive and recommendations for the 2nd Watch List, 2018.

[75] H.K. Painter, M. M., Buerkly, M. A., Julius, M. L., Vajda, A. M., Norris, D. O., Barber L. B., Furlong, E. T., Schultz, M. M., Schoenfuss, Antidepressants at aniromentally relevant

concentrations affect predator avoidance behaviour of larval fathead (Pimephales promelas), Environ. Toxicol. Chem. 28 (2009) 2677–2684.

[76] Z. Li, G. Lu, X. Yang, C. Wang, Single and combined effects of selected pharmaceuticals at sublethal concentrations on multiple biomarkers in Carassius auratus, Ecotoxicology 21 (2012) 353–361.

[77] J. Drzyma, J. Kalka, Ecotoxic interactions between pharmaceuticals in mixtures : Diclofenac and sulfamethoxazole, Chemosphere 259 (2020) 1–8.

[78] C.H. Johansson, L. Janmar, T. Backhaus, Toxicity of ciprofloxacin and sulfamethoxazole to marine periphytic algae and bacteria, Aquat. Toxicol. 156 (2014) 248–258.

[79] L. Zheng, Y. Zheng, C. Chen, Y. Zhan, X. Lin, Facile One-Pot Synthesis of ZnO/SnO$_2$ Heterojunction Photocatalysts with Excellent Photocatalytic Activity and Photostability, Chempluschem 3800 (2012) 217–223.

[80] A.O. Oluwole, E.O. Omotola, O.S. Olatunji, Pharmaceuticals and personal care products in water and wastewater: a review of treatment processes and use of photocatalyst immobilized on functionalized carbon in AOP degradation, BMC Chem. 14 (2020) 1–30.

[81] D. Qing, R.M. Gersberg, T. Hua, J. Zhu, M. Kumar, W. Jern, S. Keat, Fate of pharmaceutical compounds in hydroponic mesocosms planted with Scirpus validus, Environ. Pollut. 181 (2013) 98–106.

[82] M. Ibanez, E. Gracia-lor, L. Bijlsma, E. Morales, L. Pastor, F. Hernández, Removal of emerging contaminants in sewage water subjected to advanced oxidation with ozone, J. Hazard. Mater. 260 (2013) 389–398.

[83] G. Li, X. Nie, Y. Gao, T. An, Can environmental pharmaceuticals be photocatalytically degraded and completely mineralized in water using g-C$_3$N$_4$/TiO$_2$ under visible light irradiation?—Implications of persistent toxic intermediates, "Applied Catal. B, Environ. 180 (2016) 726–732.

[84] Y. Wang, J. Liu, D. Kang, C. Wu, Y. Wu, Removal of pharmaceuticals and personal care products from wastewater using algae-based technologies : a review, Rev. Environ. Sci.

Bio/Technology 16 (2017) 717–735.

[85]   J. Gomes, E. Domingues, M. Gmurek, R.M. Quinta-ferreira, Advanced oxidation processes for recalcitrant compounds removal comparison with biofiltration by Corbicula fluminea, Energy Reports 6 (2020) 666–671.

[86]   N. Koprivanac, A. Lončarić Božić, S. Papić, Cleaner production processes in the synthesis of blue anthraquinone reactive dyes, Dye. Pigment. 44 (1999) 33–40.

[87]   S. Papić, N. Koprivanac, A. Lončarić Božić, A. Meteš, Removal of some reactive dyes from synthetic wastewater by combined Al(III) coagulation/carbon adsorption process, Dye Pigment 62 (2004) 291–298.

[88]   A.A. Attia, W.E. Rashwan, S.A. Khedr, Capacity of activated carbon in the removal of acid dyes subsequent to its thermal treatment, Dye Pigment 69 (2006) 128–136.

[89]   J. Berset, R. Brenneisen, C. Mathieu, Analysis of llicit and illicit drugs in waste , surface and lake water samples using large volume direct injection high performance liquid chromatography – Electrospray tandem mass spectrometry (HPLC–MS/MS), Chemosphere 81 (2010) 859–866.

[90]   M. Rosa, M. Teresa, F. Ventura, Behavior of pharmaceuticals and drugs of abuse in a drinking water treatment plant (DWTP) using combined conventional and ultra filtration and reverse osmosis (UF/RO) treatments, Environ. Pollut. 159 (2011) 1584–1591.

[91]   B. Kasprzyk-Hordern, M. Ziółek, J. Nawrocki, Catalytic ozonation and methods of enhancing molecular ozone reactions in water treatment, Applied Catalysis B: Environmental 46 (2003) 639–669.

[92]   A. Kurt, B.K. Mert, N. Özengin, A. Kurt, B.K. Mert, N. Özengin, Treatment of Antibiotics in Wastewater Using Advanced Oxidation Processes (AOPs) in: Physico-Chemical Wastewater Treat. Resour. Recover., 2017.

[93]   Y. Deng, R. Zhao, Advanced Oxidation Processes (AOPs) in Wastewater Treatment, Curr. Pollut. Rep. 1 (2015) 167–176.

[94] W.A. Pryor, Oxy-radicals and related species: their formation, lifetimes, and reactions, Ann. Rev. Physiol. 48 (1986) 657–667.

[95] P.R. Gogate, A.B. Pandit, A review of imperative technologies for wastewater treatment I: Oxidation technologies at ambient conditions, Adv. Environ. Res. 8 (2004) 501–551.

[96] L. Prieto-Rodríguez, I. Oller, N. Klamerth, A. Agüera, E.M. Rodríguez, S. Malato, Application of solar AOPs and ozonation for elimination of micropollutants in municipal wastewater treatment plant effluents, Water Res. 47 (2013) 1521–1528.

[97] T. Shindhal, P. Rakholiya, S. Varjani, A. Pandey, H.H. Ngo, W. Guo, H.Y. Ng, M.J. Taherzadeh, A critical review on advances in the practices and perspectives for the treatment of dye industry wastewater, BioEngineering 12 (2021) 70–87.

[98] A.C.A. Garcia, M.A.S. Rodrigues, J.L.N. Xavier, V. Gazulla, A. Meneguzzi, A.M. Bernardes, Degradation of cyanotoxins (microcystin) in drinking water using photoelectrooxidation, Brazilian J. Biol. 75 (2015) S45–S49.

[99] C. Comninellis, A. Kapalka, S. Malato, S.A. Parsons, I. Poulios, D. Mantzavinos, Advanced oxidation processes for water treatment : advances and trends for R&D, J. of Chemical Technol. Biotechnol. 776 (2008) 769–776.

[100] M. Agulló-Barceló, M.I. Polo-López, F. Lucena, J. Jofre, P. Fernández-Ibáñez, Solar Advanced Oxidation Processes as disinfection tertiary treatments for real wastewater: Implications for water reclamation, Appl. Catal. B Environ. 136–137 (2013) 341–350.

[101] R. Andreozzi, V. Caprio, A. Insola, R. Marotta, Advanced oxidation processes (AOP) for water purification and recovery, Catal. Today. 53 (1999) 51–59.

[102] H. Kušić, N. Koprivanac, B.R. Locke, Decomposition of phenol by hybrid gas/liquid electrical discharge reactors with zeolite catalysts, J. Hazard. Mater. 125 (2005) 190–200.

[103] S. Giannakis, S. Rtimi, C. Pulgarin, Light-assisted advanced oxidation processes for the elimination of chemical and microbiological pollution of wastewaters in developed and developing countries, Molecules 22 (2017) 1–21.

[104] J.A. LaVerne, OH radicals and oxidizing products in the gamma radiolysis of water, Radiat. Res. 153 (2000) 196–200.

[105] H.K. Fujishima A., Electrochemical photolysis of water at a semiconductor electrode, Nature. 238 (1972) 38–40.

[106] M.R. Hoffmann, S.T. Martin, W. Choi, D.W. Bahnemann, Environmental Applications of Semiconductor Photocatalysis, Chem. Rev. 95 (1995) 69–96.

[107] V. Maroga Mboula, V. Héquet, Y. Gru, R. Colin, Y. Andrès, Assessment of the efficiency of photocatalysis on tetracycline biodegradation, J. Hazard. Mater. 209–210 (2012) 355–364.

[108] X. Wang, W. Bi, P. Zhai, X. Wang, H. Li, G. Mailhot, W. Dong, Adsorption and photocatalytic degradation of pharmaceuticals by $BiOCl_xI_y$ nanospheres in aqueous solution, Appl. Surf. Sci. 360 (2016) 240–251.

[109] C.M. Lee, P. Palaniandy, I. Dahlan, Pharmaceutical residues in aquatic environment and water remediation by TiO_2 heterogeneous photocatalysis: a review, Environ. Earth Sci. 76 (2017) 1–19.

[110] C.B. Ong, L.Y. Ng, A.W. Mohammad, A review of ZnO nanoparticles as solar photocatalysts: Synthesis, mechanisms and applications, Renew. Sustain. Energy Rev. 81 (2018) 536–551.

[111] C.A. Bignozzi, S. Caramori, V. Cristino, R. Argazzi, L. Meda, A. Tacca, Nanostructured photoelectrodes based on WO_3: Applications to photooxidation of aqueous electrolytes, Chem. Soc. Rev. 42 (2013) 2228–2246.

[112] J. Zhang, B. Tian, L. Wang, M. Xing, J. Lei, Mechanism of Photocatalysis, in: Photocatal. Springer Singapore, (2018) 1–15.

[113] A.O. Ibhadon, P. Fitzpatrick, Heterogeneous photocatalysis: Recent advances and applications, Catalysts 3 (2013) 189–218.

[114] A.P. J. Dharma, Simple method of measuring the band gap energy value of TiO_2 in the

powder form using a UV/Vis/NIR spectrometer, PerkinElmer, Waltham, (2012).

[115] Q. Guo, C.Y. Zhou, Z.B. Ma, Z.F. Ren, H.J. Fan, X.M. Yang, Fundamental processes in surface photocatalysis on TiO_2, in: Wuli Huaxue Xuebao/Acta Phys. - Chim. Sin., (2016) 28–47.

[116] F. Saadati, N. Keramati, M.M. Ghazi, Influence of parameters on the photocatalytic degradation of tetracycline in wastewater: A review, Crit. Rev. Environ. Sci. Technol. 46 (2016) 757–782.

[117] A.M. Al-Hamdi, U. Rinner, M. Sillanpää, Tin dioxide as a photocatalyst for water treatment: A review, Process Saf. Environ. Prot. 107 (2017) 190–205.

[118] L. Yang, L.E. Yu, M.B. Ray, Degradation of paracetamol in aqueous solutions by TiO_2 photocatalysis, Water Res. 42 (2008) 3480–3488.

[119] V. Belgiorno, L. Rizzo, D. Fatta, C. Della Rocca, G. Lofrano, A. Nikolaou, V. Naddeo, S. Meric, Review on endocrine disrupting-emerging compounds in urban wastewater: occurrence and removal by photocatalysis and ultrasonic irradiation for wastewater reuse, Desalination 215 (2007) 166–176.

[120] N.A. Laoufi, S. Hout, D. Tassalit, A. Ounnar, A. Djouadi, N. Chekir, F. Bentahar, Removal of a persistent pharmaceutical micropollutant by UV/TiO_2 process using an immobilized titanium dioxide catalyst: Parametric study, Chem. Eng. Trans. 32 (2013) 1951–1956.

[121] Y. Ji, L. Zhou, C. Ferronato, X. Yang, A. Salvador, C. Zeng, J.M. Chovelon, Photocatalytic degradation of atenolol in aqueous titanium dioxide suspensions: Kinetics, intermediates and degradation pathways, J. Photochem. Photobiol. A Chem. 254 (2013) 35–44.

[122] D. Chen, Y. Cheng, N. Zhou, P. Chen, Y. Wang, K. Li, S. Huo, P. Cheng, P. Peng, R. Zhang, L. Wang, H. Liu, Y. Liu, R. Ruan, Photocatalytic degradation of organic pollutants using TiO_2-based photocatalysts: A review, J. Clean. Prod. 268 (2020) 1–14.

[123] A. Di Paola, G. Cufalo, M. Addamo, M. Bellardita, R. Campostrini, M. Ischia, R. Ceccato, L. Palmisano, Photocatalytic activity of nanocrystalline TiO_2 (brookite, rutile and brookite-based) powders prepared by thermohydrolysis of $TiCl_4$ in aqueous chloride solutions,

Colloids Surfaces A Physicochem. Eng. Asp. 317 (2008) 366–376.

[124] Y. Nosaka, A. Nosaka, Understanding Hydroxyl Radical (•OH) Generation Processes in Photocatalysis, ACS Energy Lett. 1 (2016) 356–359.

[125] D. Spasiano, R. Marotta, S. Malato, P. Fernandez-Ibañez, I. Di Somma, Solar photocatalysis: Materials, reactors, some commercial, and pre-industrialized applications. A comprehensive approach, Appl. Catal. B Environ. 170–171 (2015) 90–123.

[126] R. Hao, X. Xiao, X. Zuo, J. Nan, W. Zhang, Efficient adsorption and visible-light photocatalytic degradation of tetracycline hydrochloride using mesoporous BiOI microspheres, J. Hazard. Mater. 209–210 (2012) 137–145.

[127] C. Lalhriatpuia, D. Tiwari, A. Tiwari, S.M. Lee, Immobilized Nanopillars-TiO_2 in the efficient removal of micro-pollutants from aqueous solutions: Physico-chemical studies, Chem. Eng. J. 281 (2015) 782–792.

[128] A.K. Ray, Photocatalytic Reactor Configurations for Water Purification. Experimentation and Modeling, First Edit, Elsevier, 2009.

[129] M. Bouchy, O. Zahraa, Photocatalytic reactors, Int. J. Photoenergy. 5 (2003) 191–197.

[130] A.A. Abdel-Khalek, S.A. Mahmoud, A.H. Zaki, Visible light assisted photocatalytic degradation of crystal violet, bromophenol blue and eosin Y dyes using AgBr-ZnO nanocomposite, Environ. Nanotechnology, Monit. Manag. 9 (2018) 164–173.

[131] A. Elhalil, R. Elmoubarki, M. Farnane, A. Machrouhi, M. Sadiq, F.Z. Mahjoubi, S. Qourzal, N. Barka, Photocatalytic degradation of caffeine as a model pharmaceutical pollutant on Mg doped $ZnO-Al_2O_3$ heterostructure, Environ. Nanotechnology, Monit. Manag. 10 (2018) 63–72.

[132] S.H. Borji, S. Nasseri, A.H. Mahvi, R. Nabizadeh, A.H. Javadi, Investigation of photocatalytic degradation of phenol by Fe(III)-doped TiO_2 and TiO_2 nanoparticles, J. Environ. Heal. Sci. Eng. 12 (2014) 1–10.

[133] A.S. R. Saravanan, F. Gracia, Basic Principles, Mechanism, and Challenges of

Photocatalysis, in: Khan M., Pradhan D. SY Nanocomposites Visible Light. Photocatal. Springer Ser. Polym. Compos. Mater., (2017) 19–40.

[134] D. Ghime, P. Ghosh, Heterogeneous Fenton degradation of oxalic acid by using silica supported iron catalysts prepared from raw rice husk, J. Water Process Eng. 19 (2017) 156–163.

[135] S.G. Babu, P. Karthik, M.C. John, S.K. Lakhera, M. Ashokkumar, J. Khim, B. Neppolian, Synergistic effect of sono-photocatalytic process for the degradation of organic pollutants using CuO-TiO$_2$/rGO, Ultrason. Sonochem. 50 (2019) 218–223.

[136] I.K. Konstantinou, T.A. Albanis, TiO$_2$-assisted photocatalytic degradation of azo dyes in aqueous solution: Kinetic and mechanistic investigations: A review, Appl. Catal. B Environ. 49 (2004) 1–14.

[137] D.F. Ollis, E. Pelizzetti, N. Serpone, Photocatalyzed destruction of water contaminants, Environ. Sci. Technol. 25 (1991) 1522–1529.

[138] B. Neppolian, H.C. Choi, S. Sakthivel, B. Arabindoo, V. Murugesan, Solar light induced and TiO$_2$ assisted degradation of textile dye reactive blue 4, Chemosphere 46 (2002) 1173–1181.

[139] S.O. Fatin, H.N. Lim, W.T. Tan, N.M. Huang, Comparison of photocatalytic activity and cyclic voltammetry of zinc oxide and titanium dioxide nanoparticles toward degradation of methylene blue, Int. J. Electrochem. Sci. 7 (2012) 9074–9084.

[140] D. Bahnemann, Photocatalytic detoxification of polluted waters, in: Boule P Handb. Environ. Chem. 2. Part L Environ. Photochem. Springer, Berlin, (1999) 285–351.

[141] A. Zawawi, R. Ramli, N. Yub Harun, Photodegradation of 1-Butyl-3-methylimidazolium Chloride [Bmim]Cl via Synergistic Effect of Adsorption–Photodegradation of Fe-TiO$_2$/AC, Technologies 5 (2017) 1–13.

[142] M.S.T. Gonçalves, A.M.F. Oliveira-Campos, E.M.M.S. Pinto, P.M.S. Plasência, M.J.R.P. Queiroz, Photochemical treatment of solutions of azo dyes containing TiO$_2$, Chemosphere 39 (1999) 781–786.

[143] A. García, J. Matos, Photocatalytic activity of TiO_2 on activated carbon under visible light in the photodegradation of phenol, Open Mater. Sci. J. 4 (2010) 2–4.

[144] K.M. Reza, A. Kurny, F. Gulshan, Parameters affecting the photocatalytic degradation of dyes using TiO_2: a review, Appl. Water Sci. 7 (2017) 1569–1578.

[145] K. Mehrotra, G.S. Yablonsky, A.K. Ray, Macro kinetic studies for photocatalytic degradation of benzoic acid in immobilized systems, Chemosphere 60 (2005) 1427–1436.

[146] E.T. Soares, M.A. Lansarin, C.C. Moro, A study of process variables for the photocatalytic degradation of rhodamine B, Brazilian J. Chem. Eng. 24 (2007) 29–36.

[147] S. Zhou, A.K. Ray, Kinetic Studies for Photocatalytic Degradation of Eosin B on a Thin Film of Titanium Dioxide, Ind. Eng. Chem. Res. 42 (2003) 6020–6033.

[148] C.M. Myers, R. H., Montgomery, D. C., Anderson-Cook, Response Surface Methodology: Process and Product Optimization using Designed Experiments, 3rd ed., John Wiley & Sons, Hoboken, USA, 2009

[149] A.R. Khataee, M.B. Kasiri, Artificial neural networks modeling of contaminated water treatment processes by homogeneous and heterogeneous nanocatalysis, J. Mol. Catal. A Chem. 331 (2010) 86–100.

[150] H. Kusic, M. Jovic, N. Kos, N. Koprivanac, V. Marin, The comparison of photooxidation processes for the minimization of organic load of colored wastewater applying the response surface methodology, J. Hazard. Mater. 183 (2010) 189–202.

[151] M. Dopar, H. Kusic, N. Koprivanac, Treatment of simulated industrial wastewater by photo-Fenton process. Part I: The optimization of process parameters using design of experiments (DOE), Chem. Eng. J. 173 (2011) 267–279.

[152] T. Bolanča, Š. Ukić, I. Peternel, H. Kušić, A. Lončarić Božić, Artificial neural network models for advanced oxidation of organics in water matrix-Comparison of applied methodologies, Indian J. Chem. Technol. 21 (2014) 21–29.

[153] P. Kralik, H. Kusic, N. Koprivanac, A. Loncaric Bozic, Degradation of chlorinated

hydrocarbons by UV/H$_2$O$_2$: The application of experimental design and kinetic modeling approach, Chem. Eng. J. 158 (2010) 154–166.

[154] A. Tomic, M. Cvetnic, M. Kovacic, H. Kusic, P. Karamanis, A. Loncaric, Structural features promoting adsorption of contaminants of emerging concern onto - TiO$_2$ P25: experimental and computational approaches, Environ. Sci. Pollut. Res. 28 (2022) 1–17.

[155] R. Xiao, T. Ye, Z. Wei, S. Luo, Z. Yang, R. Spinney, Quantitative Structure-Activity Relationship (QSAR) for the Oxidation of Trace Organic Contaminants by Sulfate Radical, Environ. Sci. Technol. 49 (2015) 13394–13402.

[156] R. Yin, L. Ling, S. Lu, H. Li, C. Li, C. Shang, Degradation of aliphatic halogenated contaminants in water by UVA/CueTiO$_2$ and UVA/TiO$_2$ photocatalytic processes: Structure-activity relationship and role of reactive species, Chemosphere. 260 (2020) 1-9

[157] S. Ghosh, P.K. Ojha, K. Roy, Exploring QSPR modeling for adsorption of hazardous synthetic organic chemicals (SOCs) by SWCNTs, Chemosphere 228 (2019) 545–555.

[158] S. Karimifard, M. R. A. Moghaddam, Application of response surface methodology in physicochemical removal of dyes from wastewater: A critical review, Sci. Total Environ. 640–641 (2018) 772–797.

[159] S.L.C. Ferreira, R.E. Bruns, H.S. Ferreira, G.D. Matos, J.M. David, G.C. Brandão, E.G.P. da Silva, L.A. Portugal, P.S. dos Reis, A.S. Souza, W.N.L. dos Santos, Box-Behnken design: An alternative for the optimization of analytical methods, Anal. Chim. Acta. 597 (2007) 179–186.

[160] H. Xu, S.W.S. Wu, Optimization Methods, Theory and Applications, Springer, 2015.

[161] A.K. Das, S. Dewanjee, Optimization of Extraction Using Mathematical Models and Computation, Elsevier Inc., 2018.

[162] L. Murray, R.L. Mason, R.F. Gunst, J.L. Hess, Statistical Design and Analysis of Experiments: With Applications to Engineering and Science, Journal of the American Statistical Association 85 (1990) 1170-1171.

[163] A. Witek-Krowiak, K. Chojnacka, D. Podstawczyk, A. Dawiec, K. Pokomeda, Application of response surface methodology and artificial neural network methods in modelling and optimization of biosorption process, Bioresour. Technol. 160 (2014) 150–160.

[164] L. Zhang, Y. Zeng, Z. Cheng, Removal of heavy metal ions using chitosan and modified chitosan: A review, J. Mol. Liq. 214 (2016) 175–191.

[165] A.I. Khuri, S. Mukhopadhyay, Response surface methodology, Wiley Interdiscip. Rev. Comput. Stat. 2 (2010) 128–149.

[166] E. Stalidzans, M. Zanin, P. Tieri, F. Castiglione, A. Polster, S. Scheiner, J. Pahle, B. Stres, M. List, J. Baumbach, M. Lautizi, K. Van Steen, H.H.H.W. Schmidt, Mechanistic Modeling and Multiscale Applications for Precision Medicine: Theory and Practice, Netw. Syst. Med. 3 (2020) 36–56.

[167] G. Camera-Roda, F. Santarelli, M. Panico, Study and optimization of an annular photocatalytic slurry reactor, Photochem. Photobiol. Sci. 8 (2009) 712–718.

[168] U. Stafford, K. A. Gray, P.V. Kamat, Photocatalytic degradation of 4-chlorophenol: a mechanistically-base model, Res. Chem. Lntermed. 23 (1997) 355–388.

[169] L. del C. Cid, C.M.C. Vera, P.A. Sorichetti, Modelling and simulation of a photocatalytic reactor at high TiO_2 concentrations, Can. J. Chem. Eng. 100 (2022) 1530–1546.

[170] M. Cvetnić, A. Tomić, M. Sigurnjak, M.N. Stankov, Š. Ukić, H. Kušić, T. Bolanča, A. Lončarić Božić, Structural features of contaminants of emerging concern behind empirical parameters of mechanistic models describing their photooxidative degradation, J. Water Process Eng. 33 (2020) 1-11.

[171] M. Simunovic, H. Kusic, N. Koprivanac, A.L. Bozic, Treatment of simulated industrial wastewater by photo-Fenton process: Part II. The development of mechanistic model, Chem. Eng. J. 173 (2011) 280–289.

[172] P. Atkins, J. de Paula, Physical Chemistry, Eighth Edi, Oxford University Press, Great Britain, 2006.

[173] M. Kwon, S. Kim, Y. Yoon, Y. Jung, T.M. Hwang, J. Lee, J.W. Kang, Comparative evaluation of ibuprofen removal by UV/H$_2$O$_2$ and UV/S$_2$O$_8^{2-}$ processes for wastewater treatment, Chem. Eng. J. 269 (2015) 379–390.

[174] H. Kubinyi, QSAR and 3D QSAR in Drug Design Part 2: Applications and Problems, Drug Discov. Today 2 (1997) 538–546.

[175] M.T.D.C. Tomasz Puzyn, Jerzy Leszczynski, In silico approaches for predicting adame properties, Recent Advances in QSAR Studies: Methods and Applications (2010) 283–304.

[176] N.L. Kruhlak, J.F. Contrera, R.D. Benz, E.J. Matthews, Progress in QSAR toxicity screening of pharmaceutical impurities and other FDA regulated products, Adv. Drug Deliv. Rev. 59 (2007) 43–55.

[177] M. Smidt, H. Kusic, D. Juretic, M.N. Stankov, S. Ukic, T. Bolanca, M. Rogosic, A.L. Bozic, Modeling Photo-oxidative Degradation of Aromatics in Water. Optimization Study Using Response Surface and Structural Relationship Approaches, Ind. Eng. Chem. Res. 54 (2015) 5427–5441.

[178] B. Gui, X. Xu, S. Zhang, Y. Wang, C. Li, D. Zhang, L. Su, Y. Zhao, Prediction of organic compounds adsorbed by polyethylene and chlorinated polyethylene microplastics in freshwater using QSAR, Environ. Res. 197 (2021) 1-8.

[179] W. Bunmahotama, W.N. Hung, T.F. Lin, Predicting the adsorption of organic pollutants from water onto activated carbons based on the pore size distribution and molecular connectivity index, Water Res. 85 (2015) 521–531.

[180] B. Chen, T. Zhang, T. Bond, Y. Gan, Development of quantitative structure activity relationship (QSAR) model for disinfection byproduct (DBP) research: A review of methods and resources, J. Hazard. Mater. 299 (2015) 260–279.

[181] D. Awfa, M. Ateia, D. Mendoza, C. Yoshimura, Application of Quantitative Structure–Property Relationship Predictive Models to Water Treatment: A Critical Review, ACS ES&T Water 1 (2021) 498–517.

[182] D.J. de Ridder, L. Villacorte, A.R.D. Verliefde, J.Q.J.C. Verberk, S.G.J. Heijman, G.L.

Amy, J.C. van Dijk, Modeling equilibrium adsorption of organic micropollutants onto activated carbon, Water Res. 44 (2010) 3077–3086.

[183] A. Golbraikh, A. Tropsha, Beware of q^2!, J. Mol. Graph. Model. 20 (2002) 269–276.

[184] P. Gramatica, Chemometric Methods and Theoretical Molecular Descriptors in Predictive QSAR Modeling of the Environmental Behavior of Organic Pollutants, In: Puzyn, T., Leszczynski, J., Cronin, M. (eds) Recent Advances in QSAR Studies. Challenges and Advances in Computational Chemistry and Physics, Springer, 2010.

[185] D.D. Varsou, S. Nikolakopoulos, A. Tsoumanis, G. Melagraki, A. Afantitis, Molecular Descriptors for Structure–Activity Applications: A Hands-On Approach, in: Methods Mol. Biol., (2018) 3–53.

[186] Vikas, Chayawan, Externally predictive quantitative modeling of supercooled liquid vapor pressure of polychlorinated-naphthalenes through electron-correlation based quantum-mechanical descriptors, Chemosphere 95 (2014) 448–454.

[187] E. Estrada, E. Molina, Novel local (fragment-based) topological molecular descriptors for QSPR/QSAR and molecular design, J. Mol. Graph. Model. 20 (2001) 54–64.

[188] R. Put, Y. Vander Heyden, Review on modelling aspects in reversed-phase liquid chromatographic quantitative structure-retention relationships, Anal. Chim. Acta. 602 (2007) 164–172.

[189] N.H.M. S. Lundqvist, Theory of inhomogeneous electron gas, in: Plenum Press. New York, 1983.

[190] K. Roy, S. Kar, R.N. Das, A Primer on QSAR/QSPR Modeling: Fundamental Concepts, 2015.

[191] D. Whitley, An overview of evolutionary algorithms: Practical issues and common pitfalls, Inf. Softw. Technol. 43 (2001) 817–831.

[192] S. Nagarajan, N.C. Skillen, F. Fina, G. Zhang, C. Randorn, L.A. Lawton, J.T.S. Irvine, P.K.J. Robertson, Comparative assessment of visible light and UV active photocatalysts by

hydroxyl radical quantification, J. Photochem. Photobiol. A Chem. 334 (2017) 13–19.

[193] H. Kusic, N. Koprivanac, A.L. Bozic, Application of Sensitivity and Flux Analyses for the Reduction of Model Predicting the Photooxidative Degradation of an Azo Dye in Aqueous Media, Environ. Model. Assess. 17 (2012) 653–671.

[194] H. Kusic, I. Peternel, S. Ukic, N. Koprivanac, T. Bolanca, S. Papic, A.L. Bozic, Modeling of iron activated persulfate oxidation treating reactive azo dye in water matrix, Chem. Eng. J. 172 (2011) 109–121.

[195] H. Kusic, D. Juretic, N. Koprivanac, V. Marin, A.L. Božić, Photooxidation processes for an azo dye in aqueous media: Modeling of degradation kinetic and ecological parameters evaluation, J. Hazard. Mater. 185 (2011) 1558–1568.

[196] G. Li Puma, A. Brucato, Dimensionless analysis of slurry photocatalytic reactors using two-flux and six-flux radiation absorption-scattering models, Catal. Today. 122 (2007) 78–90.

[197] S.M. Jacob, Photoreactor Engineering, Northwestern University ProQuest Dissertations, 1967.

[198] A. Brucato, L. Rizzuti, Simplified Modeling of Radiant Fields in Heterogeneous Photoreactors. 1. Case of Zero Reflectance, Ind. Eng. Chem. Res. 36 (1997) 4740–4747.

[199] J. Meseguer, I. Pérez-Grande, A. Sanz-Andrés, Thermal radiation heat transfer, Spacecraft Thermal Control, 2012.

[200] E.W. M. Born, Electromagnetic theory ofpropagation, interference and diffraction of light, Cambridge University Press, 1961.

[201] A. Turolla, A. Piazzoli, J. Farner Budarz, M.R. Wiesner, M. Antonelli, Experimental measurement and modelling of reactive species generation in TiO$_2$ nanoparticle photocatalysis, Chem. Eng. J. 271 (2015) 260–268.

[202] O. Fónagy, E. Szabó-Bárdos, O. Horváth, 1,4-Benzoquinone and 1,4-hydroquinone based determination of electron and superoxide radical formed in heterogeneous photocatalytic systems, J. Photochem. Photobiol. A Chem. 407 (2021) 1–14.

[203] H. Kušić, N. Koprivanac, A.L. Božić, I. Selanec, Photo-assisted Fenton type processes for the degradation of phenol: A kinetic study, J. Hazard. Mater. 136 (2006) 632–644.

[204] H. Gallard, J. De Laat, Kinetic modelling of Fe(III)/H$_2$O$_2$ oxidation reactions in dilute aqueous solution using atrazine as a model organic compound, Water Res. 34 (2000) 3107–3116.

[205] N. Kang, D.S. Lee, J. Yoon, Kinetic modeling of Fenton oxidation of phenol and monochlorophenols, Chemosphere 47 (2002) 915–924.

[206] D. Juretic, H. Kusic, D.D. Dionysiou, B. Rasulev, A. Loncaric Bozic, Modeling of photooxidative degradation of aromatics in water matrix; combination of mechanistic and structural-relationship approach, Chem. Eng. J. 257 (2014) 229–241.

[207] G. V. Buxton, C.L. Greenstock, W.P. Helman, A.B. Ross, Critical Review of rate constants for reactions of hydrated electrons, hydrogen atoms and hydroxyl radicals (·OH/·O$^-$) in Aqueous Solution, J. Phys. Chem. Ref. Data. 17 (1988) 513–886.

[208] I. Arslan, I.A. Balcioglu, D.W. Bahnemann, Heterogeneous photocatalytic treatment of simulated dyehouse effluents using novel TiO$_2$-photocatalysts, Appl. Catal. B Environ. 26 (2000) 193–206.

[209] D. Lambropoulou, E. Evgenidou, V. Saliverou, C. Kosma, I. Konstantinou, Degradation of venlafaxine using TiO$_2$/UV process: Kinetic studies, RSM optimization, identification of transformation products and toxicity evaluation, J. Hazard. Mater. 323 (2017) 513–526.

[210] Koltsakidou, M. Antonopoulou, Evgenidou, I. Konstantinou, A.E. Giannakas, M. Papadaki, D. Bikiaris, D.A. Lambropoulou, Photocatalytical removal of fluorouracil using TiO$_2$-P25 and N/S doped TiO$_2$ catalysts: A kinetic and mechanistic study, Sci. Total Environ. 578 (2017) 257–267.

[211] Y. Ling, M.J. Klemes, S. Steinschneider, W.R. Dichtel, D.E. Helbling, QSARs to predict adsorption affinity of organic micropollutants for activated carbon and B-cyclodextrin polymer adsorbents, Water Res. 154 (2019) 217–226.

[212] S. Ghosh, P.K. Ojha, K. Roy, Eadsorption of hazardous syntheticxploring QSPR modeling

for organic chemicals (SOCs) by SWCNTs, Chemosphere 228 (2019) 545–555.

[213] P. Gramatica, Principles of QSAR models validation: internal and external, QSAR Comb. Sci. 26 (2007) 694–701.

[214] M. Cvetnic, D. Juretic Perisic, M. Kovacic, H. Kusic, J. Dermadi, S. Horvat, T. Bolanca, V. Marin, P. Karamanis, A. Loncaric Bozic, Prediction of biodegradability of aromatics in water using QSAR modeling, Ecotoxicol. Environ. Saf. 139 (2017) 139–149.

[215] G. Li, L. Lv, H. Fan, J. Ma, Y. Li, Y. Wan, X.S. Zhao, Effect of the agglomeration of TiO_2 nanoparticles on their photocatalytic performance in the aqueous phase, J. Colloid Interface Sci. 348 (2010) 342–347.

[216] F. Xu, Review of analytical studies on TiO_2 nanoparticles and particle aggregation, coagulation, flocculation, sedimentation, stabilization, Chemosphere 212 (2018) 662–677.

[217] J.Q. Jiang, Z. Zhou, V.K. Sharma, Occurrence, transportation, monitoring and treatment of emerging micro-pollutants in waste water - A review from global views, Microchem. J. 110 (2013) 292–300.

[218] D. Uretic, H. Kusic, D.D. Dionysiou, B. Rasulev, A. Loncaric Bozic, Modeling of photooxidative degradation of aromatics in water matrix; combination of mechanistic and structural-relationship approach, Chem. Eng. J. 257 (2014) 229–241.

[219] H. Czili, A. Horváth, Applicability of coumarin for detecting and measuring hydroxyl radicals generated by photoexcitation of TiO_2 nanoparticles, Appl. Catal. B Environ. 81 (2008) 295–302.

[220] M. Wojtoniszak, B. Zielinska, R.J. Kalenczuk, E. Mijowska, Photocatalytic performance of titania nanospheres deposited on graphene in coumarin oxidation reaction, Mater. Sci. Pol. 30 (2012) 32–38.

[221] T. Sharifi, D. Crmaric, M. Kovacic, M. Popovic, M.K. Rokovic, H. Kusic, D. Jozić, G. Ambrožić, D. Kralj, J. Kontrec, B. Zener, U.L. Stangar, D.D. Dionysiou, A.L. Bozic, Tailored BiVO4 for enhanced visible-light photocatalytic performance, J. Environ. Chem. Eng. 9 (2021) 1–15.

[222] D. Juretic, H. Kusic, A. Papic, M. Smidt, O. Jezovita, I. Peternel, A.L. Bozic, Modeling of photodegradation kinetics of aromatic pollutants in water matrix, J. Photochem. Photobiol. A Chem. 271 (2013) 65–76.

[223] L.A. Pérez-Estrada, S. Malato, W. Gernjak, A. Agüera, E.M. Thurman, I. Ferrer, A.R. Fernández-Alba, Photo-fenton degradation of diclofenac: Identification of main intermediates and degradation pathway, Environ. Sci. Technol. 39 (2005) 8300–8306.

[224] M. Torun, Ö. Gültekin, D. Şolpan, O. Güven, Mineralization of paracetamol in aqueous solution with advanced oxidation processes, Environ. Technol. 36 (2015) 970–982.

[225] D. Juretic, H. Kusic, D.D. Dionysiou, B. Rasulev, I. Peternel, A. Loncaric Bozic, Prediction of key structural features responsible for aromaticity of single-benzene ring pollutants and their photooxidative intermediates, Chem. Eng. J. 276 (2015) 261–273.

[226] M. Cvetnić, M. Novak Stankov, M. Kovačić, Š. Ukić, T. Bolanča, H. Kušić, B. Rasulev, D.D. Dionysiou, A. Lončarić Božić, Key structural features promoting radical driven degradation of emerging contaminants in water, Environ. Int. 124 (2019) 38–48.

[227] M. Smidt, H. Kusic, D. Juretic, M.Novak Stankov, S. Ukic, T. Bolanca, M. Rogosic, A. Loncaric Bozic, Modeling Photo-oxidative Degradation of Aromatics in Water. Optimization Study Using Response Surface and Structural Relationship Approaches, Ind. Eng. Chem. Res. 54 (2015) 5427–5441.

[228] R. Wehrens, H. Putter, L.M.C. Buydens, The bootstrap: A tutorial, Chemom. Intell. Lab. Syst. 54 (2000) 35–52.

[229] M. Cvetnic, D. Juretic Perisic, M. Kovacic, S. Ukic, T. Bolanca, B. Rasulev, H. Kusic, A. Loncaric Bozic, Toxicity of aromatic pollutants and photooxidative intermediates in water: A QSAR study, Ecotoxicol. Environ. Saf. 169 (2019) 918–927.

[230] C. Rücker, G. Rücker, M. Meringer, Y-randomization and its variants in QSPR/QSAR, J. Chem. Inf. Model. 47 (2007) 2345–2357.

[231] H. Liu, E. Papa, P. Gramatica, Evaluation and QSAR modeling on multiple endpoints of estrogen activity based on different bioassays, Chemosphere 70 (2008) 1889–1897.

[232] R. Todeschini, V. Consonni, Handbook of Molecular Descriptors, In: Gasteiger, J. (Ed.), Handbook of Chemoinformatics: From Data to Knowledge, Wiley-VCH Verlag GmbH, Weinheim, 2003.

[233] J. Dreher, J. Scheiber, N. Stiefl, K. Baumann, XMaP - An Interpretable Alignment-Free Four-Dimensional Quantitative Structure-Activity Relationship Technique Based on Molecular Surface Properties and Conformer Ensembles, J. Chem. Inf. Model. 58 (2018) 165–181.

[234] J. Leszczynski, A. Kaczmarek-Kedziera, T. Puzyn, M.G. Papadopoulos, H. Reis, M.K. Shukla, Handbook of computational chemistry, 2017.

[235] V. Consonni, R. Todeschini, Multivariate Analysis of Molecular Descriptors, (2012) 111–147.

[236] S.C. Basak, B.D. Gute, G.D. Grunwald, Use of topostructural, topochemical, and geometric parameters in the prediction of vapor pressure: A hierarchical QSAR approach, J. Chem. Inf. Comput. Sci. 37 (1997) 651–655.

[237] E. Estrada, A. Ramírez, Edge adjacency relationships and molecular topographic descriptors. Definition and QSAR applications, J. Chem. Inf. Comput. Sci. 36 (1996) 837–843.

[238] A. Mauri, V. Consonni, M. Pavan, R. Todeschini, DRAGON software: An easy approach to molecular descriptor calculations, Match. 56 (2006) 237–248.

[239] K. Roy, I. Mitra, Electrotopological State Atom (E-State) Index in Drug Design, QSAR, Property Prediction and Toxicity Assessment, Curr. Comput. Aided-Drug Des. 8 (2012) 135–158.

[240] M. Kovacic, H. Kusic, M. Fanetti, U.L. Stangar, M. Valant, D.D. Dionysiou, A.L. Bozic, TiO_2-SnS_2 nanocomposites: solar-active photocatalytic materials for water treatment, Environ. Sci. Pollut. Res. 24 (2017) 19965–19979.

[241] M.O.P. Kovacic, H. Kusic, A. Loncaric Bozic, D.D. Dionysiou, Advanced Oxidation Processes, in: Encycl. Water Sci. Technol. Soc., (2020) 1925–1940.

[242] F.M. dela Rosa, J. Papac, S. Garcia-Ballesteros, M. Kovačić, Z. Katančić, H. Kušić, A.L. Božić, Solar Light Activation of Persulfate by TiO_2/Fe_2O_3 Layered Composite Films for Degradation of Amoxicillin: Degradation Mechanism, Matrix Effects, and Toxicity Assessments, Adv. Sustain. Syst. 5 (2021) 1–14.

[243] X. Luo, X. Wei, J. Chen, Q. Xie, X. Yang, W.J.G.M. Peijnenburg, Rate constants of hydroxyl radicals reaction with different dissociation species of fluoroquinolones and sulfonamides: Combined experimental and QSAR studies, Water Res. 166 (2019) 1–7.

[244] Y. Zhang, Y. Xiao, Y. Zhang, T.T. Lim, UV direct photolysis of halogenated disinfection byproducts: Experimental study and QSAR modeling, Chemosphere 235 (2019) 719–725.

[245] F. Lai, F.X. Tian, B. Xu, W.K. Ye, Y.Q. Gao, C. Chen, H.B. Xing, B. Wang, M.J. Xie, X.J. Hu, A comparative study on the degradation of phenylurea herbicides by UV/persulfate process: Kinetics, mechanisms, energy demand and toxicity evaluation associated with DBPs, Chem. Eng. J. 428 (2022) 1–12.

7. APPENDIX

Table A1 Experimentally determined K adsorption coefficients according to 3^2 FFD:

					K, $L \cdot g^{-1}$				
pH		**γ(TiO₂ P25), mg·L⁻¹**		**ALC**	**o-aminoBenzAc**	**AMX**	**AZN**	**BenzAc**	
-1	4	-1	0.4	0.458	0.677	2.173	2.825	0.823	
0	7	-1	0.4	0.304	0.551	2.066	2.372	0.866	
1	10	-1	0.4	0.458	0.677	3.708	1.073	1.010	
-1	4	0	0.8	0.387	0.622	2.686	2.560	0.789	
0	7	0	0.8	0.281	0.530	2.120	2.393	0.802	
1	10	0	0.8	0.387	0.622	3.280	1.485	0.881	
-1	4	1	1.2	0.329	0.574	2.784	2.611	0.777	
0	7	1	1.2	0.215	0.464	1.960	2.558	0.757	
1	10	1	1.2	0.384	0.619	3.065	1.613	0.814	
pH		**γ(TiO₂ P25), mg·L⁻¹**		**BPA**	**CIP**	**DSL**	**DVF**	**DCP**	
-1	4	-1	0.4	0.375	12.538	1.312	0.141	0.952	
0	7	-1	0.4	0.274	5.488	0.983	0.075	0.928	
1	10	-1	0.4	2.655	0.151	1.010	7.051	0.952	
-1	4	0	0.8	0.344	13.115	1.132	0.119	0.942	
0	7	0	0.8	0.240	7.661	0.871	0.058	0.924	
1	10	0	0.8	2.019	0.387	0.860	4.078	0.942	
-1	4	1	1.2	0.391	14.435	1.079	0.153	0.933	
0	7	1	1.2	0.421	6.929	0.830	0.177	0.909	
1	10	1	1.2	1.756	0.311	0.814	3.082	0.942	
pH		**γ(TiO₂ P25), mg·L⁻¹**		**DCF**	**1,4-DMB**	**2,6-DMP**	**DIU**	**DPH**	
-1	4	-1	0.4	23.638	1.040	0.842	0.652	1.962	
0	7	-1	0.4	1.652	0.880	0.861	0.458	1.305	
1	10	-1	0.4	0.100	0.801	0.794	1.216	1.145	
-1	4	0	0.8	28.084	0.898	0.637	0.675	1.245	
0	7	0	0.8	0.970	0.793	0.738	0.421	0.950	
1	10	0	0.8	0.307	0.725	0.724	0.675	0.742	
-1	4	1	1.2	35.993	0.815	0.528	1.089	1.000	
0	7	1	1.2	0.824	0.676	0.658	0.358	0.733	
1	10	1	1.2	0.420	0.687	0.666	0.479	0.616	

Table A2 Experimentally determined K coefficients according to 3^2 FFD:

				EE2	ETD	HCTZ	IBP	*p*-MP
				K, L·g⁻¹				

pH		γ(TiO₂ P25), mg·L⁻¹		EE2	ETD	HCTZ	IBP	*p*-MP
-1	4	-1	0.4	2.964	13.533	1.722	1.910	1.082
0	7	-1	0.4	0.934	5.128	0.966	0.285	0.774
1	10	-1	0.4	1.042	1.761	1.021	0.246	0.642
-1	4	0	0.8	1.640	7.596	1.281	1.359	0.806
0	7	0	0.8	0.575	2.898	0.758	0.381	0.628
1	10	0	0.8	0.548	2.416	0.740	0.279	0.526
-1	4	1	1.2	1.357	5.873	1.165	1.156	0.664
0	7	1	1.2	0.476	2.503	0.690	0.553	0.458
1	10	1	1.2	0.439	2.968	0.662	0.390	0.471

pH		γ(TiO₂ P25), mg·L⁻¹		*m*-NP	*p*-NP	OMP	OXY	Ph
-1	4	-1	0.4	1.171	0.823	1.401	7.982	0.907
0	7	-1	0.4	0.600	0.742	1.142	5.625	0.862
1	10	-1	0.4	0.412	0.823	1.070	1.151	0.907
-1	4	0	0.8	0.649	0.789	1.116	6.555	0.888
0	7	0	0.8	0.395	0.728	0.974	5.724	0.853
1	10	0	0.8	0.277	0.789	0.861	2.206	0.888
-1	4	1	1.2	0.441	0.757	1.000	6.818	0.870
0	7	1	1.2	0.209	0.681	0.856	6.541	0.825
1	10	1	1.2	0.222	0.787	0.785	2.603	0.887

pH		γ(TiO₂ P25), mg·L⁻¹		SalAc	SZM	SA	TB	VZD
-1	4	-1	0.4	0.677	0.458	0.710	3.835	2.772
0	7	-1	0.4	0.750	0.562	0.741	6.871	2.400
1	10	-1	0.4	1.021	1.042	0.631	4.819	5.318
-1	4	0	0.8	0.622	0.387	0.405	2.626	1.659
0	7	0	0.8	0.643	0.413	0.545	3.995	1.991
1	10	0	0.8	0.776	0.603	0.524	2.644	3.200
-1	4	1	1.2	0.604	0.365	0.279	1.975	1.199
0	7	1	1.2	0.574	0.329	0.433	3.142	1.468
1	10	1	1.2	0.662	0.439	0.444	1.912	2.734

Table A3 Accuracy and significance of derived RSM models in a form of quadratic polynomial equations for 30 studied organics compounds using 3^2 FFD with square root transformation of the response ($Y' = \sqrt{Y}$):

Abbreviation	RSM models	R^2	$p<0.05$
ALC	$Y = 0.008X_1 + 0.117X_1^2 - 0.041X_2 + 0.002X_2^2 + 0.011X_1X_2 + 0.514$	0.9791	0.0101
o-aminoBenzAc	$Y = 0.095X_1 - 0.092X_1^2 - 0.02X_2 + 0.002X_1X_2 + 0.657$	0.9658	0.0208
AMX	$Y = 0.118X_1 + 0.28X_1^2 - 0.003X_2 - 0.026X_2^2 - 0.092X_1X_2 + 1.448$	0.9861	0.0055
AZN	$Y = 0.183X_1 + 0.218X_1^2 - 0.072X_2 + 0.026X_2^2 - 0.03X_1X_2 + 0.435$	0.9853	0.0059
BenzAc	$Y = -0.256X_1 + 0.275X_1^2 - 0.057X_2 + 0.088X_2^2 - 0.147X_1X_2 + 0.303$	0.9524	0.0338
BPA	$Y = -0.024X_1 + 0.529X_1^2 - 0.721X_2 - 0.079X_2^2 - 0.782X_1X_2 + 2.804$	0.9555	0.0306
CIP	$Y = -1.566X_1 - 0.493X_1^2 + 0.12X_2 - 0.127X_2^2 - 0.022X_1X_2 + 2.665$	0.9975	0.0004
DSL	$Y = 0.197X_1 + 0.377X_1^2 - 0.172X_2 + 0.043X_2^2 - 0.17X_1X_2 + 0.969$	0.9712	0.0162
DVF	$Y = 0.887X_1 + 0.945X_1^2 - 0.123X_2 + 0.111X_2^2 - 0.229X_1X_2 + 0.238$	0.9823	0.0078
DCP	$Y = 0.039X_1 + 0.007X_1^2 + 0.103X_2 - 0.141X_2^2 - 0.019X_1X_2 + 0.523$	0.9685	0.0185
DCF	$Y = -2.44X_1 + 1.887X_1^2 + 0.182X_2 + 0.057X_2^2 - 0.202X_1X_2 + 1.021$	0.9902	0.0033
1,4-DMB	$Y = -0.094X_1 + 0.291X_1^2 + 0.144X_2 + 0.053X_2^2 - 0.187X_1X_2 + 0.544$	0.9708	0.0165
2,6-DMP	$Y = 0.037X_1 + 0.136X_1^2 - 0.045X_2 + 0.028X_2^2 - 0.014X_1X_2 + 0.329$	0.9646	0.0219
DIU	$Y = -0.009X_1 + 0.24X_1^2 - 0.042X_2 + 0.056X_2^2 - 0.126X_1X_2 + 0.604$	0.9799	0.0095
DPH	$Y = -0.133X_1 + 0.048X_1^2 - 0.162X_2 + 0.058X_2^2 + 0.029X_1X_2 + 0.952$	0.9918	0.0025
EE2	$Y = -0.291X_1 + 0.294X_1^2 - 0.199X_2 + 0.111X_2^2 + 0.05X_1X_2 + 0.731$	0.9856	0.0058
ETD	$Y = -0.709X_1 + 0.394X_1^2 - 0.257X_2 + 0.162X_2^2 + 0.413X_1X_2 + 1.742$	0.9868	0.0051
HCTZ	$Y = -0.329X_1 + 0.35X_1^2 + 0.095X_2 + 0.077X_2^2 - 0.191X_1X_2 + 0.259$	0.9809	0.0088
IBP	$Y = -0.329X_1 + 0.247X_1^2 + 0.005X_2 + 0.039X_2^2 + 0.109X_1X_2 + 0.606$	0.9643	0.0221
p-MP	$Y = 0.02X_1 - 0.089X_1^2 + 0.016X_2 - 0.008X_2^2 + 0.007X_1X_2 + 0.325$	0.9643	0.0222
m-NP	$Y = -0.152X_1 + 0.078X_1^2 - 0.151X_2 + 0.028X_2^2 + 0.062X_1X_2 + 0.601$	0.9925	0.0022
p-NP	$Y = -0.025X_1 - 0.05X_1^2 + 0.055X_2 + 0.04X_2^2 + 0.036X_1X_2 + 0.309$	0.9661	0.0206
OMP	$Y = -0.223X_1 + 0.044X_1^2 - 0.065X_2 + 0.178X_2^2 + 0.427X_1X_2 + 1.866$	0.9727	0.0150
OXY	$Y = -0.628X_1 - 0.413X_1^2 + 0.085X_2 + 0.029X_2^2 + 0.189X_1X_2 + 2.421$	0.9893	0.0037
Ph	$Y = -0.008X_1 + 0.013X_1^2 - 0.003X_2 + 0.009X_2^2 + 0.025X_1X_2 + 0.184$	0.9642	0.0223
SalAc	$Y = -0.667X_1 + 0.176X_1^2 + 0.165X_2 - 0.053X_2^2 - 0.143X_1X_2 + 1.013$	0.9778	0.0110
SZM	$Y = 0.93X_1 + 0.072X_1^2 - 0.101X_2 + 0.034X_2^2 - 0.071X_1X_2 + 0.633$	0.9901	0.0033
SA	$Y = 0.029X_1 - 0.054X_1^2 - 0.107X_2 + 0.026X_2^2 + 0.047X_1X_2 + 0.736$	0.9921	0.0024
TB	$Y = 0.037X_1 - 0.433X_1^2 - 0.369X_2 + 0.141X_2^2 - 0.065X_1X_2 + 2.037$	0.9875	0.0047
VZD	$Y = 0.283X_1 + 0.242X_1^2 - 0.26X_2 + 0.084X_2^2 - 0.021X_1X_2 + 1.335$	0.9610	0.0252

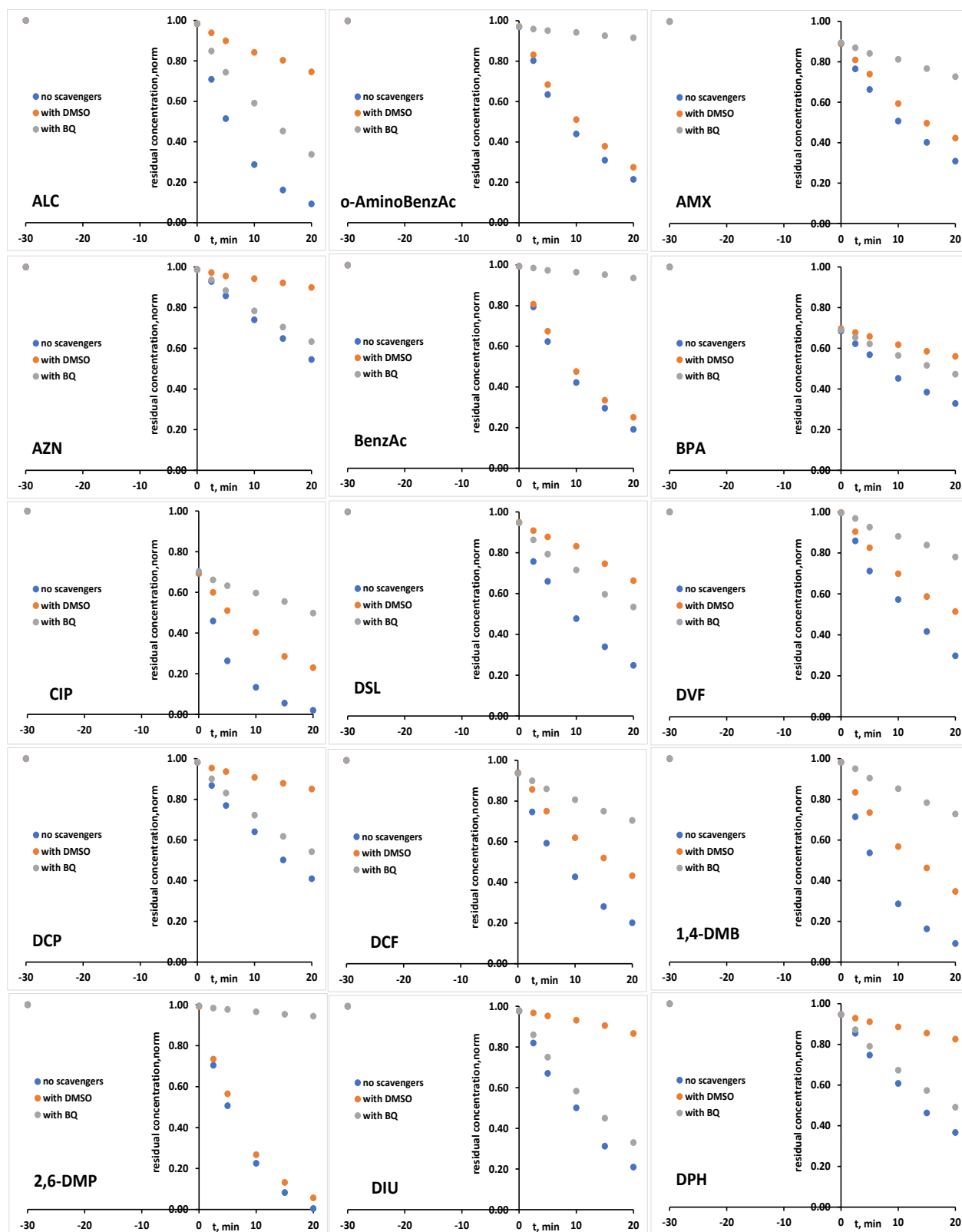**Figure A1** Degradation kinetics of studied organic compound (#1-15, Table 18) without and with the presence of scavengers for HO• and $O_2^{-•}$.
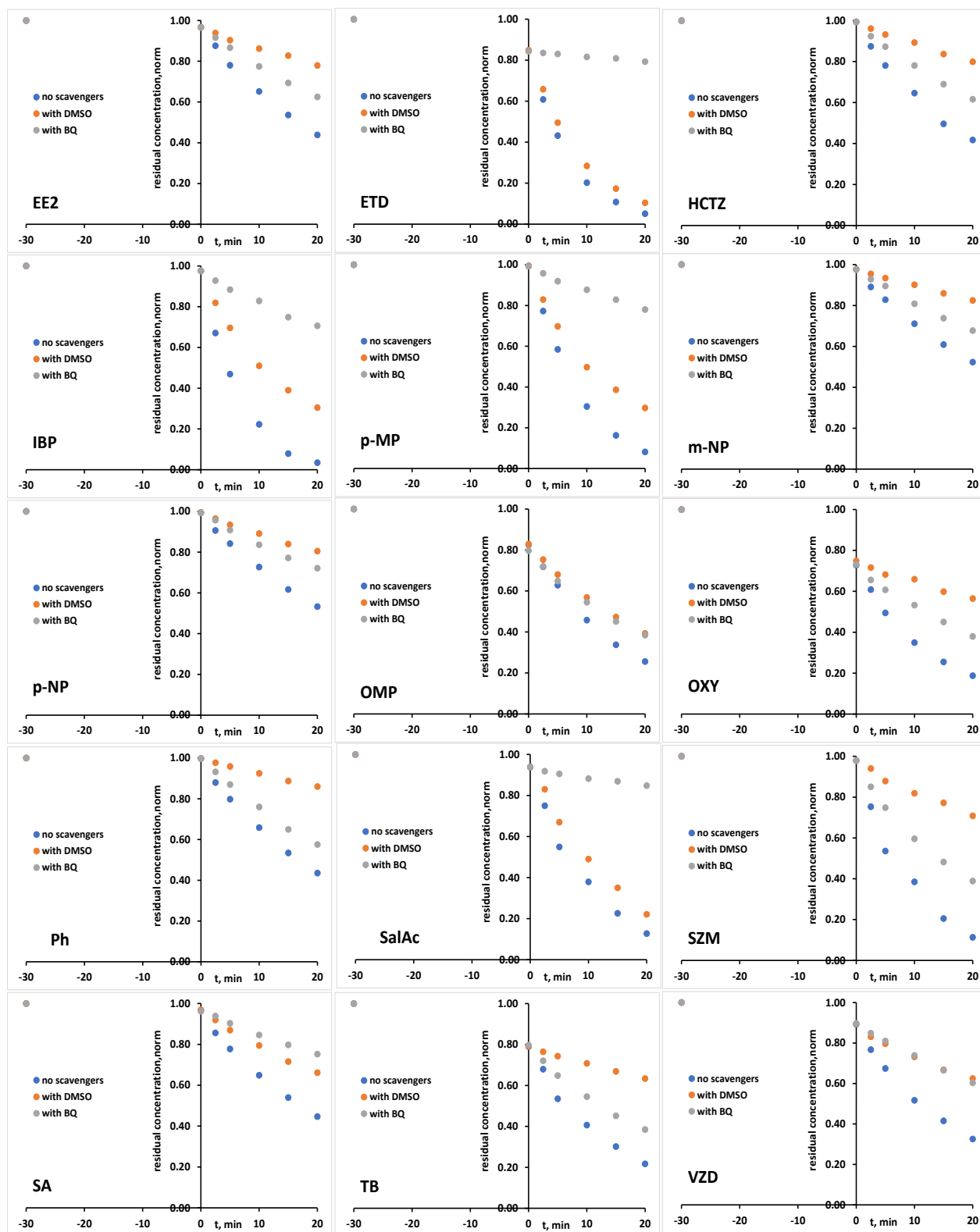
Figure A2 Degradation kinetics of studied organic compound (#16-30, Table 18) without and with the presence of scavengers for HO• and $O_2^{-•}$.

CURRICULUM VITAE

Antonija Tomić ▮▮▮▮▮▮▮▮▮▮▮▮ ▮▮ ▮▮▮▮▮▮▮ She attended and graduated primary and secondary school in Požega. In 2011, she enrolled in undergraduate studies in chemical engineering at the Faculty of Chemical Engineering and Technology at the University of Zagreb, and after completing the undergraduate studies, she enrolled in graduate studies at the same faculty. During graduate degree, she received the Dean's Award for a prestigious student research work. She completed her graduate studies in 2017, and next year she enrolled in the doctoral studies in Chemical Engineering and Applied Chemistry. She received her doctorate in (10th January 2023) with the topic: "Modelling of photocatalytic degradation of pharmaceuticals in water by multi-faceted approach."

Since July 2018, she has been an employee at the Department of Polymer Engineering and Organic Chemical Technology, Faculty of Chemical Engineering and Technology, University of Zagreb. In addition to scientific research at the department, she is involved as a direct supervisor in the implementation of student theses and laboratory exercises. In December of the same year, she joined the Croatian Science Foundation project team: *Modeling of Environmental Aspects of Advanced Water Treatment for degradation of Priority Pollutants* (Project IP-09-2014-7992 MEAoWT) under the supervision of prof. Tomislav Bolanča, Ph. D. Since 2019 she was member of project team the Croatian Science Foundation: *Nano-sized Solar-active Catalysts for Environmental Technologies* (Project IP-01-2018, NaSCEnT) under the supervisor of prof. Hrvoje Kušić, Ph. D. As part of scientific research, she participated in 9 scientific conference and 1 professional conference and is co-author of 3 scientific publications cited in the Web of Science database and 1 review paper published in a journal cited in secondary publications.

BIBLIOGRAPHY

Original scientific papers in CC journals:

[1] A. Tomić, M. Cvetnić, M. Kovačić, H. Kušić, P. Karamanis, A. Lončaric Bozić, Structural features promoting adsorption of contaminants of emerging concern onto TiO_2 P25: experimental and computational approaches, *Environmental science and pollution research* 29 (2022) 1-17.

[2] M. Kovačić, K. Perović, J. Papac, A. Tomić, L. Matoh, B. Žener, T. Brodar, I. Capan, A. K. Surca, H. Kušić, U. Lavrenčič Štangar, A. Lončarić Božić, One-Pot Synthesis of Sulfur-Doped TiO_2/Reduced Graphene Oxide Composite (S-TiO_2/rGO) with Improved Photocatalytic Activity for the Removal of Diclofenac from Water, *Materials* 13 (2020) 1-14.

[3] M. Cvetnić, A. Tomić, M. Sigurnjak, M. Novak Stankov, Š. Ukić, H. Kušić, T. Bolanča, A. Lončarić Božić, Structural features of contaminants of emerging concern behind empirical parameters of mechanistic models describing their photooxidative degradation*, Journal of water process engineering* 33 (2020) 1-11.

Rewiev paper in secondary publications:

[1] A. Tomić, H. Kušić, T. Bolanča, A. Lončarić Božić, Nova mikroonečišćivala u vodenom okolišu, *Hrvatske Vode* 118 (2021) 241-254.

Conference presentations:

[1] A. Tomić, M. Cvetnić, H. Kušić, A. Lončarić Božić, Modelling and prediction of adsorption coefficients of various pollutants in water by multi-faceted approach, 11th European Conference on Solar Chemistry and Photocatalysis: Environmental Applications (SPEA11) // Book of Abstracts / D. Fabbri, A. Bianco, P. E. Laurenti (ed.), Turin, (2022) 428-428 (poster).

[2] A. Tomić, M. Cvetnić, H. Kušić, M. Kovačić, A. Lončarić Božić, Predictive quantitative structure-property relationship (QSPR) and response surface modelling for adsorption processes of contaminants of emerging concern in water onto TiO_2, 27th Croatian meeting of chemist and chemical engineers (27th HSKIKI) // Book of abstracts / D. Marković, E. Meštrović, D. Namjesnik, V. Tomašić (ed.), Veli Lošinj: Croatian Society of Chemical Engineers and Technologists, (2021)

337-337 (poster).

[3] A. Tomić, M. Gavran, M. Kovačić, H. Kušić, A. Lončarić Božić, Experimental and computational study on the adsorption of contaminants of emerging concern on TiO_2 photocatalyst, 2020 EFCATS Summer School (EFCATS) // Book of abstracts: Engineering materials for catalysis / A. Pintar, N. Novak Tušar, G. Rupprechter (ed.), Portorose, (2020) 53-53 (poster).

[4] F. dela Rosa, J. Papac, A. Tomić, M. Kovačić, M. Kraljić Roković, H. Kušić, U. Lavrenčič Štangar, A. Lončarić Božić, Facile preparation of TiO_2/Fe_2O_3 layered composite films for solar-driven photocatalytic degradation of pharmaceuticals, XIII Meeting of young chemical engineers (XIII SMLKI) // Book of abstracts / I. Dejanović, D. Vrsaljko, K. Žižek (ed.), Zagreb: Croatian Society of Chemical Engineers, (2020) 83-83 (poster).

[5] A. Tomić, F. dela Rosa, M. Kovačić, H. Kušić, A. Lončarić Božić, Photocatalytic degradation of pharmaceuticals in water: Response surface modeling approach, XIII Meeting of young chemical engineers (XIII SMLKI) // Book of abstracts / I. Dejanović, D. Vrsaljko, K. Žižek (ed.), Zagreb: Croatian Society of Chemical Engineers, (2020) 101-101 (poster).

[6] A. Tomić, M. Cvetnić, T. Bolanča, M. Novak Stankov, Š. Ukić, H. Kušić, A. Lončarić Božić, Photooxidative degradation of pharmaceuticals and pesticides in water: mechanistic modelling approach, 26th Croatian meeting of chemist and chemical engineers (26th HSKIKI) // Book of abstracts / N. Galić, M. Rogošić (ed.), Šibenik: Croatian Society of Chemical Engineers, (2019) 219-219 (poster).

[7] V. Gilja, A. Tomić, I. Živković, Z. Katančić, I. Peternel, Z. Hrnjak- Murgić, Optimization of photocatalytic activity of waste fly ash/TiO_2 composite in wastewater polluted by C.I. Reactive Red 45 // Abstracts of The 22nd International Conference on Advanced Oxidation Technologies for Treatment of Water, Air and Soil / Hussain Al-Ekabi (ed.), London, (2016) 68-68 (poster).

[8] M. Kovačić, S. Salaeh, A. Čović, A. Tomić, D. Juretić Perišić, H. Kušić, A. Lončarić Božić, Degradation of 17β-estradiol in aqueous medium by application of composite TiO_2-FeZ photocatalyst, XI Meeting of young chemical engineers (XI SMLKI) // Book of abstracts / G. Matijašić (ed.), Zagreb: Croatian Society of Chemical Engineers, (2016) 122-122 (poster).

[9] M. Perlog, A. Tomić, V. Gilja, Z. Hrnjak-Murgić, Lj. Kratofil Krehula, Z. Katančić, Synthesis

and characterization of fly ash/TiO$_2$ photocatalytic nanocomposites, XI Meeting of young chemical engineers (XI SMLKI) // Book of abstracts / G. Matijašić (ed.), Zagreb: Croatian Society of Chemical Engineers, (2016) 36-36 (lecture).

Professional conference:

[1] A. Tomić H. Kušić T. Bolanča, A. Lončarić Božić, Nova onečišćivala koja izazivaju zabrinutost u okolišu // 2nd Conference on Water Treatment, Preparation, Purification and Protection, Zagreb: Croatian Professional Scientific Association for Energy, Mechanical Technologies and Renewable Energy Sources (HESO) and Energy marketing d.o.o, (2022) (lecture).